Virginia Polytechnic Institute and State University
Department of Engineering Science and Mechanics
Blacksburg, VA 24061-0219

Final Technical Report on the
Research Grant AFOSR-91-0351
Entitled

A COMPREHENSIVE PROGRAM FOR THE PERFORMANCE IMPROVEMENT OF COMPOSITE AIRCRAFT WINGS THROUGH AEROLASTIC TAILORING AND MODERN CONTROL

Covering the Period
September 1991 - 31 August 1994

Submitted to
Dr. Spencer T. Wu
Air Force Office of Scientific Research
January 23, 1995

Principal Investigator: Leonard Meirovitch
University Distinguished Professor

Principal Coinvestigator: Liviu Librescu
Professor

1. AGENCY USE ONLY (Leave blank)	2. REPORT DATE	3. REPORT TYPE AND DATES COVERED
	23 Jan 95	Final, 1 Sep 91 - 31 Aug 94

4. TITLE AND SUBTITLE
Performance Improvement of Composite Wings through Aeroelastic Tailoring and Modern Control

5. FUNDING NUMBERS
AFOSR-91-0351
2302/DS

6. AUTHOR(S)
L. Meirovitch and L. Librescu

VA Polytechnic Inst. + State Univ
BLACKSBURG, VA 24061

7. PERFORMING ORGANIZATION NAME(S) AND ADDRESS(ES)
AFOSR
110 Duncan Avenue, Suite B115
Bolling AFB, DC 20332-0001
NA

8. PERFORMING ORGANIZATION REPORT NUMBER
AFOSR-TR- 95-0326

9. SPONSORING/MONITORING AGENCY NAME(S) AND ADDRESS(ES)
AFOSR/NA
Bolling AFB DC 20332-6448
NA

10. SPONSORING/MONITORING AGENCY REPORT NUMBER
AFOSR-
91-0351

11. SUPPLEMENTARY NOTES

Approved for Public Release; Distributions Unlimited

Approved for public release,
distribution unlimited

13. ABSTRACT (Maximum 200 words)

The research has been carried out simultaneously on three aspects of aircraft wings performance optimization, as follows:

i. Structural tailoring and modern control of thin-walled model of composite aircraft wings.

ii. Structural tailoring of a low-aspect ratio plate model of composite aircraft wings.

iii. Integrated structural design and vibration control by multiobjective optimization.

Significant progress has been made on all fronts.

14. SUBJECT TERMS	15. NUMBER OF PAGES
Composite Aircraft Wings; Thin-walled Structures; Structural Tailoring; Vibration Control	16. PRICE CODE

17. SECURITY CLASSIFICATION OF REPORT	18. SECURITY CLASSIFICATION OF THIS PAGE	19. SECURITY CLASSIFICATION OF ABSTRACT	20. LIMITATION OF ABSTRACT
Unclassified	Unclassified	Unclassified	Unclassified

Abstract

The research has been carried out simultaneously on three aspects of aircraft wings performance optimization, as follows:

i. Structural tailoring and modern control of thin-walled model of composite aircraft wings.

ii. Structural tailoring of a low-aspect ratio plate model of composite aircraft wings.

iii. Integrated structural design and vibration control by multiobjective optimization.

Significant progress has been made on all fronts.

Introduction

The research can be divided into the following areas:

i. Structural tailoring and modern control of thin-walled model of composite aircraft wings.

ii. Structural tailoring of a low-aspect ratio plate model of composite aircraft wings.

iii. Integrated structural design and vibration control by multiobjective optimization.

Five technical papers have resulted from the research. The research is reported according to these papers.

1. *Refined Structural Modeling For Enhancing Vibrational and Aeroelastic Characteristics of Composite Aircraft Wings*, L. Librescu, L. Meirovitch and O. Song*

An analytical study, including tailoring, of the vibrational and static aeroelastic response characteristics of anisotropic composite aircraft wings in the form of thin-walled beams is presented. The theoretical analysis and numerical results encompass effects such as transverse shear flexibility exhibited by the advanced composite materials, warping restraint characterizing cantilevered structures, elastic anisotropy and induced structural couplings. The complex effects of these factors are highlighted and the power of the tailoring technique toward enhancing the dynamic and static structural characteristics is demonstrated.

The paper has been presented at the *AIAA/ASME/ASCE/AHS/ASC 34th Structures, Structural Dynamics, and Materials Conference*, La Jolla, CA, April 19-22, 1993, and has been accepted for publication in the journal *La Recherche Aérospatiale.* A copy of the paper is enclosed.

2. *Integrated Structural Tailoring and Adaptive Control for Advanced Aircraft Wings*, L. Librescu, L. Meirovitch and O. Song*

This paper presents an integrated approach combining structural tailoring with the converse piezoelectric effect for the purpose of actively controlling the vibration and static aeroelastic characteristics of advanced aircraft wings. The structural model incorporating a number of nonclassical features consists of a thin/thick-walled closed cross section cantilevered beam whose constituent layers exhibit elastic anisotropic properties. In addition,

* The authors are listed in alphabetical order.

a system of piezoelectric actuators bonded to, or embedded into the structure generates a localized strain field in response to an injected electric current, thus producing a change in the static and dynamic characteristics of the structure. Results reveal that a combination of both techniques can play a major role in enhancing the vibrational and static aeroelastic response characteristics of aircraft wings.

The paper has been presented at the *AIAA/ASME/ASCE/AHS/ACS 34th Structures, Structural Dynamics, and Materials Conference*, La Jolla, CA, April 19-22, 1993, and is being considered for publication in *Journal of Aircraft.* A copy of the paper is enclosed.

3. *Structural Modeling of Low-Aspect Ratio Composite Wings*, L. Meirovitch and T.J. Seitz

This paper is concerned with the aeroelastic tailoring of a structural model consisting of a rigid fuselage and a low-aspect ratio wing made of composite materials. The wing is modeled as a trapezoidal plate with root and tip chords parallel to the flow and with general sweep. The fuselage is capable of plunge and pitch and the elastic wing model includes shear deformations but ignores rotatory inertia.

The paper has been presented at the *AIAA/ASME/ASCE/AHS/ACS 34th Structures, Structural Dynamics, and Materials Conference*, La Jolla, CA, April 19-22, 1993, and has been tentatively accepted for publication in *Journal of Aircraft.* A copy of the paper is enclosed.

4. *Integrated Structural Design and Vibration Suppression Using Independent Modal Space Control*, R. A. Canfield and L. Meirovitch

The integrated design of a structure and its control system is treated as a multiobjective optimization problem. Structural mass and a quadratic performance index constitute the vector objective function. The closed-loop performance index is taken as the time integral of the Hamiltonian. Constraints on natural frequencies, closed-loop damping, and actuator forces are also considered. Derivatives of the objective and constraint functions with respect to structural and control design variables are derived for a finite element beam model of the structure and constant feedback gains determined by independent modal space control. Pareto optimal designs generated for a simple beam demonstrate the benefit of solving the

integrated structural and control optimization problem.

The paper has been presented at the *AIAA/ASME/ASCE/AHS/ACS 34th Structures, Structural Dynamics, and Materials Conference*, La Jolla, CA, April 19-22, 1993, and has appeared in *AIAA Journal*, Vol. 32, No. 10, 1994, pp. 2053-2060. A copy of the paper is enclosed.

5. *Vibration and Static Aeroelastic Instability of Nonuniform, Thin-Walled Beam Composite Wings*, L. Librescu, L. Meirovitch and O. Song*

The equations of motion for a nonuniform, anisotropic thin-walled beam are derived and applied to the study of vibration and static aeroelastic instability of slender tapered aircraft wings made of advanced composite materials. Numerical results illustrate the effects of anisotropy, transverse shear flexibility, primary and secondary warping, as well as of wing taper ratio, and the implications of these effects on the vibrational and divergence instability characteristics are discussed.

The paper has been presented at the *AIAA/ASME/ASCE/AHS/ACS 35th Structures, Structural Dynamics, and Materials Conference*, Hilton Head, SC, April 16-20, 1994, and is currently being revised for submission for publication in *AIAA Journal.* A copy of the paper is enclosed.

* The authors are listed in alphabetical order.

Refined Structural Modeling For Enhanced Vibrational and Aeroelastic Characteristics of Composite Aircraft Wings

L. Librescu, L. Meirovitch and O. Song*
Department of Engineering Science and Mechanics, Virginia Polytechnic Institute and State University, Blacksburg, VA 24061, USA

Abstract An analytical study focusing on the vibrational and static aeroelastic response of anisotropic composite aircraft wings modeled as thin-walled beams is presented. The theoretical analysis and numerical results encompass effects such as transverse shear flexibility exhibited by the advanced composite materials, warping restraint characterizing cantilevered structures, elastic anisotropy and induced structural couplings. The complex effects of these factors are highlighted and the power of the tailoring technique toward enhancing the dynamic and static structural characteristics is demonstrated.

Keywords: Composite materials - Vibration - Static aeroelasticity - Tailoring - Transverse shear flexibility - Warping restraint - Structural couplings

Résumé

* The authors are listed in alphabetical order.

I - INTRODUCTION

With the advent of high-performance composite materials, thick- and thin-walled beam structures made of fiber reinforced laminated composites are likely to play an increasing role in the design of aircraft wings. In addition, the ability to tailor the structural characteristics argues for extensive use of composite materials in these structures. The various elastic and structural couplings resulting from directional properties of fiber-reinforced composite materials and of ply-stacking sequence can be exploited successfully to enhance the response characteristics of flight vehicles. However, extensive use of these potential benefits can be achieved only if the effects induced by these couplings are well understood.

It is clear that, for an accurate prediction of flight vehicle response characteristics, comprehensive structural models must be developed. It is also clear that, in addition to this requirement, more powerful analytical tools than those currently available are needed for accurate prediction of structural response under complex static and dynamic excitations.

The present paper is devoted to the development of the structural theories and analytical techniques capable of treating the above problem. To this end, a refined dynamical model of laminated composite thin-/thick-walled beams of arbitrary closed cross section incorporating a number of nonclassical features is developed. In this connection, a ply-angle scheme generating the most favorable structural coupling for the problem at hand is implemented. Then, the vibrational and static aeroelastic behavior of composite swept-wings is studied and the influence of various factors on the response characteristics is demonstrated.

Two methods of solution for the problem at hand were explored and proved to be extremely efficient. An exact one, based on the Laplace transform technique in the spatial domain, and an approximate one, referred to as the extended Galerkin method, yielding numerical results in excellent agreement with the first. The analytical developments in this paper are general in the sense that they are valid for arbitrary beam cross sections. However, for illustration purposes, a biconvex profile typical of supersonic wing airplanes is adopted.

It should be remarked that, due to the incorporation of transverse shear, the ensuing beam theory is perfectly applicable to both thin- and thick-walled beams, in the sense of

$h_{max}/b \lesssim 0.1$, respectively, where h_{max} denotes the maximum thickness of the wall and b a typical cross-sectional dimension. Although the theory is applicable to thick-walled beams as well, the standard terminology of thin-walled beams is used throughout. It should be stressed here that the necessity of incorporating transverse sheer effects arises not only from the fact that composite beams tend to be thicker than the standard metallic counterpart, but also from the fact that advanced fiber composite materials exhibit high flexibilities in transverse shear.

It should be emphasized here that the model of composite aircraft wings almost universally used to date has been the simple *solid* beam [1]. Hence, the composite thin-walled beam model developed and used in this paper represents a significant advance in the state of the art as it permits not only the incorporation of effects not accounted for previously, but also enables one to treat a number of important problems of wing structures using a more refined structural model.

II - BASIC ASSUMPTIONS

This study uses the structural concept of single-cell, thin-walled beams of arbitrary cross-section. Pertinent quantities are referred to a global coordinate system xyz, where x and y denote the cross-sectional coordinates and z is the spanwise coordinate (Fig. 1a). The theory is based on the following assumptions: i) beam cross-sections do not deform in their own planes, ii) transverse shear effects are significant, iii) the twist varies along the span, i.e., the rate of twist $d\phi/dz$ is no longer assumed to be constant (as in the Saint-Venant torsional model) but a function of the spanwise coordinate, where $\phi' \equiv d\phi/dz$ constitutes a measure of the torsion-related nonuniform warping, iv) primary and secondary warping effects are sufficiently important to be included. (The first one is related to the warping displacement of points on the midline cross section and the second one is related to points off the midline contour.) and v) in the absense of an internal pressure field, the hoop stress resultant is negligibly small compared to the remaining stresses.

III - KINEMATICAL EQUATIONS

Consistent with assumption iv), the primary warping function $F_\omega(s)$ is taken as [2-4]

$$F_\omega(s) = \int_o^s [r_n(\bar{s}) - \psi]\, d\bar{s} \tag{1}$$

where

$$\psi = \frac{\oint r_n(\bar{s}) d\bar{s}}{\oint d\bar{s}} = \frac{2A_c}{\beta} \tag{2}$$

denotes the torsional function, A_c the cross-sectional area of the beam bounded by the midline contour, s the arc-length measured along the circumferential coordinate, whose origin is arbitrarily but conveniently chosen, $\bar{s}$ is a dummy coordinate associated with the s-coordinate, $\oint(\cdot)ds$ the integral along the closed midline contour, $r_n(s) = x(s)\ell + y(s)m$ a geometric quantity (see Fig. 1b), where $\ell = \cos(n,x)$, $m = \cos(n,y)$ denote direction cosines, and $\beta = \oint d\bar{s}$ is the circumferential contour length.

In accordance with assumptions i) - iv), and in order to reduce the three-dimensional elasticity theory of thin-walled beams to an equivalent one-dimensional one, the components of the displacement vector are expressed as [4]

$$u(x,y,z,t) = u_o(z,t) - y\phi(z,t),\ v(x,y,z,t) = v_o(z,t) + x\phi(z,t) \tag{4a,b}$$

$$\begin{aligned} w(x,y,z,t) =& w_o(z,t) + \theta_x(z,t)\,[y(s) + nm] \\ &+ \theta_y(z,t)\,[x(s) + n\ell] - \phi'(z,t)\,[F_\omega(s) + na(s)] \end{aligned} \tag{4c}$$

In the above equation, $F_\omega(s)$ and $na(s)$ play the role of primary and secondary warping functions (see also [5]), respectively, where n denotes the coordinate in the thickness direction, and

$$\theta_x(z,t) = \gamma_{yz}(z,t) - v_o'(z,t),\ \theta_y(z,t) = \gamma_{xz}(z,t) - u_o'(z,t),\ a(s) = -y(s)\ell + x(s)m \tag{5a-c}$$

in which $\theta_x(z,t)$ and $\theta_y(z,t)$ denote the rotations about axes x and y, respectively, and γ_{yz} and γ_{xz} are the transverse shear strains in the planes yz and xz, respectively; we note that primes denote derivatives with respect to z. When transverse shear effects are ignored, $\theta_x \to -v_0'$ and $\theta_y \to -u_0'$. In agreement with Eqs. (4), it can be readily verified that the assumption of cross-sectional nondeformability, implying $\epsilon_{xx} = 0$, $\epsilon_{yy} = 0$, and $\epsilon_{xy} = 0$, or

equivalently $\epsilon_{nn} = \epsilon_{ss} = \epsilon_{sn} = 0$, and the continuity requirement of w along the midline contour, i.e., $\oint(\partial w/\partial s)ds = 0$, are fulfilled.

The quantities $u_0(z,t)$, $v_0(z,t)$ and $w_0(z,t)$, denoting the rigid-body translations along the x, y and z axis, respectively, and $\theta_x(z,t), \theta_y(z,t)$ and $\phi(z,t)$, denoting the rigid-body rotations about the x- and y-axes and the twist about the z-axis, respectively, constitute the variables of the problem.

IV - CONSTITUTIVE EQUATIONS

Consider the case of composite thin-walled beams consisting of a finite number N of homogeneous layers. It is assumed that the material of each constituent layer is linearly elastic and anisotropic and that the bonding between the layers is perfect. The three-dimensional constitutive equations for a generally orthotropic elastic material can be expressed as

$$\begin{bmatrix} \sigma_{ss} \\ \sigma_{zz} \\ \sigma_{nn} \\ \sigma_{zn} \\ \sigma_{ns} \\ \sigma_{sz} \end{bmatrix} = \begin{bmatrix} \bar{Q}_{11} & \bar{Q}_{12} & \bar{Q}_{13} & 0 & 0 & \bar{Q}_{16} \\ \bar{Q}_{12} & \bar{Q}_{22} & \bar{Q}_{23} & 0 & 0 & \bar{Q}_{26} \\ \bar{Q}_{13} & \bar{Q}_{23} & \bar{Q}_{33} & 0 & 0 & \bar{Q}_{36} \\ 0 & 0 & 0 & \bar{Q}_{44} & \bar{Q}_{45} & 0 \\ 0 & 0 & 0 & \bar{Q}_{45} & \bar{Q}_{55} & 0 \\ \bar{Q}_{16} & \bar{Q}_{26} & \bar{Q}_{36} & 0 & 0 & \bar{Q}_{66} \end{bmatrix} \begin{bmatrix} \epsilon_{ss} \\ \epsilon_{zz} \\ \epsilon_{nn} \\ \gamma_{zn} \\ \gamma_{ns} \\ \gamma_{sz} \end{bmatrix} \tag{6}$$

where $\bar{Q}_{ij}$ denote the transformed elastic coefficients associated with the kth layer in the global coordinate system of the structure and $\gamma_{pr} = 2\epsilon_{pr}$, $p \neq r$ and ϵ_{ij} denote the components of the strain tensor. The three-dimensional dependence in Eqs. (6) can be reduced to an equivalent one-dimensional dependence in two steps. The first step, yielding the two-dimensional local constitutive equations, consists of the integration of the original three-dimensional form through the laminate thickness, while the second step, resulting in the one-dimensional form, consists of the integration of the previous form of constitutive equations along the midline contour of the beam cross section.

In light of assumptions i) and v), the local constitutive equations, expressed in terms of the strain measures, become the equations for the membrane stress resultants

$$N_{zz} = K_{11}\epsilon^0_{zz} + K_{12}\tilde{\gamma}_{sz} + K_{13}\phi' + K_{14}\epsilon^n_{zz} \tag{7a}$$

$$N_{sz} = K_{21}\epsilon^0_{zz} + K_{22}\tilde{\gamma}_{sz} + K_{23}\phi' + K_{24}\epsilon^n_{zz} \tag{7b}$$

transverse shear stress resultant

$$N_{zn} = A_{44}\gamma_{zn} \tag{8}$$

and stress couples

$$L_{zz} = K_{41}\epsilon^0_{zz} + K_{42}\tilde{\gamma}_{sz} + K_{43}\phi' + K_{44}\epsilon^n_{zz} \tag{9a}$$

$$L_{sz} = K_{51}\epsilon^0_{zz} + K_{52}\tilde{\gamma}_{sz} + K_{53}\phi' + K_{54}\epsilon^n_{zz} \tag{9b}$$

where K_{ij} denote the modified local stiffness coefficients, (see Appendix). Consistent with Eqs. (4) and (5), the strain components entering into the above constitutive equations are $\epsilon_{zz} = \epsilon^o_{zz} + n\epsilon^n_{zz}$, $\gamma_{sz} = \tilde{\gamma}_{sz} + \tilde{\tilde{\gamma}}_{sz}$ and γ_{zn}, where

$$\epsilon^o_{zz} = w_0' + x(s)\theta_y' + y(s)\theta_x' - F_\omega(s)\phi'', \ \epsilon^n_{zz} = \theta_y'\ell + \theta_x' m - a(s)\phi'' \tag{10a,b}$$

$$\tilde{\gamma}_{sz} = -(u_0' + \theta_y)m + (v_0' + \theta_x)\ell, \ \tilde{\tilde{\gamma}}_{sz} = 2\frac{Ac}{\beta}\phi', \ \gamma_{zn} = (u_0' + \theta_y)\ell + (v_0' + \theta_x)m \tag{10c-e}$$

In the above equations, ϵ^o_{zz} and ϵ^n_{zz} denote the axial strain components associated with the primary and secondary warping, respectively, $\tilde{\gamma}_{sz}$ and $\tilde{\tilde{\gamma}}_{sz}$ stand for the tangential shear strains of the beam midsurface induced by transverse shear and by twist, respectively, and γ_{zn} denotes the transverse shear strain component. The stress resultants, the stress couples and the strain measures appearing in Eqs. (7) - (9) exhibit a two-dimensional spatial dependence, the dependence being on s- and z-coordinates. In the dynamical problem, they also depend on time.

V - THE BOUNDARY-VALUE PROBLEM

The boundary-value problem, consisting of the differential equations and the boundary conditions, can be derived conveniently by means of the extended Hamilton's principle, which can be stated as follows [6]:

$$\int_{t_1}^{t_2} (\delta T - \delta V + \delta W)\, dt = 0, \ \delta u_0 = \delta v_0 = \delta w_0 = \delta\theta_x = \delta\theta_y = \delta\phi = 0 \text{ at } t = t_1, t_2 \tag{11}$$

where T and V denote the kinetic energy and strain energy, respectively, while δW is the virtual work due to nonconservative forces. The kinetic energy has the form

$$T = \frac{1}{2}\int_0^L \oint \sum_{k-1}^{N} \int_{h_{(k)}} \rho^{(k)} \Big[\left(\dot{u}_0 - y\dot{\phi}\right)^2 + \left(\dot{v}_0 + x\dot{\phi}\right)^2 + \Big\{ \left(\dot{w}_0 + y\dot{\theta}_x + x\dot{\theta}_y - F_\omega\dot{\phi}'\right) + n\left(\ell\dot{\theta}_y + m\dot{\theta}_x - a\dot{\phi}'\right) \Big\}^2 \Big] dn ds dz \tag{12}$$

whereas the strain energy can be shown to have the expression

$$V = \frac{1}{2}\int_0^L \oint \sum_{k=1}^{N} \int_{h(k)} \left\{ \sigma_{zz}^{(k)} \Big[w_0' + x\theta_y' + y\theta_x' - F_\omega \phi'' + n\left(\ell\theta_y' + m\theta_x' - a\phi''\right)\Big] + \sigma_{sz}^{(k)} \Big[-\left(u_0' + \theta_y\right) m + \left(v_0' + \theta_x\right)\ell + \frac{2Ac}{\beta}\phi' \Big] + \sigma_{nz}^{(k)} \left[\left(u_0' + \theta_y\right)\ell + \left(v_0' + \theta_x\right) m \right] \right\} dn\,ds\,dz \tag{13}$$

where L denotes the wing semispan. Moreover, the virtual work of the nonconservative forces can be written as

$$\delta W = \int_0^L \left(p_y \delta v_0 + m_z \delta\phi\right) dz \tag{14}$$

where p_y and m_z denote the lift force per unit length and aerodynamic twist moment (positive nose up) about the elastic axis.

Carrying out integrations with respect to n, s and t, we can write

$$\int_{t_0}^{t_1} \delta T\, dt = -\int_{t_0}^{t_1} \Big[\int_0^L \big(I_1 \delta u_0 + I_2 \delta v_0 + I_3 \delta w_0 + \left(I_4 - I_9'\right)\delta\phi + I_5 \delta\theta_y + I_7 \delta\theta_x \big)\, dz - I_9 \phi \Big|_0^L \Big] dt \tag{15}$$

where I_i denote the inertia terms, given in the Appendix. Integration with respect to n and s in Eq. (13) and consideration of Eqs. (1), (5), (7) and (10), yields

$$\delta V = -\int_0^L \Big[T_z' \delta w_0 + \left(M_y' - Q_x\right)\delta\theta_y + \left(M_x' - Q_y\right)\delta\theta_x + \left(B_\omega'' + M_z'\right)\delta\phi + Q_x' \delta u_0 + Q_y' \delta v_0 \Big] dz + \Big[T_z \delta w_0 + M_y \delta\theta_y + M_x \delta\theta_x - B_\omega \delta\phi' + \left(B_\omega' + M_z\right)\delta\phi + Q_x \delta u_0 + Q_y \delta v_0 \Big] \Big|_0^L \tag{16}$$

where

$$\begin{aligned} &T_z(z,t) = \oint N_{zz}\, ds,\ Q_x(z,t) = \oint \left(-N_{sz} m + N_{zn}\ell\right) ds \\ &Q_y(z,t) = \oint \left(N_{sz}\ell + N_{zn} m\right) ds,\ M_x(z,t) = \oint \left(y N_{zz} + L_{zz} m\right) ds \\ &M_y(z,t) = \oint \left(x N_{zz} + L_{zz}\ell\right),\ M_z(z,t) = 2\oint N_{sz}\psi ds \\ &B_\omega(z,t) = \oint \left[F_\omega(s) N_{zz} + a(s) L_{zz}\right] ds \end{aligned} \tag{17a-g}$$

In Eqs. (17),T_z, Q_x and Q_y denote the axial force and shear forces in the x- and y- directions, M_x, M_y and M_z denote the moments about the x-, y- and z-axes, respectively, and B_ω

denotes the bimoment. Introducing Eqs. (14)-(16) into Eq. (11) and following the usual steps [7], we obtain the boundary-value problem for the most general case of anisotropy. The boundary-value problem consists of six differential equations of motion for the displacements $u_0, v_0, w_o, \theta_x, \theta_y$ and ϕ, together with the corresponding boundary conditions. Such a set exhibits complete coupling between the various modes, i.e., primary and secondary warping, vertical and lateral bending, twist and transverse shear. However, the principal goal of structural tailoring lies in the appropriate selection of fiber orientation so as to produce desired elastic couplings between certain modes. For the problem at hand, the induced elastic couplings must play a decisive role in the enhancement of the free vibration and aeroelastic response characteristics of wing structures. At the same time, the selected ply-angle orientation should not generate undesired couplings, producing unwanted effects on the response characteristics. In this sense, the bending-twist coupling is most important in the design of aircraft wings. Its beneficial effects, demonstrated for the solid beam model in [1], will be considered here in the context of a thin-walled beam model. Additional beneficial effects of this cross-coupling have been highlighted recently in [8]. The above criteria for selecting fiber orientation, together with ease of implementation in design and manufacturing, result in the ply-angle distribution

$$\theta(y) = -\theta(-y). \tag{18}$$

This ply configuration is shown in Fig. 2. According to terminology used in [9], structures displaying this ply-angle distribution are said to exhibit *circumferentially asymmetric stiffness configuration.*

In the case of the ply-angle distribution given by Eq. (18), the extended Hamilton's principle, Eq. (11), yields two independent boundary-value problems. The first boundary-value problem is of eighth order and involves the coupling of the twist ϕ, the vertical bending v_0 and the flapwise transverse shear θ_x. On the other hand, the second boundary-value is of sixth order and involves the coupling of the extension w_0, the lateral bending u_0 and the chordwise transverse shear θ_y. The first boundary-value problem is governed by the

differential equations of motion

$$\underline{-a_{66}\phi''''} + a_{73}\theta_x'' - \underline{a_{65}(v_0''' + \theta_x'')} + a_{77}\phi'' + m_z = (b_4 + b_5)\ddot{\phi} - \underline{\underline{(b_{10} + b_{18})\ddot{\phi}''}} \quad (19a)$$

$$a_{55}(v_o'' + \theta_x') + \underline{a_{56}\phi'''} + p_y = b_1\ddot{v}_o \quad (19b)$$

$$a_{33}\theta_x'' + a_{37}\phi'' - \underline{a_{65}(v_o'' + \theta_x')} - \underline{a_{56}\phi''} = (b_4 + b_{14})\ddot{\theta}_x \quad (19c)$$

to be satisfied over $0 < z < L$. For cantilevered thin-walled beams, the solution of Eqs. (19) must satisfy the boundary conditions

$$\phi = 0,\ v_0 = 0,\ \theta_x = 0,\ \underline{\phi'} = 0 \quad (20a\text{-}d)$$

at $z = 0$ and

$$\underline{-a_{66}\phi'''} + a_{73}\theta_x' - \underline{a_{65}(v_0'' + \theta_x')} + a_{77}\phi' = -\underline{\underline{(b_{10} + b_{18})\ddot{\phi}'}}$$
$$a_{55}(v_o' + \theta_x) + \underline{a_{56}\phi''} = 0,\ a_{33}\theta_x' + a_{37}\phi' = 0, \quad \underline{a_{66}\phi''} + \underline{a_{65}(v_0' + \theta_x)} = 0 \quad (21a\text{-}d)$$

at $z = L$. Note that singly and doubly underlined terms in Eqs. (19)-(21) are associated with the warping restraint and warping inertia effects, respectively.

The couplings exhibited by the second boundary-value problem are of no interest here, so that the problem will not be pursued any further.

The boundary-value problem associated with the bending-twist-transverse shear motions, Eqs. (19)-(21), can be used to enhance the vibrational and aeroelastic response characteristics of wing structures. It should be mentioned here that the stiffness terms $a_{37} = a_{73}$ and $a_{56} = a_{65}$ appearing in Eqs. (19) and (21) are responsible for the coupling between bending and twist, with the effect of a_{56} due to warping being much weaker than the effect of a_{37} (see Fig. 11). It should be pointed out that deletion of the warping restraint results in a reduction in the order of the boundary-value problem from eight to six, so that only three boundary conditions must be satisfied at each end. On the other hand, if transverse shear effects are ignored, then the order of the boundary-value problem is preserved. The stiffness coefficients a_{ij} and the inertia coefficients b_i appearing in Eqs. (19) and (21) are displayed in the Appendix.

VI - STRUCTURAL TAILORING FOR IMPROVED VIBRATION AND STATIC AEROELASTIC RESPONSE

Static aeroelastic behavior, which includes both divergence instability and aeroelastic lift distribution is an important consideration in the design of modern aircraft. The analysis performed here addresses the problem of designing the wing so as to take advantage of structural couplings from a static aeroelastic viewpoint. This is done by using the unique directional properties of advanced composite materials. The same importance should be afforded to the vibrational characteristics, which are basic to the dynamic response, flutter instability and aeroservoelasticity studies of flight vehicles.

In the case of free vibration, the terms associated with the external loadings are omitted. Moreover, for static aeroelastic problems, the inertia terms must be discarded from Eqs. (19) and (21), and the only loading terms to be retained are the ones associated with the aerodynamic lift p_y and the torsional aerodynamic moment m_z. Using strip-theory aerodynamics, we can write [10]

$$p_y(z) = q_n c a_o(\phi_o + \phi - v_o' \tan\Lambda) - NW/2L \tag{22a}$$

$$m_z(z) = q_n c a_o e(\phi_o + \phi - v_o' \tan\Lambda) + q_n c^2 C_{MAC} - NWd/2L \tag{22b}$$

Here $q_n = \frac{1}{2}\rho U_n^2$ denotes the dynamic pressure normal to the leading edge of the swept wing, c the chord of the wing, a_o the *corrected lift* curve slope coefficient, Λ the angle of sweep (considered positive for swept-back), e the offset between the aerodynamic and reference axis, ϕ_o the rigid angle of attack (measured in planes normal to the leading edge), C_{MAC} the wing section pitching moment coefficient (whose influence, as usual, is disregarded), $W/2L$ the wing weight per unit length and N the load factor normal to the wing surface, whose expression is

$$N = \frac{2c\ q_n a_o}{W} \int_o^L (\phi_o + \phi - v_o' \tan\ \Lambda) dz \tag{23}$$

The static aeroelastic response is analyzed here both in the subcritical range, i.e., for the range of velocities $q_n < (q_n)_D$, where $(q_n)_D$ denotes divergence dynamic pressure, and in the critical case as well. As a general remark, Eqs. (22) reveal that for $\Lambda < 0$,

i.e., for swept-forward wings, the aeroelastic bending-twist coupling results in an increase in $p_y(z)$ and $m_z(z)$, which in turn reduces dramatically the divergence speed, whereas for $\Lambda > 0$, i.e., for swept-back wings, the opposite trend takes place. These two phenomena are referred to as wash-in and wash-out [11], respectively. Whereas the goal of the subcritical aeroelastic analysis consists of the determination of the distribution of the effective angle of attack ϕ_{eff} and of the lift force, as affected by the elastic deformations, the study of the critical case involves the determination of divergence instability conditions. Clearly, the main target of tailoring applied to swept-forward wing is to yield a decrease of the effective angle of attack, and implicitly of the aeroelastic lift and, as a result, an increase of the critical divergence speed. Whereas the study of the subcritical static aeroelastic response requires the solution of an integral-differential system of equations, obtained by inserting Eqs. (22) and (23) into Eqs. (19), the determination of the divergence speed leads to the solution of an eigenvalue problem, where the divergence speed plays the role of eigenvalue. Structural tailoring applied to the vibration of wing structures must result in an increase in the eigenfrequencies without weight penalties. To determine the natural frequencies, one must solve an eigenvalue problem.

In spite of the mathematical complexities involved, the two previously mentioned solution techniques used here proved to be extremely powerful, as demonstrated by the following numerical illustrations. Details of the techniques can be found in [12-14].

VII - SPECIAL CASES INVOLVING DIVERGENCE INSTABILITY

In the most general case, closed-form solutions for the divergence speed are not feasible. However, in a number of special cases closed-form solutions can be obtained. These cases are concerned with i) pure bending divergence of swept wings infinitely rigid in transverse shear and ii) pure torsion divergence.

In the first case, eliminating $a_{56}\phi''$ from Eqs. (19b) and (19c), assuming very large torsional stiffness, letting $\theta_x \rightarrow -v_0'$, ignoring the inertia terms and implementing a Rayleigh-

quotient procedure, the expression of the divergence speed can be shown to have the form

$$(q_n)_D = -\frac{2a_{33}\int_0^L (v_0'')^2 dz}{a_0 c \tan\Lambda \int_0^L (v_0^2)' dz} \tag{24}$$

where v_0 must satisfy the boundary conditions

$$v_0 = 0,\ v_0' = 0 \text{ at } z = 0 \tag{25a}$$

$$v_0'' = 0,\ v_0''' = 0 \text{ at } z = L \tag{25b}$$

Equation (24) reveals that only swept-forward wings, $\Lambda \rightarrow -\Lambda$, can exhibit divergence instability in pure bending. This result represents an extension to wings modeled as thin-walled beams of results obtained in [16]. Also from Eq. (24), one can conclude that the bending stiffness term a_{33} must be maximized to increase $(q_n)_D$ as much as possible. This can be achieved by designing the wing so that $K_{14} \rightarrow 0$.

In the pure torsion case, assuming infinite bending stiffness and implementing a Rayleigh-quotient procedure in conjunction with the static counterpart of Eq. (19a), it can be shown that

$$(q_n)_D = q_D = \frac{\int_0^L \left[a_{66}(\phi'')^2 + a_{77}(\phi')^2\right] dz}{a_0 c e \int_0^L \phi^2 dz} \tag{26}$$

in which the underdashed term is connected with the warping inhibition, and note that ϕ must satisfy the boundary conditions

$$\phi = 0,\ \phi' = 0 \text{ at } z = 0 \tag{27a}$$

$$\phi'' = a_{77}\phi' - a_{66}\phi''' = 0 \text{ at } z = L \tag{27b}$$

As in the case of wings modeled as solid beams [16], Eq. (26) reveals that pure torsion divergence can occur for straight wings only.

VIII - APPROXIMATE EXPRESSION FOR THE DIVERGENCE OF SWEPT-FORWARD WINGS

An approximate expression for the coupled divergence of swept-forward wings can be derived using the conditions corresponding to decoupled divergence in bending and torsion,

Eqs. (24) and (26). The expression is based on a linear algebraic relation between the two decoupled expressions of the divergence instability obtained previously. The linear relation yields the expression for the divergence in the form

$$(q_n)_D = \frac{1}{a_0 c L^2}\frac{P}{S} \tag{28}$$

where

$$P = \frac{\int_0^1 \left[\frac{a_{66}}{L^2 a_{77}}\left(\frac{d^2\phi}{d\eta^2}\right)^2 + \left(\frac{d\phi}{d\eta}\right)^2\right] d\eta}{\int_0^1 \phi^2 d\eta} \tag{29a}$$

$$S = \frac{e}{a_{77}} - \frac{PL\tan\Lambda \int_0^1 \frac{d(v_0^2)}{d\eta} d\eta}{2a_{33}\int_0^1 \left(\frac{d^2 v_0}{d\eta^2}\right)^2 d\eta} \tag{29b}$$

where $\eta = z/L$. As in Eqs. (24) and (26), the warping restraint effect is included but the transverse shear flexibility is ignored. Equation (28) represents the extension to wings modeled as thin-walled beams of the divergence expression obtained in [16] for solid beams.

IX - NUMERICAL ILLUSTRATIONS

Wing structures modeled as cantilevered thin-walled beams of biconvex cross sections made of the graphite-epoxy material are considered. The material properties used are

$$E_L = 30 \times 10^6 \text{ psi}, \; E_T = 0.75 \times 10^6 \text{ psi}$$

$$G_{LT} = 0.37 \times 10^6 \text{ psi}, \; G_{TT} = 0.45 \times 10^6 \text{ psi}$$

$$\mu_{LT} = \mu_{TT} = 0.25, \; \rho = 14.3 \times 10^{-5} \text{ lb sec}^2/\text{in}^4$$

where L and T denote directions parallel and transverse to the fibers, respectively.

The geometrical characteristics of the wing are displayed in Fig. 1a. Figure 3a shows the first three in vacuo eigenfrequencies associated with Problem A as functions of the ply angle θ with the bending-twist coupling stiffness first included, $a_{37} \neq 0$, and then discarded, $a_{37} = 0$. In both cases, plots of the frequencies versus θ are symmetric about $\theta = 90°$ and experience as many peaks as the eigenfrequency number. When $a_{37} = 0$, the second

eigenfrequency has a local maximum in the vicinity of $\theta = 75°$ and $\theta = 105°$, and at these ply angles it comes in close proximity to the third eigenfrequency. On the other hand, when the effect of bending-twist coupling is included, implying $a_{37} \neq 0$, Fig. 3a reveals that frequency near merging is precluded. This phenomenon was also observed in Ref. 15, in which a solid beam model was used. The frequency of the fundamental mode has a maximum at $\theta = 90°$. At $\theta = 0°$ (and 180°), where the bending and twist become decoupled, the fundamental mode can be identified as a pure bending mode, denoted by B. The frequency associated with the second mode first increases for $0° < \theta \leq 80°$ and then decreases for $80° \leq \theta \leq 90°$, the trend being symmetric about $\theta = 90°$. Another notable trend is that, in the absence of cross-coupling rigidity, the second eigenfrequency is overestimated compared to the real case, in which the cross-coupling rigidity is included. At $\theta = 0°$ (or $\theta = 180°$) and $\theta = 90°$, where decoupling occurs, the second mode can be identified as the second pure bending mode and the first pure torsional mode, respectively, where the latter is denoted by T. As far as the third eigenfrequency is concerned, a more complex variation with the ply angle is observed. Indeed, the variation about $\theta = 90°$ is drastically attenuated when the cross coupling is ignored. At $\theta = 0°$ (or $\theta = 180°$) and $\theta = 90°$, this mode can be identified as the first pure torsional mode and second pure bending mode, respectively.

Figure 3b displays the first three eigenfrequencies for Problem A as functions of the ply angle for the cases in which the transverse shear effects are incorporated and ignored. Clearly, for ply angles such that the bending is dominant, omission of the transverse shear causes an overestimation of frequencies.

Figure 4a portrays plots of the first three eigenfrequencies for Problem B versus the ply angle θ. In this case, the lateral bending-extension cross-coupling parameter a_{14} plays a similar role to the bending-twist stiffness a_{37}. However, these three eigenfrequencies are well separated within the entire range of ply angles θ and, in addition, removal of a_{14} does not cause the second and third eigenfrequencies to approach each other, regardless of the value of θ. The plots are symmetric about $\theta = 90°$ and, as expected, the lateral eigenfrequencies are much higher than the transverse counterpart frequencies. At $\theta = 90°$ the first three modes

are identified as the first three pure lateral bending modes, denoted by B, and at $\theta = 0°$ and $\theta = 180°$ as the first two pure lateral bending modes and the first pure axial mode, where the latter is denoted by A.

Figure 4b portrays the first three eigenfrequencies in lateral vibration versus the ply angle θ for the cases in which the transverse shear is included and ignored. A comparison of Figs. 3b and 4b reveals that the overestimation of eigenfrequencies for the case in which the transverse shear effects are ignored is more pronounced in chordwise vibration than in the flapping vibration counterpart.

Figure 5 presents the bending and twist in the three lowest modes as functions of the normalized position $\eta = z/L$ for $\theta = 45°$. The modes are normalized so that the value at the tip is equal to unity. For other ply angles and for the case of lateral bending, similar plots were obtained, but they are not displayed here. As a general comment, the position of the nodal points changes in general with θ. This trend, coupled with large variations of these modes with θ, is likely to have a significant effect on the flutter behavior.

The effect of the ply angle on the divergence speed is illustrated in Fig. 6 for the swept-back, swept-forward and straight wing aircraft. The figure shows plots of the normalized divergence speed $(q_n)_D \,/\, (q_n)^*_D$ versus the ply angle θ, where $(q_n)^*_D = (q_n)_D \Big|_{\Lambda=\theta=0} = 35.566$psi. It reveals that the range of ply angles for which divergence instability is avoided decreases with increasing forward sweep and increases with increasing sweep back angles. Figure 7 displays the normalized divergence speed versus the ply angle for various values of the wall thickness and for $\Lambda = 0$ and $\Lambda = -60°$. It reveals that, when an increase in the wall thickness is an option for increasing the divergence speed, then it must be considered in conjunction with the proper ply angle, thus yielding a maximum increase of the divergence speed.

In Fig. 8a plots of the divergence speed versus the ply angle for two swept angles, $\Lambda = 0°$ and $\Lambda = -60°$, and for the cases $a_{37} = 0$ and $a_{37} \neq 0$ are displayed. As the figure reveals, for $a_{37} = 0$ the divergence speed exhibits symmetry about $\theta = 90°$, whereas for $a_{37} \neq 0$ it is not symmetric. Moreover, results for straight wings reveal that a larger range of ply angles corresponding to infinite divergence speed is exhibited than for the forward-

swept wing counterpart. Although the bending-twist cross coupling is not the only factor influencing the aeroelastic static behavior, it is clear that its effect is dominant. By increasing its negative value as much as possible, the bending of the swept wings and the resulting twist tend to produce a wash-out effect.

Figure 8b displays a plot of the ratio $(q_n)_{D,FW} / (q_n)_{D,WR}$ as a function of the ply angle θ for $\Lambda = -30°$ and $\Lambda = 0$, where $(q_n)_{D,FW}$ is the divergence speed for a free warping model and $(q_n)_{D,WR}$ is the divergence speed for the case in which the warping restraint effect is included. It essentially demonstrates the effect of warping restraint on the divergence speed. It can be concluded from this figure that the warping inhibition does not always result in an increase in the divergence speed. In other words, the free warping model does not yield the most conservative results from the divergence instability point of view. Hence, for a rational design, the warping restraint effect must always be taken into consideration. A similar result was obtained for a solid beam wing model in [16-18].

In view the importance of this cross-coupling rigidities, in Fig. 9 plots of a_{37}, a_{33}, a_{77}, a_{56} and a_{14} versus θ are portrayed. Based on these plots, a value of θ resulting in a more rational design can be achieved. Within the theory of solid beams, the importance of the bending-twist coupling was underscored in [1,11-13, 15-17]

Figures 10a and 10b display plots of the normalized effective angle of attack, ϕ_{eff}/ϕ_0, versus the normalized position $\eta = z/L$ for a swept and a straight wing, and with the ply angle θ and sweep angle Λ acting as parameters, where $\phi_{eff} = \phi_0 + \phi - v_0' \tan\Lambda$ is the effective angle of attack and $\phi_0 = 5°$ is the rigid angle of attack. The plots provide a measure of the subcritical static aeroelastic response. The effective angle of attack constitutes a measure of the induced aeroelastic loads. For ply angles $\theta < 90°$, the aeroelastic loads are amplified, whereas for $\theta > 90°$, for both forward swept and swept back wings, they are attenuated. In all cases, the flight speed corresponds to a dynamic pressure $(q_n)_{\text{flight}} = 3.446$ psi. The basic conclusion is that tailoring can play a significant role not only in counteracting the detrimental wash-in effect, but also in diminishing the effect of elastic twist. This change of the traditional subcritical static aeroelastic response of forward swept wing is basically due

to the bending-twist coupling stiffness a_{37}.

The results obtained here confirm that the coupling stiffness a_{37} plays a key role in controlling the wing behavior as far as the subcritical static aeroelastic response and divergence instability are concerned. By increasing the negative value of a_{37} as much as possible for $\Lambda < 0$, the wash-in effect turns into a wash-out effect. The effect of transverse shear flexibility on the subcritical aeroelastic response of swept-forward wings is in general detrimental, in the sense that it exacerbates the wash-in effect. This conclusion, based on results obtained in this study but not displayed here, is reinforced by results obtained in [13]. However, in contrast to other cases of ply angles, results for $55° < \theta < 90°$ and for $\Lambda > 0$ reveal that the coupling rigidities play a significant role also in this respect and can render the effect of transverse shear flexibility either immaterial or slightly beneficial.

Finally, Fig. 11 displays the subcritical aeroelastic responses of $\tilde{v}_o = v_0/L$, θ_x and ϕ as functions of η for a straight wing with ply angles $\theta = 45°$ and $\theta = 135°$. As before, $(q_n)_{\text{flight}} = 3.448$ psi was prescribed. These plots reveal again that, for values of the ply angle θ for which the cross-coupling parameter a_{37} reaches a negative value, smaller displacements are experienced as compared to the case in which a_{37} is positive.

X - CONCLUSIONS

A dynamic theory of aircraft wings modeled as thin-walled composite beams of closed cross-sectional contour was presented. The theory incorporates a number of features essential for a reliable prediction of the free vibration and aeroelastic response characteristics.

A specific ply-angle distribution, inducing a bending-twist cross-coupling, was considered and its influence on the eigenvibration, divergence instability and static aeroelastic response was investigated. As the numerical illustrations reveal, the bending-twist cross-coupling term a_{37}, considered in conjunction with the tailoring technique, plays a key role in the enhancement of swept wings performance. Physically, this coupling stiffness generates a wash-out effect, alleviating the excessive build-up of aerodynamic loads. This is achieved by using ply angles so as to minimize or completely nullify the wash-in effect, as well as the detrimental transverse shear flexibility effect. A similar conclusion can be drawn in connec-

tion with the warping restraint effect, which is always present and should be used to enhance the aeroelastic characteristics of wing structures.

The various results obtained here are expected to contribute to the understanding of the role played by a number of nonclassical factors, which, as shown, can affect in a complex way the behavior of aircraft wings made of composite materials.

XI - REFERENCES

1. Weisshaar, T.A., "Aeroelastic Tailoring - Creative Use of Unusual Materials," AIAA Paper 87-0976, *AIAA/ASME/ASCE/AHS 28th Structures, Structural Dynamics, and Materials Conference*, Monterey, CA, April 9-10, 1987.
2. Rehfield, L.W., "Design Analysis Methodology for Composite Rotor Blades," *Proceedings of the Seventh DoD/NASA Conference on Fibrous Composites in Structural Design*, AFWAL-TR-85-3094, June 1983, pp. v(a)-1 - v(a)-15.
3. Libove, C.,"Stresses and Rate of Twist in Single-Cell Thin-Walled Beames With Anisotropic Walls," *AIAA Journal*, Vol. 26, No. 9, September 1988, pp. 1107-118.
4. Librescu, L. and Song, O., "Behavior of Thin-Walled Beams Made of Advanced Composite Materials and Incorporating Non-Classical Effects," *Applied Mechanics Review*, (Eds.), R.A. Kitte and D.T. Mook, Vol. 44, No. 11, Part 2, November 1991, pp. 174-180.
5. Gjelsvik, A., *The Theory of Thin Walled Bars*, John Wiley and Sons, New York, 1981.
6. Meirovitch, L., *Computational Methods in Structural Dynamics*, Sijthoff & Noordhoff International Publishers, The Netherlands, 1980.
7. Librescu, L., *Elastostatics and Kinetics of Anisotropic and Heterogeneous Shell-Type Structures*, Noordhoff International Publishers, Leyden, The Netherlands, 1975.
8. Garfinkle, M., "Twisting Smartly in the Wind," *Aerospace America*, July 1994, pp. 18-20.
9. Rehfield, L. W. and Atilgan, A. R., "Toward Understanding the Tailoring Mechanisms for Thin-Walled Composite Tubular Beams," *Proceedings of the First U.S.S.R.-U.S.A.*

Symposium on Mechanics of Composite Materials, Riga, Lituania, May 23-26, 1989.

10. Bisplinghoff, R.L. and Ashley, H., *Principles of Aeroelasticity*, Wiley, New York, 1962.
11. Weisshaar, T. A., "Aeroelastic Tailoring of Forward Swept Composite Wings," *Journal of Aircraft*, Vol. 18, No. 8, Aug. 1981, pp. 669-676.
12. Librescu, L. and Thangjitham, S., "Analytical Studies on Static Aeroelastic Behavior of Forward Swept Composite Wing Structures," *Journal of Aircraft*, Vol. 28, No. 2, February 1991, pp. 151-157.
13. Karpouzian, G. and Librescu, L., "A Comprehensive Model of Anisotropic Composite Aircraft Wings and Its Use in Aeroelastic Analyses," *Journal of Aircraft*, Vol. 31, No. 3, May-June 1994, pp. 702-712.
14. Palazotto, A.N. and Linnermann, I.E., "Vibration and Buckling Characteristics of Composite Cylindrical Panels Incorporating the Effects of a Higher Order Shear Theory," *International Journal of Solids and Structures*, Vol. 28, No. 3, 1991, pp. 341-361.
15. Weisshaar, T.A. and Foist, B.L., "Vibration Tailoring of Advanced Composite Lifting Surfaces," *Journal of Aircraft*, Vol. 22, No. 2, February 1985, pp. 141-147.
16. Librescu, L. and Simovich, J., "General Formulation for the Aeroelastic Divergence of Composite Swept-Forward Wing Structures," *Journal of Aircraft*, Vol. 25, No. 4, April 1988, pp. 364-371.
17. Librescu, L. and Khdeir, A.A., "Aeroelastic Divergence of Swept-Forward Composite Wings Including Warping Restraint Effect," *AIAA Journal*, Vol. 26, No. 11, November 1988, pp. 1373-1377.
18. Oyibo, G.A. "Some Implications of Warping Restraint on the Behavior of Composite Anisotropic Beams," *Journal of Aircraft*, Vol. 26, No. 2, February 1989, pp. 187-189.

Acknowledgement

The authors gratefully acknowledge the support of AFOSR through Research Grant 91-0351. The grant monitors were Drs. Spencer T. Wu and Walter F. Jones.

Appendix

The reduced rigidity quantities are as follows:

$$
\begin{aligned}
&K_{11} = A_{22} - \frac{A_{12}^2}{A_{11}}, \quad K_{12} = A_{26} - \frac{A_{12}A_{16}}{A_{11}} = K_{21}, \quad K_{13} = 2K_{12}\frac{A_c}{\beta} \\
&K_{14} = B_{22} - \frac{A_{12}B_{12}}{A_{11}} = K_{41}, \quad K_{22} = A_{66} - \frac{A_{16}^2}{A_{11}}, \quad K_{23} = 2K_{22}\frac{A_c}{\beta} \\
&K_{24} = B_{26} - \frac{A_{16}B_{12}}{A_{11}} = K_{42}, \quad K_{43} = 2K_{24}\frac{A_c}{\beta} \\
&K_{44} = D_{22} - \frac{B_{12}^2}{A_{11}}, \quad K_{51} = B_{26} - \frac{B_{16}A_{12}}{A_{11}}, \quad K_{52} = B_{66} - \frac{B_{16}A_{16}}{A_{11}} \\
&K_{53} = 2K_{52}\frac{A_c}{\beta}, \quad K_{54} = D_{26} - \frac{B_{12}B_{16}}{A_{11}}
\end{aligned}
\tag{A.1}
$$

where A_{ij}, B_{ij} and D_{ij} denote local stretching, stretching-bending coupling and bending rigidity quantities, respectively.

The inertia terms are

$$
\begin{aligned}
&I_1 = \oint (\ddot{u}_0 - y\ddot{\phi}) m_0 ds, \quad I_2 = \oint (\ddot{v}_0 + x\ddot{\phi}) m_0 ds \\
&I_3 = \oint (\ddot{w}_0 + x\ddot{\theta}_y + y\ddot{\theta}_x - F_\omega \ddot{\phi}') m_0 ds, \; I_4 = \oint [(x^2 + y^2)\ddot{\phi} - y\ddot{u}_0 + x\ddot{v}_0] m_0 ds \\
&I_5 = \oint [x\ddot{w}_0 + x^2\ddot{\theta}_y + xy\ddot{\theta}_x - xF_\omega(s)\ddot{\phi}'] m_0 ds \\
&\quad + \oint \left(\ell^2\ddot{\theta}_y + \ell m\ddot{\theta}_x - \ell a(s)\ddot{\phi}'\right) m_2 ds \\
&I_7 = \oint [y\ddot{w}_0 + y^2\ddot{\theta}_x + xy\ddot{\theta}_y - yF_\omega(s)\ddot{\phi}'] m_0 ds \\
&\quad + \oint \left[m^2\ddot{\theta}_x + m\ell\ddot{\theta}_y - ma(s)\ddot{\phi}'\right] m_2 ds \\
&I_9 = \oint [-F_\omega(s)\ddot{w}_0 - xF_\omega\ddot{\theta}_y - yF_\omega(s)\ddot{\theta}_x + F_\omega(s)^2\ddot{\phi}'] m_0 ds \\
&\quad + \oint \left[-ma(s)\ddot{\theta}_x - \ell a(s)\ddot{\theta}_y + a^2(s)\ddot{\phi}'\right] m_2 ds
\end{aligned}
\tag{A.2}
$$

where

$$
(m_0, m_2) = \sum_{k=1}^{N} \int_{h_{(k-1)}}^{h_{(k)}} \rho_{(k)}(1, n^2) dn \tag{A.3}
$$

denote the mass terms.

The rigidity terms are symmetric, $a_{ij} = a_{ji}$, and the terms of interests in this paper have the expressions

$$
a_{33} = \oint \left(K_{11}y^2 + 2yK_{14}m + K_{44}m^2\right) ds
$$

$$
\begin{aligned}
a_{37} &= \oint (yK_{13} + K_{43}m)\, ds,\ a_{55} = \oint \left(K_{22}\ell^2 + A_{44}m^2\right) ds \\
a_{56} &= -\oint (F_\omega K_{21}\ell + K_{24}a\ell)\, ds \\
a_{66} &= \oint \left(K_{11}F_\omega^2 + 2K_{14}F_\omega a + K_{44}a^2\right) ds,\ a_{77} = \oint 2\frac{A_c}{\beta}K_{23}ds
\end{aligned}
\tag{A.4}
$$

The reduced mass terms are as follows:

$$
\begin{aligned}
(b_1,\ b_4,\ b_5,\ b_{10}) &= \oint m_o(1,\ y^2,\ x^2,\ F_\omega^2)ds \\
(b_{14},\ b_{18}) &= \oint m_2 \left(m^2,\ a^2\right) ds
\end{aligned}
\tag{A.5}
$$

List of Figures

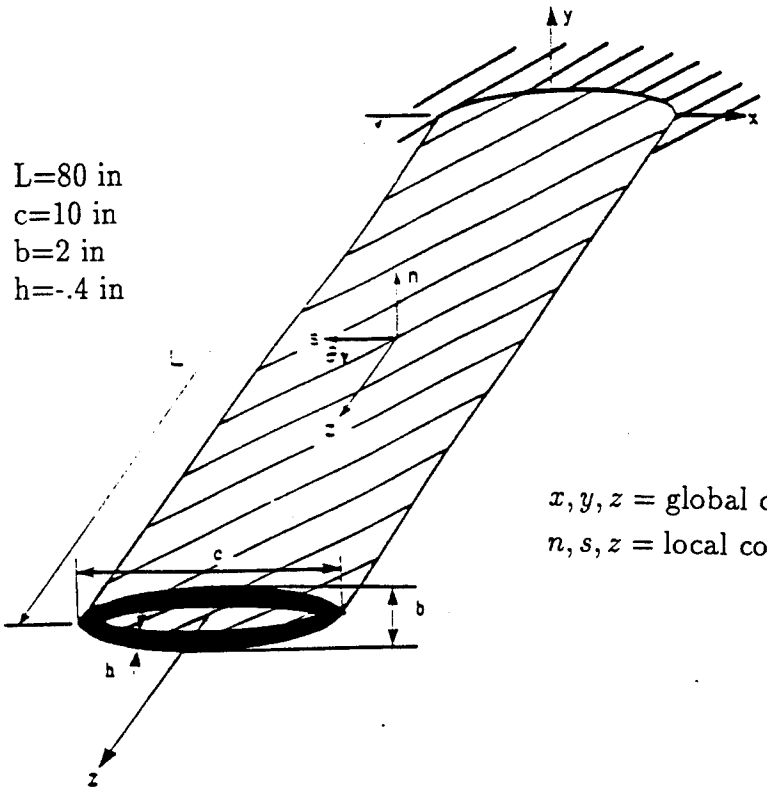

a. Coordinates and Dimensions for the Cantilevered Wing

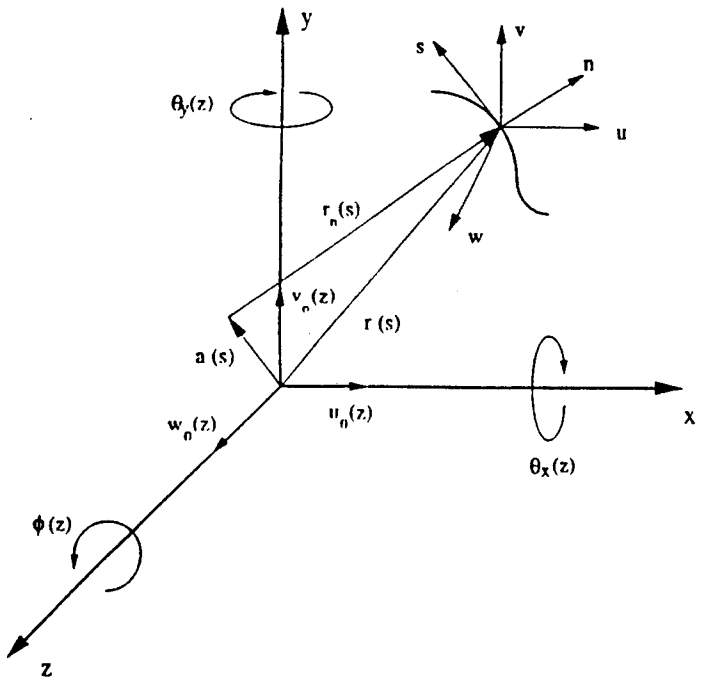

b. Displacement Field

Fig. 1 - Geometry of the Thin-Walled Wing Model

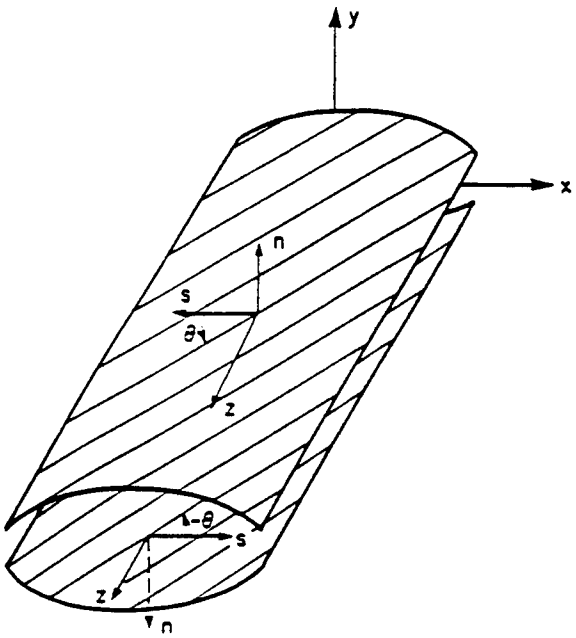

Fig. 2 - Circumferentially Asymmetric Stiffness Configuration: $\theta(y) = -\ell(-y)$

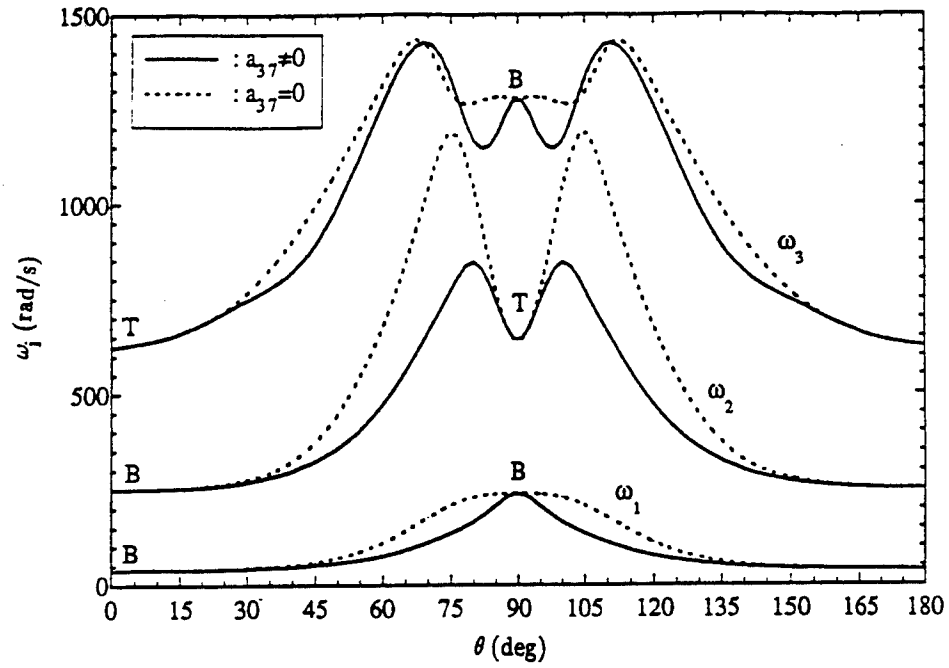

a. With and without bending-twist coupling

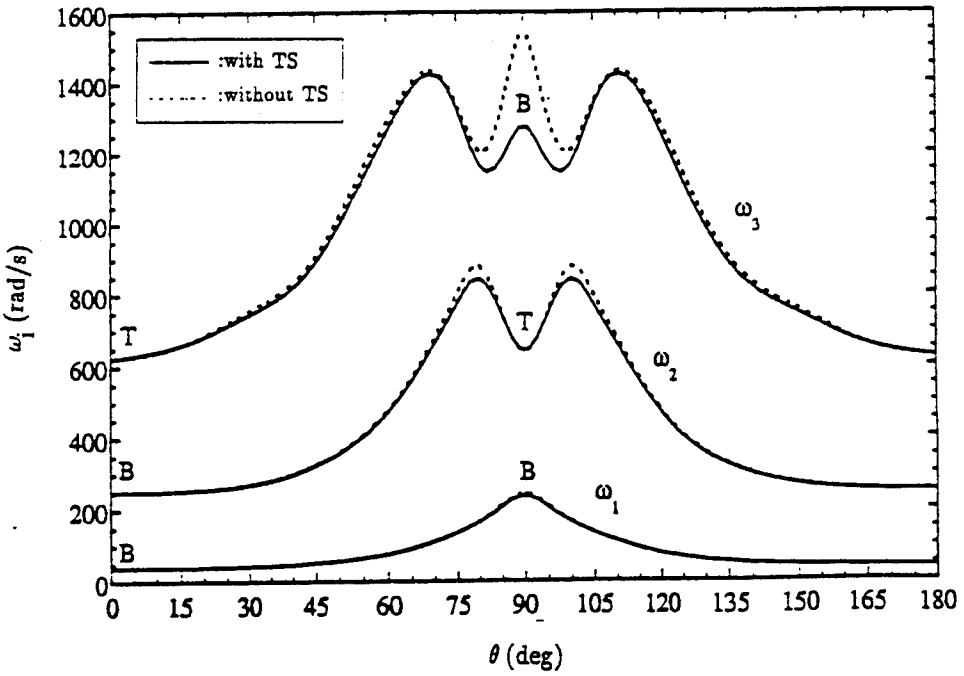

b. With and without transverse shear

Fig. 3 - The Three Lowest Eigenfrequencies Versus the Ply Angle for Froblem A

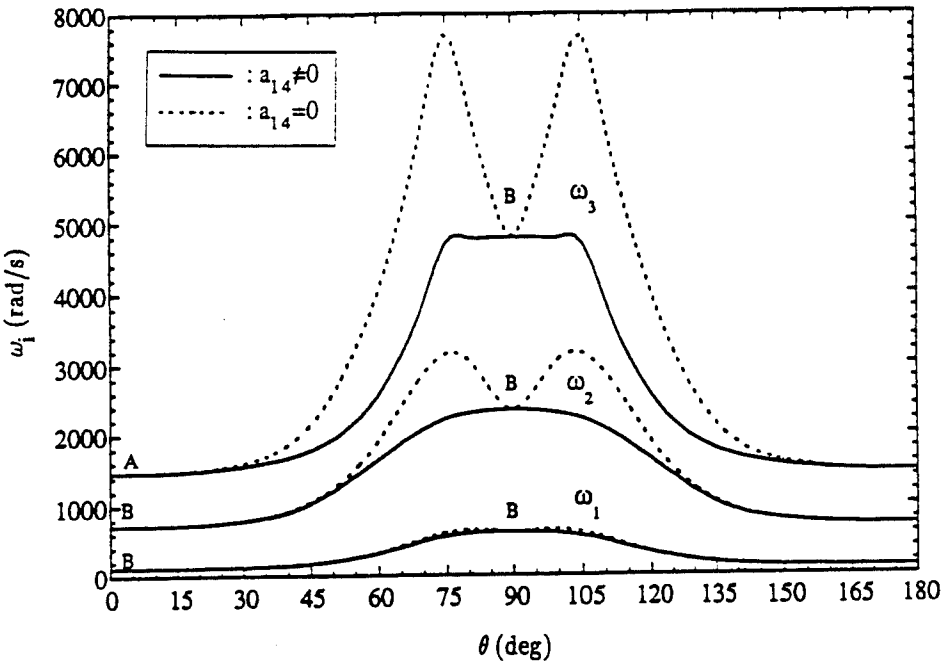

a. With and without lateral bending-extension coupling

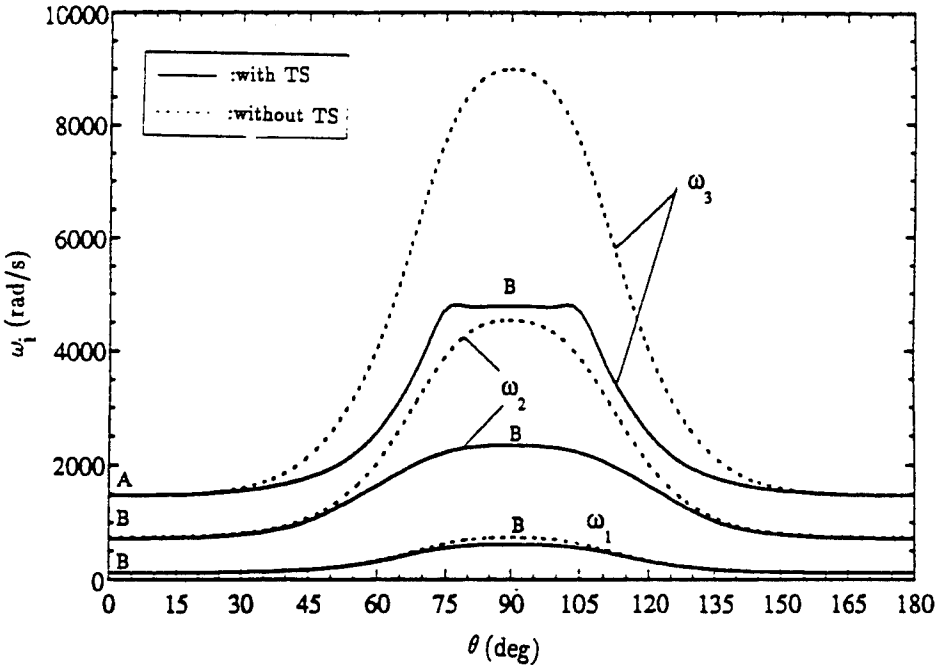

b. With and without transverse shear

Fig. 4 - The Three Lowest Eigenfrequencies Versus the Ply Angle for Problem B

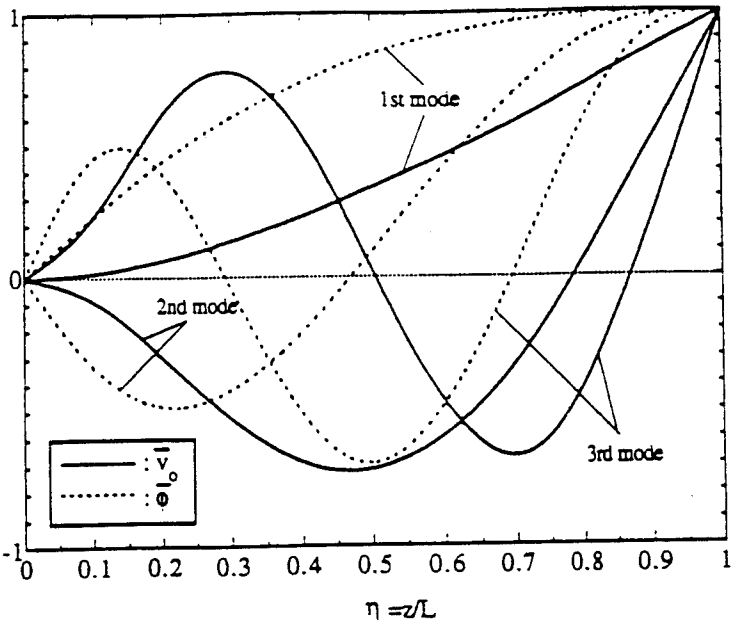

Fig. 5 - The Normalized Vertical Displacement and Normalized Twist in the Lowest Three Modes for $\theta = 45°$

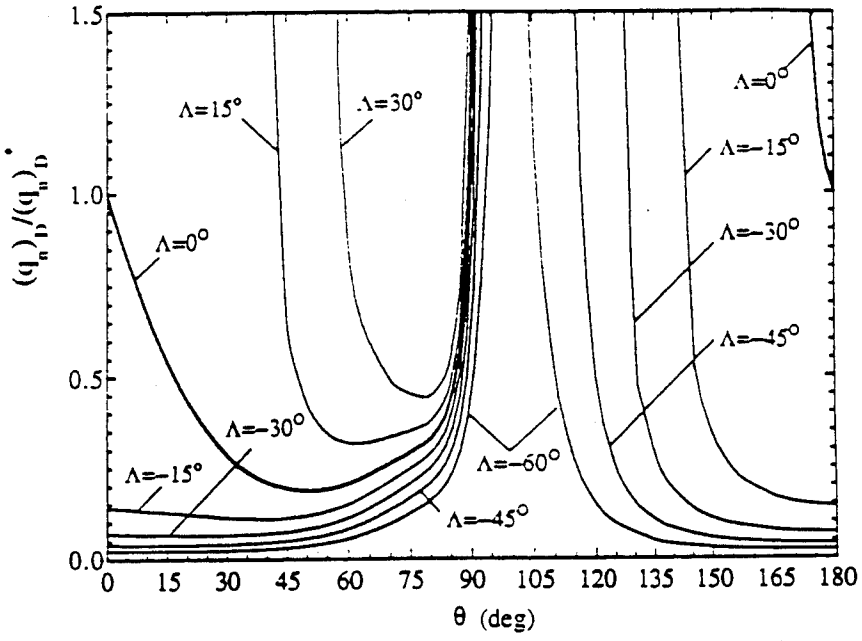

Fig. 6 - The Normalized Divergence Speed Versus the Ply Angle for Swept ($\Lambda \lessgtr 0$) and Straight ($\Lambda = 0$) Wings

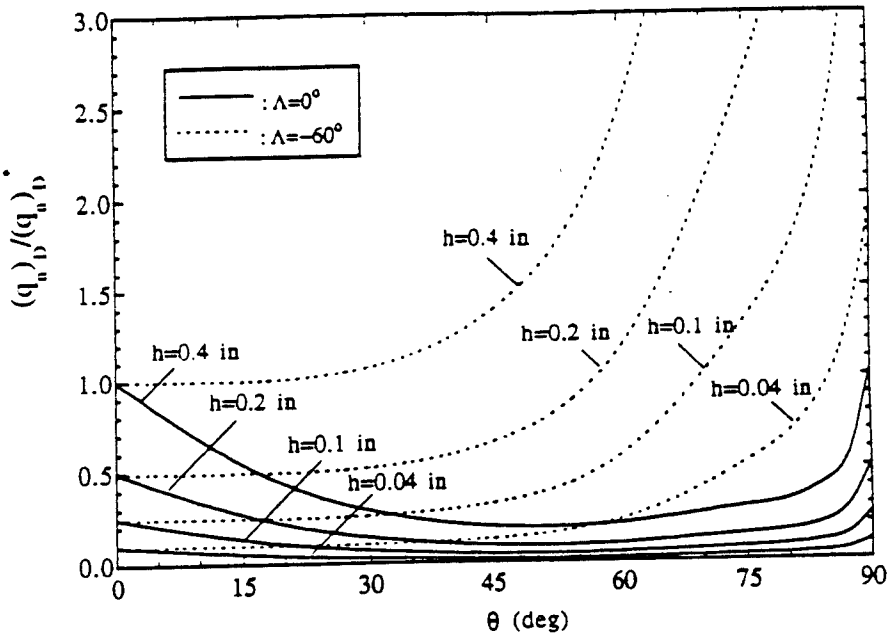

Fig. 7 - The Normalized Divergence Speed Versus the Ply Angle for Various Values of the Wall Thickness and for $\Lambda = 0°, -60°$.

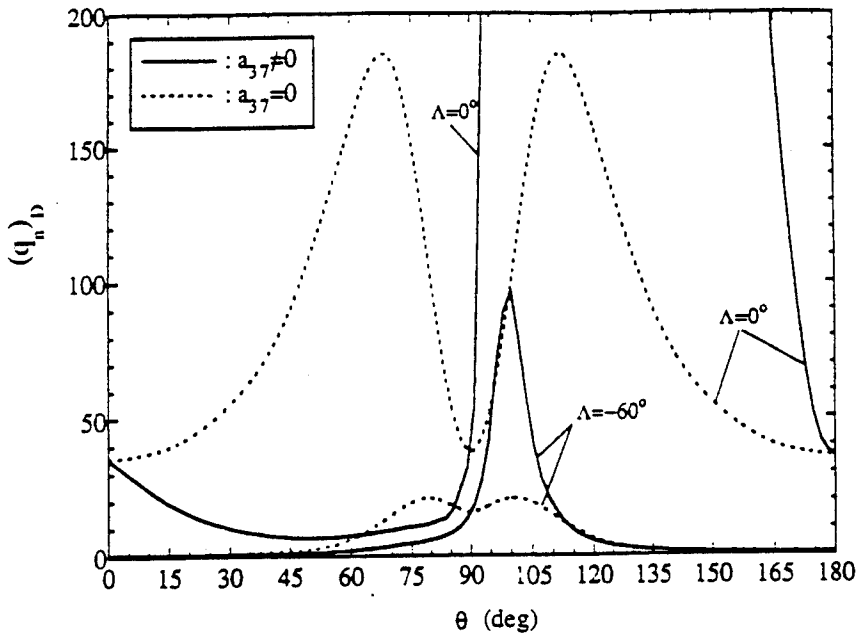

a. With and without bending-twist coupling ($\Lambda = 0°,\ -60°$)

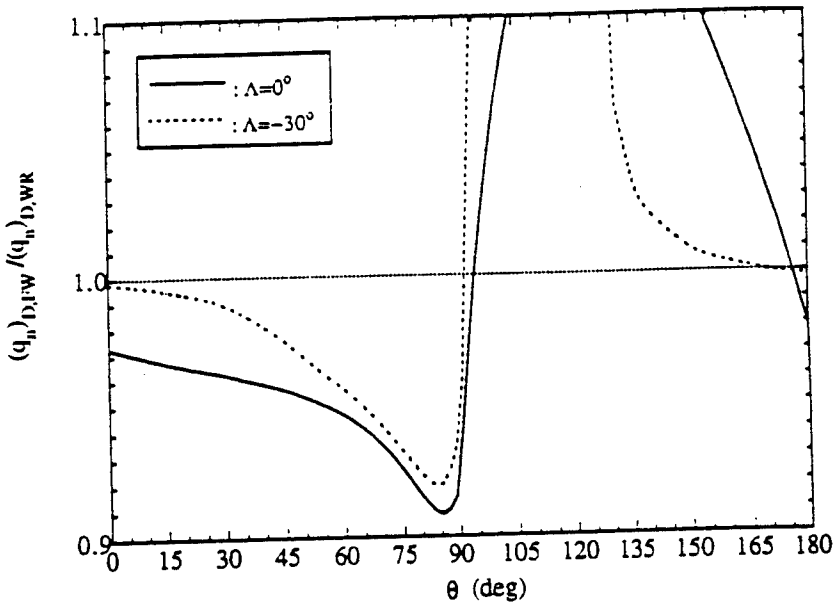

b. Effect of warping restraint ($\Lambda = 0°$,$-30°$)

Fig. 8 - The Divergence Speed for Unswept and Swept Composite Wings

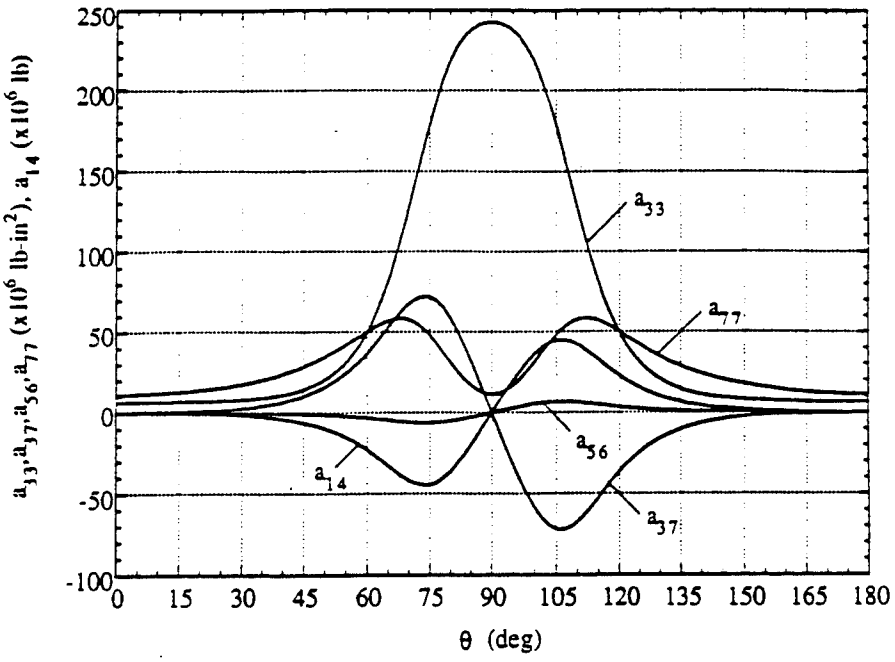

Fig. 9 - Stiffness Terms for Problems A and B Versus the Ply Angle

a_{33} = bending, a_{37} = bending-twist

a_{56} = transverse shear-warping, a_{77} = twist

a_{14} = extension-transverse shear

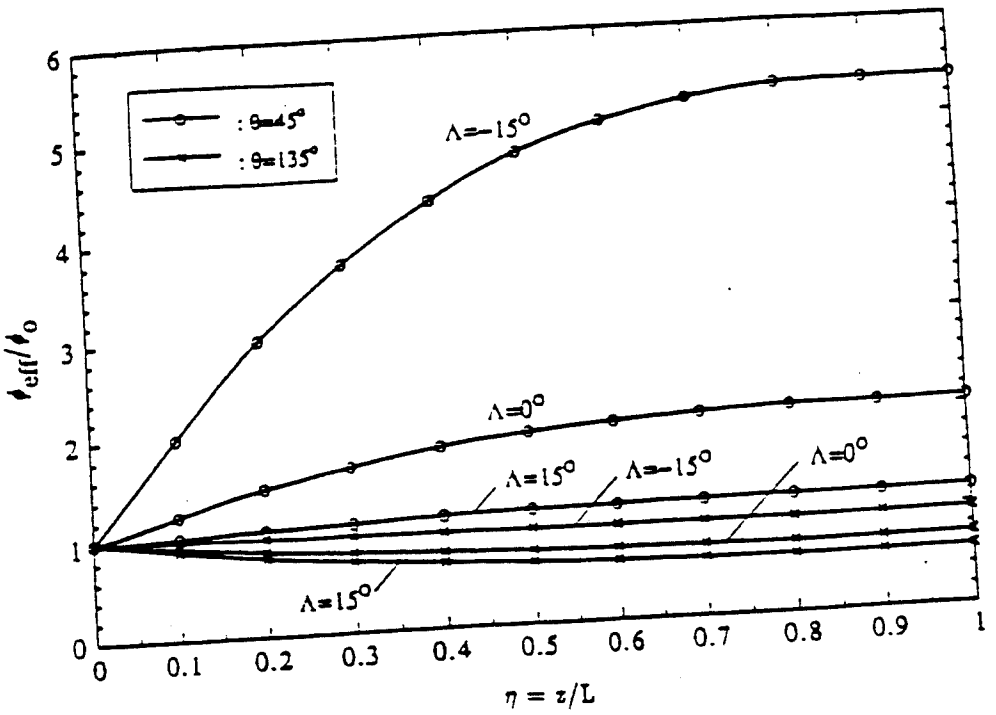

a. Swept wings

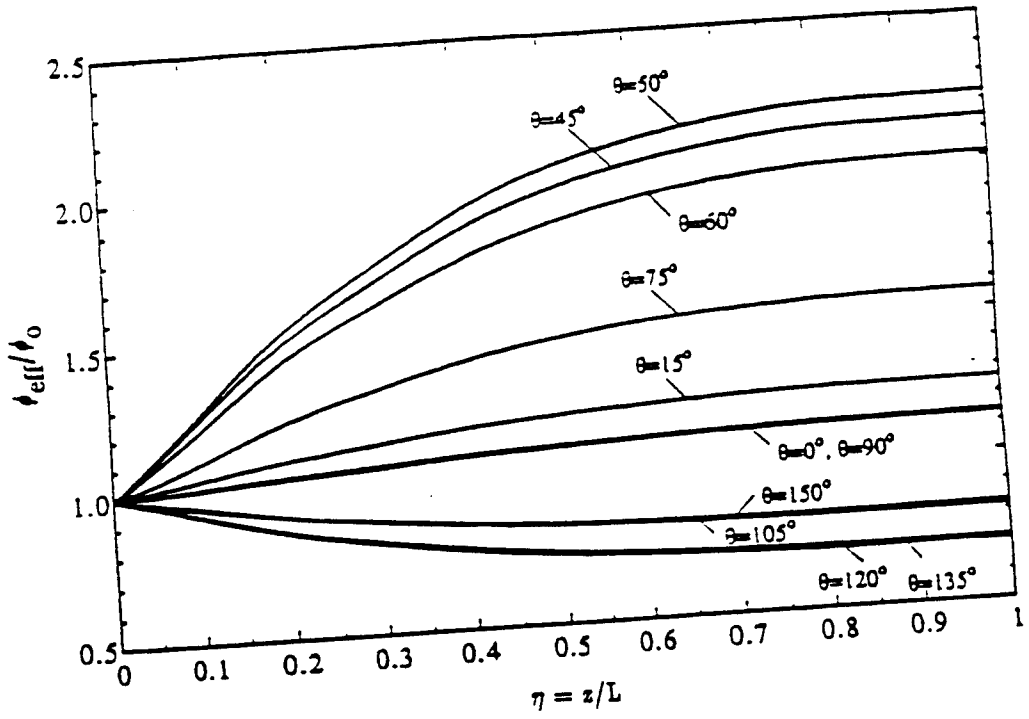

b. Straight wings

Fig. 10 - The Normalized Effective Angle of Attack Versus the Spanwise Position for a Number of Ply Angles

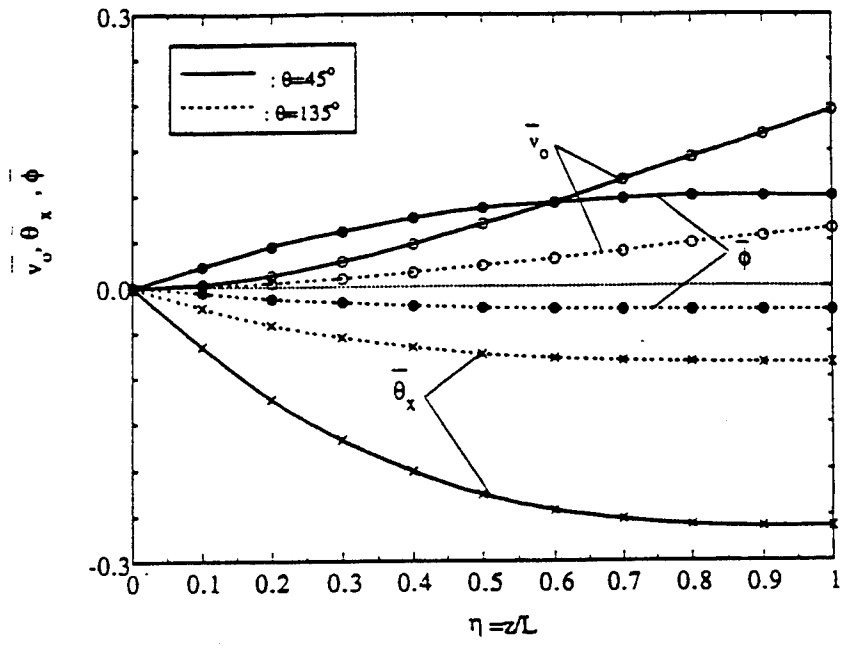

Fig. 11 - Subcritical Normalized Responses in Bending ($\overline{v}_0$) and Twist $\left(\overline{\phi}\right)$ for a Straight Wing and for $\theta = 45°,\ 135°$

Integrated Structural Tailoring and Adaptive Control for Advanced Aircraft Wings†

L. Librescu*, L. Meirovitch** and O. Song***
Department of Engineering Science and Mechanics
Virginia Polytechnic Institute and State University
Blacksburg, VA 24061

Abstract

This paper presents an integrated approach combining structural tailoring with the converse piezoelectric effect for the purpose of actively controlling the vibration and static aeroelastic characteristics of advanced aircraft wings. The structural model incorporating a number of nonclassical features consists of a thin/thick-walled closed cross section cantilevered beam whose constituent layers exhibit elastic anisotropic properties. In addition, a system of piezoelectric actuators bonded to, or embedded into the structure generates a localized strain field in response to an injected electric current, thus producing a change in the static and dynamic characteristics of the structure. Results reveal that a combination of both techniques can play a major role in enhancing the vibrational and static aeroelastic response characteristics of aircraft wings.

1. Introduction

Due to their outstanding properties, such as high strength/stiffness to weight ratio, fiber-reinforced laminated thick/thin-walled structures are likely to play an increasing role in the design of advanced aircraft wings. In addition, a number of elastic couplings resulting from anisotropy and ply-angle sequence of the composite materials can be exploited so as to enhance the response characteristics. In this regard, within the last two decades, a technique referred to as *structural tailoring* has been used with spectacular results.[1] It should be noted,

---

† The authors are listed in alphabetical order.
* Professor.
** University Distinguished Professor. Fellow AIAA.
*** Post-Doctoral Research Associate.

however, that structural tailoring is a passive design technique, in the sense that the control law is fixed in terms of the considered constitutive equations. This implies that the structure cannot respond adaptively to changes in its parameters or external stimuli. To overcome this shortcoming, additional capabilities must be built into the structure. This is particularly true in view of the fact that future generations of flight vehicles are likely to operate under increasingly severe conditions.

An approach showing good promise is adaptive control, which amounts to the integration of adaptive materials possessing sensing and actuating capabilities into the structure.[2-4] Piezoelectric materials are excellent candidates for the role of sensors and actuators. In contrast to passive structures, in which the vibrational and aeroelastic response characteristics, are predetermined, in adaptive structures these characteristics can be altered in a known and predictable manner. These adaptive capabilities can be used to prevent structural resonance and/or any other type of instability, as well as to improve the static and dynamic response of the structure.

In this paper, the task of improving the static aeroelastic response and free vibration characteristics of aircraft wings made of advanced composite materials is accomplished through the synergistic effect of combining structural tailoring and adaptive control techniques. The structural wing model consists of a thin/thick-walled closed cross-sectional cantilevered beam whose constituent layers feature elastic anisotropic properties. The adaptive control capability is achieved by a voltage feedback via the converse piezoelectric effect. The induced localized strain field produces a change in the dynamic characteristics of the structure.

The global constitutive equations of wing structures made of advanced composite materials and incorporating adaptive capabilities are first derived. These adaptive capabilities are provided by piezoelectric layers bonded or embedded into the structure and serving both as sensors and actuators. Then, based on related work,[5] the equations of motion and the associated boundary conditions of composite adaptive structures are derived. Feedback control laws relating the applied electric field to the mechanical characteristics of the vibrating

structure are implemented, thus altering the frequencies and mode shapes of the system. The obtained results underline the fact that simultaneous implementation of tailoring and adaptive materials technology can enhance the static aeroelastic response and dynamic characteristics of flight vehicle structures significantly.

2. The Structural Model

A structural model consisting of a thin-walled beam of arbitrary cross-section aiming at simulating the lifting surface of advanced flight vehicles is used. Two systems of coordinates, namely s, z, n and x, y, z, are used to describe the kinematics of thin-walled beams, as shown in Fig. 1. The theory of thin-walled beams used herein incorporates the following nonclassical features: i) Anisotropy of constituent material layers, ii) Transverse shear flexibility and iii) Primary and secondary warping effects. In the light of ii), the structural model applies not only to thin-walled beams, but also to thick-walled beams. The theory is based also on the in-plane cross-section nondeformability assumption.[6-8]

Consistent with the above statements, the components of the displacement vector are expressed as

$$u(x,y,z,t) = u_0(z,t) - y\phi(z,t) \tag{1a}$$

$$v(x,y,z,t) = v_0(z,t) + x\phi(z,t) \tag{1b}$$

$$\begin{aligned} w(x,y,z,t) = {} & w_0(z,t) + \theta_x(z,t)[y(s) + nm] \\ & + \theta_y(z,t)[x(s) + n\ell] - \phi'(z,t)[F_w(s) + na(s)] \end{aligned} \tag{1c}$$

where $\ell = \cos(n,x)$ and $m = \cos(n,y)$ denote the direction cosines. In addition

$$\theta_x(z,t) = \gamma_{yz}(z,t) - v_0'(z,t) \tag{2a}$$

$$\theta_y(z,t) = \gamma_{xz}(z,t) - u_0'(z,t) \tag{2b}$$

where $\theta_x(z,t)$ and $\theta_y(z,t)$ denote the rotations about axes x and y, respectively, while γ_{yz} and γ_{xz} denote the transverse shear strains in the planes yz and xz, respectively. Based on

Eqs. (1), the axial strain component reduces to

$$S_{zz}(n,s,z,t) = \bar{S}_{zz}(s,z,t) + n\bar{\bar{S}}_{zz}(s,z,t) \tag{3}$$

where

$$\bar{S}_{zz}(s,z,t) = w_o'(z,t) + \theta_y'(z,t)x(s) + \theta_x'(z,t)y(s) - \phi''(z,t)F_\omega(s) \tag{4a}$$

and

$$\bar{\bar{S}}_{zz}(s,z,t) = \theta_y'(z,t)\ell + \theta_x'(z,t)m - \phi''(z,t)a(s) \tag{4b}$$

are the axial strains associated with the primary and secondary warping, respectively, in which primes denote derivatives with respect to z. The membrane and transverse shear strain components can be expressed in the form

$$S_{sz}(s,z,t) = \tilde{S}_{sz}(s,z,t) + 2\frac{Ac}{\beta}\phi'(z,t) \tag{5}$$

and

$$S_{nz}(s,z,t) = \left[\theta_y(z,t) + u_o'(z,t)\right]\ell + \left[\theta_x(z,t) + v_o'(z,t)\right]m \tag{6a}$$

respectively, where

$$\tilde{S}_{sz}(s,z,t) = -\left[\theta_y(z,t) + u_o'(z,t)\right]m + \left[\theta_x(z,t) + v_o'(z,t)\right]\ell \tag{6b}$$

In the above equations, $u_o(z,t)$, $v_o(z,t)$ and $w_o(z,t)$ represent rigid-body translations in the x, y and z directions and $\phi(z,t)$ represents the twist about the z-axis, (see Fig. 2). Moreover, $h = h(s)$ denotes the wall thickness, allowed to vary in the circumferential direction, A_C the cross-sectional area bounded by the contour midline, β the total length of the contour midline and t the time. In addition, $F_\omega(s)$ denotes the warping function defined as[5-8]

$$F_\omega(s) = \int_o^s [r_n(s) - \psi]\, ds \tag{7}$$

where

$$\psi = \frac{\oint [r(s)/h(s)]\, ds}{\oint [1/h(s)]\, ds} = \frac{2A_C}{\beta} \tag{8}$$

is the torsional function, in which $\oint(\cdot)ds$ denotes the integral along the closed midline contour, and $r_n(\bar{s})$ and a are geometric quantities defined as

$$r_n(s) = x(s)\ell + y(s)m, \; a = -xm + y\ell \tag{9}$$

When the structure exhibits infinite rigidities in transverse shear, $\theta_y(z,t) \to -u_o'(z,t)$ and $\theta_x(z,t) \to -v_o'(z,t)$.

3. Constitutive Equations for Adaptive Wings

As recently conjectured,[2-4,9,10] the adaptive capabilities of piezoelectric devices can result in superior control compared to standard passive or even active control. Piezoelectric materials, integrated into the load-bearing structure by means of surface bonding or embedding, serve as networks of actuator/sensor systems.

The linear three-dimensional piezoelectric constitutive equations can be expressed in contracted index notation[11]

$$\sigma_i = C_{ij}^{\mathcal{E}} S_j - e_{ki}\,\mathcal{E}_k, \quad D_k = e_{kj} S_j + \epsilon_{k\ell}^{S}\,\mathcal{E}_\ell \tag{10a,b}$$

where σ_i and $S_j (i,j = 1,2,\ldots,6)$ denote the stress and strain components, respectively, in which

$$S_j = \begin{cases} S_{pr} \text{ for } p = r, j = 1,2,3 \\ 2S_{pr} \text{ for } p \neq r, j = 4,5,6 \end{cases} \tag{11}$$

Moreover, $C_{ij}^{\mathcal{E}}$, e_{ki} and $\epsilon_{k\ell}^{S}$ are the elastic (measured under constant electric field), piezoelectric and dielectric constants (measured under constant strain), while $\mathcal{E}_k$ and $D_k (k = 1,2,3)$ denote the electric field intensity and electric displacement vector, respectively. Summation over repeated indices is implied in Eqs. (10). Equations (10a) and (10b) describe the *converse* and *direct* piezoelectric effects, respectively.

In piezoelectric adaptive structures, the direct effect is used for sensing and the converse effect is used to generate control forces. Equations (10) are valid for the most general anisotropic case, i.e., for triclinic crystals. In the following, the piezoelectric anisotropy is restricted to the case of hexagonal symmetry, the n-axis being an axis of rotary symmetry

coinciding with the direction of polarization[11] (thickness polarization). In this case, the piezoelectric continuum is characterized by a reduced number of elastic piezoelectric and dielectric coefficients. We also assume that the electric field vector $\mathcal{E}_\ell$ is defined by the component $\mathcal{E}_3$ only, $\mathcal{E}_1 = \mathcal{E}_2 = 0$, and that the electric field intensity $\mathcal{E}_3$ is uniform over the entire area. Due to the fact that the voltage is distributed uniformly, we assume that in the static case $\mathcal{E}_3$ is constant while in the dynamic case it depends on time alone. The piezoelectric actuators are distributed over the entire span and their distribution in the circumferential and transversal directions is defined by

$$R_k(n) = H\left(n - n_{(k-)}\right) - H\left(n - n_{(k+)}\right) \tag{12a}$$

$$R_k(s) = H\left(s - s_{(k-)}\right) - H\left(s - s_{(k+)}\right) \tag{12b}$$

in which H denotes the Heaviside unit step function. It is assumed that the host structure and the actuator consist of $\mathcal{r}$ layers exhibiting general-type orthotropy, and, respectively of p piezoelectric layers exhibiting hexagonal symmetry.

Before we derive the global one-dimensional constitutive equations for adaptive wing structures, it will prove convenient to derive their two-dimensional counterparts. Integrating the actual three-dimensional constitutive equations over the wall thickness and assuming that the hoop stress-resultant N_{ss} is negligibly small when compared with the remaining stresses, the two-dimensional constitutive equations are

$$\begin{bmatrix} N_{zz} \\ N_{sz} \end{bmatrix} = \begin{bmatrix} K_{11} & K_{12} & K_{13} & K_{14} \\ K_{21} & K_{22} & K_{23} & K_{24} \end{bmatrix} \begin{bmatrix} \bar{S}_{zz} \\ \tilde{S}_{sz} \\ \phi' \\ \bar{\bar{S}}_{zz} \end{bmatrix} - \begin{bmatrix} N^a_{zz} \\ 0 \end{bmatrix} \tag{13}$$

$$N_{zn} = A_{44} S_{zn} \tag{14}$$

$$\begin{bmatrix} L_{zz} \\ L_{sz} \end{bmatrix} = \begin{bmatrix} K_{41} & K_{42} & K_{43} & K_{44} \\ K_{51} & K_{52} & K_{53} & K_{54} \end{bmatrix} \begin{bmatrix} \bar{S}_{zz} \\ \tilde{S}_{sz} \\ \phi' \\ \bar{\bar{S}}_{zz} \end{bmatrix} - \begin{bmatrix} L^a_{zz} \\ 0 \end{bmatrix} \tag{15}$$

where N_{zz} and N_{sz} denote tangential stress resultants, N_{zn} denotes the transverse shear stress resultant and L_{zz} and L_{sz} denote the stress couples, all quantities depending on s, z and t. Moreover, K_{ij} denote the modified local stiffness coefficients, listed in the Appendix, and N^a_{zz} and L^a_{zz} denote the piezoelectrically induced-stress resultant and stress couple, respectively, expressed as

$$N^a_{zz}(s,t) = \left(1 - \frac{A_{12}}{A_{11}}\right) \sum_{k=1}^{\ell} \mathcal{E}_3^{(k)}(t) \left(n_{(k+)} - n_{(k-)}\right) e_{31}^{(k)} R_{(k)}(s) \tag{16a}$$

$$L^a_{zz}(s,t) = \sum_{k=1}^{\ell} \mathcal{E}_3^{(k)}(t) R_{(k)}(s) \left(n_{(k+)} - n_{(k-)}\right) e_{31}^{(k)} \left[\underline{\frac{1}{2}\left(n_{(k+)} + n_{(k-)}\right)} - \frac{B_{12}}{A_{11}}\right] \tag{16b}$$

where, in the case of symmetrically located piezoactuators, the term underscored vanishes.

4. The Equations of Motion for Adaptive Wing Structures

From Ref. 5, the one-dimensional stress-resultants and stress couples are given by

$$T_z(z,t) = \oint N_{zz} ds, \; Q_x(z,t) = \oint (-N_{sz} m + N_{zn} \ell)\, ds \tag{17a,b}$$

$$Q_y(z,t) = \oint (N_{sz} \ell + N_{zn} m)\, ds, \; M_x(z,t) = \oint (y N_{zz} + L_{zz} m)\, ds \tag{17c,d}$$

$$M_y(z,t) = \oint (x N_{zz} + L_{zz} \ell)\, ds, \; M_z(z,t) = \oint N_{sz} \frac{2A_C}{\beta} ds \tag{17e,f}$$

and

$$B_\omega(z,t) = \oint [F_\omega(s) N_{zz} + a(s) L_{zz}]\, ds \tag{17g}$$

where T_z is the axial force, Q_x and Q_y are shear forces, M_x, M_y and M_z are the bending and twist moments, respectively, while B_ω is a bimoment global quantity. In view of Eqs. (13) and (15), the stress quantities T_z, M_x, M_y and B_ω can be cast in the more convenient form

$$T_z = \hat{T}_z - \hat{\hat{T}}_z, \; M_x = \hat{M}_x - \hat{\hat{M}}_x, \; M_y = \hat{M}_y - \hat{\hat{M}}_y, \; B_\omega = \hat{B}_\omega - \hat{\hat{B}}_\omega \tag{18a-d}$$

where single and double overcarets identify purely mechanical and piezoelectrically induced terms, respectively. The latter terms are

$$\hat{\hat{T}}_z = \oint \sum_{k=1}^{\ell} \mathcal{E}_3^{(k)} R_{(k)}(s) \left(n_{(k+)} - n_{(k-)}\right) e_{31}^{(k)} \left[\underline{\frac{1}{2}\left(n_{(k+)} + n_{(k-)}\right)} - \frac{B_{12}}{A_{11}}\right] ds \tag{19a}$$

$$\hat{\hat{M}}_x = \oint \sum_{k=1}^{\ell} \mathcal{E}_3^{(k)} \left(n_{(k+)} - n_{(k-)}\right) e_{31}^{(k)} R_{(k)}(s) \left[y\left(1 - \frac{A_{12}}{A_{11}}\right) - m\frac{B_{12}}{A_{11}}\right] ds$$
$$+ \frac{1}{2}\oint \underline{\left[m \sum_{k=1}^{\ell} \mathcal{E}_3^{(k)} \left(n_{(k+)}^2 - n_{(k-)}^2\right) e_{31}^{(k)} R_{(k)}(s)\right] ds} \tag{19b}$$

$$\hat{\hat{M}}_y = \oint \sum_{k=1}^{\ell} \mathcal{E}_3^{(k)} \left(n_{(k+)} - n_{(k-)}\right) e_{31}^{(k)} R_{(k)}(s) \left[x\left(1 - \frac{A_{12}}{A_{11}}\right) + \ell\frac{B_{12}}{A_{11}}\right] ds$$
$$+ \frac{1}{2}\oint \underline{\left[\ell \sum_{k=1}^{\ell} \mathcal{E}_3^{(k)} \left(n_{(k+)}^2 - n_{(k-)}^2\right) e_{31}^{(k)} R_{(k)}(s)\right] ds} \tag{19c}$$

$$\hat{\hat{B}}_\omega = \oint \sum_{k=1}^{\ell} \mathcal{E}_3^{(k)} \left(n_{(k+)} - n_{(k-)}\right) e_{31}^{(k)} R_{(k)}(s) \left[F_\omega\left(1 - \frac{A_{12}}{A_{11}}\right) - a(s)\frac{B_{12}}{A_{11}}\right] ds$$
$$+ \frac{1}{2}\oint \underline{\left[a(s) \sum_{k=1}^{\ell} \mathcal{E}_3^{(k)} \left(n_{(k+)}^2 - n_{(k-)}^2\right) e_{31}^{(k)} R_{(k)}(s)\right] ds} \tag{19d}$$

It is readily seen from Eqs. (19*a-d*) that the piezoelectrically induced stress resultants are proportional to the injected electric current $\mathcal{E}_3$. In the case of actuators placed symmetrically throughout the thickness of the beam, the underlined terms in Eqs. (19) vanish.

One reason for employing advanced composite materials in flight vehicle design lies in the fact that they permit the use of specific lay-up and fiber orientations so as to induce preferred elastic couplings having enhanced effects on the response characteristics. As studies on vibration and subcritical/critical aeroelastic behavior of wing structures reveal,[1,18,19] the bending-twist coupling plays a major role. Additional beneficial effects of this cross coupling have been discussed recently in Ref. 20. In the case of wing structures modeled as thin-walled beams, the ply-configuration inducing such an elastic coupling is referred to in Refs. 12 as the *circumferentially antisymmetric stiffness* configuration and in Ref. 13 as the *symmetric configuration.* The associated ply-angle distribution is governed by the law (see Fig. 3)

$$\theta(y) = -\theta(-y) \tag{20}$$

The resulting equations for adaptive wing structures characterized by the above mentioned ply-angle configuration are:

$$-\underline{a_{66}\phi''''} + a_{73}\theta_x'' - \underline{a_{65}(v_0''' + \theta_x'')} + a_{77}\phi'' + m_z = (b_4 + b_5)\ddot{\phi} - \underline{(b_{10} + b_{18})}\ddot{\phi}'' \tag{21a}$$

$$a_{55}\left(v_o'' + \theta_x'\right) + \underline{a_{56}\phi'''} + p_y = b_1\ddot{v}_o \tag{21b}$$

$$a_{33}\theta_x'' + a_{37}\phi'' \underline{-a_{65}(v_0'' + \theta_x')} - a_{55}\left(v_o' + \theta_x\right) - \underline{a_{56}\phi''} = (b_4 + b_{14})\ddot{\theta}_x \tag{21c}$$

as well as by the boundary conditions at the root ($z = 0$)

$$\phi = 0, \quad \underline{\phi' = 0}\ , \ v_0 = 0, \ \theta_x = 0 \tag{22a-d}$$

and at the tip ($z = L$)

$$-\underline{a_{66}\phi'''} + a_{73}\theta_x' + a_{77}\phi' = -\underline{(b_{10} + b_{18})}\ddot{\phi}', \quad \underline{a_{66}\phi''} + \underline{a_{65}(v_0' + \theta_x)} = 0 \tag{23a, b}$$

$$a_{55}\left(v_o' + \theta_x\right) + \underline{a_{56}\phi''} = 0, \ a_{33}\theta_x' + a_{37}\phi' = \hat{\hat{M}}_x \tag{23c, d}$$

The coefficients appearing in Eqs. (21) and (23) stand for the stiffness and mass quantities and are given in the Appendix. The existence of two bending-twist stiffness coupling terms, namely, $a_{37} = a_{73}$ and $a_{56} = a_{65}$, should be noted. The latter is induced by the warping restraint effect and its influence is in general somewhat less important than that of the former. Their variation with the ply-angle is presented in Fig. 16 of Ref. 5. The singly and doubly dashed underlined terms in Eqs. (21)-(23) are associated with the warping restraint and warping inertia, respectively. Because the piezoactuators are distributed over the entire wing span, derivatives with respect to z of piezoelectrically-induced terms in Eqs. (21) vanish. This explains why their contribution does not appear in the equations of motion; it appears only as a nonhomogeneous term in the boundary conditions.

It should be observed here that for the free vibration problem the transverse load p_y and the twisting moment m_z must be ignored in Eqs. (21) and for the static aeroelastic problem the inertia terms must be omitted from Eqs. (21) and (23). Consistent with strip-theory aerodynamics, the unsteady lift force p_y and torsional aerodynamic moment m_z, both per unit span, can be expressed as

$$p_y(z) = q_n c a_o\left(\phi_o + \phi - v_o' \tan\Lambda\right) - NW/2L$$

$$m_z(z) = q_n c a_o e \left(\phi_o + \phi - v_o' \tan\Lambda\right) + q_n c^2 C_{MAC} - NWd/2L \qquad (24a,b)$$

Here $q_n = \frac{1}{2}\rho U_n^2$ denotes the dynamic pressure normal to the leading edge of the swept wing, c the chord of the wing, a_o the "corrected lift" curve slope coefficient, Λ the angle of sweep (considered positive for swept-back), e the offset between the aerodynamic and reference axis, ϕ_o the rigid angle of attack (measured in planes normal to the leading edge), C_{MAC} the wing section pitching moment coefficient (whose influence, as usual, is disregarded), $W/2L$ the weight per unit length of wing and N the load factor normal to the wing surface, whose expression is

$$N = \frac{2cq_n a_o}{W} \int_o^L \left(\phi_o + \phi - v_o' \tan\Lambda\right) dz \qquad (25)$$

The static aeroelastic response is analyzed both in the subcritical range, i.e., for velocities $q_n < (q_n)_D$, and in the critical case as well, where $(q_n)_D$ denotes the divergence dynamic pressure. As a general remark, Eqs. (24) reveal that for $\Lambda < 0$, i.e., for swept-forward wings, the aeroelastic bending-twist coupling results in an increase in $p_y(z)$ and $m_z(z)$, which in turn results in a deterioration of the subcritical static aeroelastic response and in a dramatic decrease of the divergence speed. Whereas the goal of the subcritical static aeroelastic analysis consists of the determination of the distribution of the effective angle of attack ϕ_{eff} and of the lift force, as affected by the elastic deformations, the study of the critical case involves the determination of divergence instability conditions. Clearly, the main target of tailoring applied to swept-forward wings is to yield a decrease in the effective angle of attack, and implicitly in the aeroelastic lift and, as a result, an increase in the critical divergence speed. Whereas the study of the subcritical static aeroelastic response requires the solution of the integral-differential system of equations obtained by inserting Eqs. (24) and (25) into Eqs. (21), the determination of the divergence speed leads to the solution of an eigenvalue problem, where the divergence speed plays the role of eigenvalue. Structural tailoring applied to the vibration of wing structures must result in an increase in the eigenfrequencies without weight penalties. The determination of natural frequencies

requires the solution of an eigenvalue problem.[21]

In spite of the mathematical complexities involved in the solution of the above mentioned problems, in which the eigenvalue appears both in the differential equations and the boundary conditions, the computational methodologies used proved to be extremely powerful. The spatial Laplace transform method yields exact solutions,[19,22] but is computationally laborious. On the other hand, the extended Galerkin method yields approximate solutions in excellent agreement with the exact ones and with less computational effort.[23]

5. The Control Law and the Closed-Loop Eigenvalues

For feedback control, the applied electric field $\mathcal{E}_3$, upon which the piezoelectrically induced moment depends, is a function of the wing motion. Two simple control laws are being considered. The first control law, denoted by $CL1$, requires that the injected electric field $\mathcal{E}_3$ is proportional to the bending moment $\hat{M}_x(0)$ at the wing root, which implies that

$$\mathcal{E}_3 = G\theta_x'(0) \tag{26}$$

Upon considering the boundary condition (23d), as well as Eq. (19b), the control law given by Eq. (26) can be rewritten as

$$\theta_x'(L) + f_3\phi'(L) - k_p\theta_x'(0) = 0 \tag{27}$$

where $f_3 = a_{37}/a_{33}$ and k_p denotes the feedback gain. This control law expresses the fact that the bending moment at the wing tip induced by piezoelectric strain actuation is proportional to the mechanical bending moment at the wing root. This control law was used in Refs. 14-16. The second control law, denoted by $CL2$, requires that the applied electric field $\mathcal{E}_3$ is proportional to the vertical deflection of the beam tip $v_0(L)$. This results in the condition

$$\theta_x'(L) + f_3\phi'(L) = \overline{k}_p v_0(L) \tag{28}$$

Equation (28) expresses the fact that the boundary moment control at the wing tip, induced by piezoelectric strain actuation, is proportional to the transversal deflection at the wing

tip. Control law (28) is similar to the one proposed in Ref. 24. It should be noticed that the feedback gains k_p and $\overline{k}_p$ are nondimensional and dimensional quantities, respectively. The nondimensional counterpart of $\overline{k}_p$ is $\check{k}_p = \overline{k}_p L^2$.

6. Numerical Examples

The equations derived here are general, in the sense that they are valid for a beam of arbitrary cross section, as well as for piezoelectric actuators arbitrarily located throughout the wall thickness and along the circumference of the beam. However, in the present case a biconvex profile, typical of supersonic wing airplanes, is adopted. It is assumed that the piezoceramic actuators used here are mounted symmetrically on the upper and bottom surfaces of the wing. The host structure is assumed to be of a graphite/epoxy material whose elastic characteristics are

$$E_L = 30\times10^6 \text{ psi}, \; E_T = 0.75\times10^6 \text{ psi}$$

$$G_{LT} = 0.37\times10^6 \text{ psi}, \; G_{TT} = 0.45\times10^6 \text{ psi}$$

$$\mu_{TT} = \mu_{LT} = 0.25, \; \rho = 14.3\times10^{-5} \text{ lbsec}^2/\text{in}^4$$

where the subscripts L and T denote directions parallel and transversal to the fibers, respectively. The geometrical wing characteristics are displayed in Fig. 1 and the piezoelectric actuators are made of PZT-4 ceramic, whose properties are given in Ref. 17.

The associated differential eigenvalue problem has been discretized in space by the extended Galerkin method.[23] The obtained results were checked by means of an exact solution based on a spatial Laplace transform[19,21] and the agreement was excellent.

Tailoring and adaptive control are applied simultaneously to enhance the vibrational characteristics of wing structures. Results are displayed in Figs. 4 and 5 and Figs. 7 and 8 for $CL1$ and $CL2$, respectively. It should be mentioned that for $\theta \neq 0$ and $\theta \neq 90°$ the bending-twist coupling causes the adaptive control to be somewhat weaker in places where the twist is very strong. On the other hand, for $\theta = 0°$ and $90°$, where the bending decouples, the adaptive control becomes very effective. As a general rule, the frequencies were normalized with respect to the ones corresponding to the uncontrolled case $k_p = 0$, and

to on-axes ply angle configuration, $\theta = 0$. The trend in the eigenfrequencies revealed in this paper using $CL2$ agrees fully with one obtained theoretically and verified experimentally.[24] As can be concluded from Figs. 5 and 8, the first eigenfrequency changes gradually with the ply angle from one corresponding to a pure bending mode (labelled as B) at $\theta = 0$ to a coupled bending-twist mode for $0 < \theta < 90°$ to a pure bending mode for $\theta = 90°$. On the other hand, the second eigenfrequency changes from a pure bending mode at $\theta = 0$ to a pure twist mode (labelled as T) for $\theta = 90°$, and the third eigenfrequency changes from pure twist for $\theta = 0$ to pure bending for $\theta = 90°$.

Plots of the first closed-loop mode are shown in Fig. 6 for three values of feedback gains. It is easy to see that the original uncontrolled modes differ considerably from the controlled modes. In Figs. 9a and 9b, the reduced divergence speed parameter $(q_n c a_0)_D$ is displayed as a function of θ for various values of the feedback gain using $CL1$ and for the cases of a straight wing, $\Lambda = 0$, and a swept-forward wing, $\Lambda = -30°$. As readily seen, the use of both tailoring and adaptive control with negative feedback gains result in a significant increase in the divergence speed. In Figs. 10a, 10b and 11, the normalized effective angle of attack ϕ_{eff}/ϕ_o is displayed for nonadaptive wings, $k_p = 0$, and for adaptive wings, $k_p < 0$, respectively . The results reveal that a strong attenuation of aeroelastic loads is experienced for $k_p < 0$, as compared to the case corresponding to $k_p = 0$. As Fig. 11 reveals, as the magnitude of the feedback gain increases, the attenuation becomes more and more pronounced. It should be noted that in the case of $CL2$, improved vibrational characteristics are obtained for positive feedback control gains, $k_p > 0$.

The results demonstrate that the use of both tailoring and adaptive control techniques can yield dramatic improvements in the dynamic and static aeroelastic characteristics of aircraft wings.

7. Summary and Conclusions

A comprehensive structural model of aircraft wing modeled as a thin/thick-walled beam of arbitrary closed cross section, cantilevered aircraft wing structures incorporating adaptive

capabilities via the inverse piezoelectric effect was developed. The anisotropic wing model incorporates a number of nonclassical features characterizing actual wing structures.

The unique directional properties of composite materials permits tailoring, which amounts to enhancing wing structure response, whereas incorporation of piezoactuators permits vibration and static aeroelastic control of the structure. It is demonstrated here that the synergistic combination of tailoring of anisotropic composite materials and control by means of adaptive materials results in a wing with better dynamic and static aeroelastic characteristics than would have resulted from tailoring or control alone. Incorporation of both technologies can provide an expanded performance envelope of flight vehicles, without weight penalties.

8. References

1. Weisshaar, T. A., "Aeroelastic Tailoring - Creative Use of Unusual Materials," AIAA Paper 87-0976, *AIAA/ASME/ASCE/AHS 28th Structures, Structural Dynamics, and Materials Conference*, April 9-10, 1987.
2. Tzou, H. S. and Anderson, G. L. (Eds.), *Intelligent Structural Systems*, Kluwer Academic Publishers, Boston, MA, 1992.
3. Crawley, E.F. and deLuis, T, "Use of Piezoelectric Actuators as Elements of Intelligent Structures," *AIAA Journal*, Vol. 25, No. 10, 1988, pp. 1373-1385.
4. Crawley, E.F., Intelligent Structures for Aerospace: A Technology Overview and Assessment," *AIAA Journal*, Vol. 31, No.8, August 1994, pp. 1689-1699.
5. Librescu, L., Meirovitch, L. and Song, O., "A Refined Structural Model of Composite Aircraft Wings for the Enhancement of Vibrational And Aeroelastic Response Characteristics," AIAA Paper 93-1697, *AIAA/ASME/ASCE/AHS/ASC 34th Structures, Structural Dynamics, and Materials Conference*, April 19-22, 1993, La Jolla, CA.
6. Librescu, L. and Song, 0.,"Behavior of Thin-Walled Beams Made of Advanced Composite Materials and Incorporating Non-Classical Effects," *Applied Mechanics Reviews*, Vol. 44, No. 11, Part 2, November 1991, pp. 174-180.

7. Rehfield, L. W., Atilgan, A. R. and Hodges, D. H., "Nonclassical Behavior of Thin-Walled Composite Beams," *Journal of the American Helicopter Society*, Vol. 35, No. 2, April 1990, pp. 42-50.

8. Chandra, R., Stemple, A. D., and Chopra, I., "Thin-Walled Composite Beams Under Bending, Torsional and Extensional Loads," *Journal of Aircraft*, Vol. 27, No. 7, 1990, pp. 619-626.

9. Lee, C. K., "Piezoelectric Laminates: Theory and Experiments for Distributed Sensors and Actuators," *Intelligent Structural Systems*, pp. 75-167, H.S. Tzou and G.L. Anderson (Eds.), Kluwer Academic Publishers, Boston, MA, 1992.

10. Hagood, N. W., Crawley, E. F., DeLuis J. and Anderson, E. H., "Development of Integrated Components for Control of Intelligent Structures," *First Joint U.S./Japan Conference on Adaptive Structures*, November 13-15, 1990, Maui, Hawaii, U.S.A., Ben K. Wada, J.L. Fanson and N. Miura (Eds.), Technomic Publ. Co., Inc., Lancaster-Basel, 1990, pp. 80-194.

11. Eringen, A. C. and Maugin, G. A., *Electrodynamics of Continua I., Foundations and Solid Media*, Springer-Verlag, New York Inc., 1990.

12. Rehfield, L. W. and Atilgan, A. R., "Toward Understanding the Tailoring Mechanisms for Thin-Walled Composite Tubular Beams," *Proceedings of the First USSR-U.S. Symposium on Mechanics of Composite Materials*, 23-26 May, 1989, Riga, Latvia SSR, S. W. Tsai, J. M. Whitney, T-W Chou and R. M. Jones (Eds.), ASME Publ. House, pp. 187-196.

13. Smith, E. C. and Chopra, I., "Formulation and Evaluation of an Analytical Model for Composite Box-Beams," *Journal of the American Helicopter Society*, Vol. 36, 1991, pp. 23-35.

14. Song, O., Librescu, L. and Rogers, C. A., "Vibrational Behavior of Adaptive Aircraft Wing Structures Modelled as Composite Thin-Walled Beams," *Ninth DoD/ NASA/ FAA Conference on Fibrous Composites in Structural Design*, November 1991, Lake Tahoe, Nevada.

15. Ehlers, S. M. and Weisshaar, T. A., "Static Aeroelastic Behavior of an Adaptive Laminated Piezoelectric Composite Wing", *Proceedings of the 31st AIAA/ASME/ASCE/AHS Structures, Structural Dynamics and Materials Conference*, Long Beach, CA, 1990, pp. 1611-1623.

16. Weisshaar, T. A. and Ehlers, S. M., "Adaptive Aeroelastic Composite Wings - Control and Optimization Issues, *Composites Engineering*, Vol. 2, Nos. 5-7, 1992, pp. 457-476.

17. Berlincourt, D. A., Curran, D. R., and Jaffe, H., "Piezoelectric and Piezomagnetic Materials and Their Function in Transducers," *Physical Acoustics - Principles and Methods*, (Eds. W. P. Mason), Vol. 1, Part A, Academic Press, New York, 1964, pp. 169-270.

18. Librescu, L. and Simovich, J., "General Formulation for the Aeroelastic Divergence of Composite Swept Forward Wing Structures," *Journal of Aircraft*, Vol. 25, No. 4, April 1988, pp. 364-371.

19. Librescu, L., and Thangjitham, S., "Analytical Studies on Static Aeroelastic Behavior of Forward-Swept Composite Wing Structures," *Journal of Aircraft*, Vol. 28, No. 2, 1991, pp. 151-157.

20. Garfinkle, M., "Twisting Smartly in the Wind", *Aerospace America*, July 1994, pp. 18-20.

21. Meirovitch, L., *Computational Methods in Structural Dynamics*, Sijthoff & Noordhoff International Publishers, The Netherlands, 1980.

22. Karpouzian, G. and Librescu, L., "A Comprehensive Model for Anisotropic Composite Aircraft Wings Suitable for Aeroelastic Analyses," *Journal of Aircraft*, Vol. 31, No. 3, May-June 1994, pp. 703-712.

23. Palazotto, A.N. and Linnemann, P.E., "Vibration and Buckling Characteristics of Composite Cylindrical Panels Incorporating the Effects of a Higher Order Shear Theory," *International Journal of Solids and Structures*, Vol. 28, No. 3, pp. 341-361, 1991.

24. Tzou, H.S. and Zhong, J.P., "Adaptive Piezoelectric Structures: Theory and Experiment," *Active Materials and Adaptive Structures, Proceedings of the ADPA/AIAA/ASME/SPIE Conference on Active Materials and Adaptive Structures*, Ed. G. J. Knowles, 4-8 November 1991, Alexandria, VA, pp. 719-724.

Appendix

The modified local stiffness coefficients are

$$K_{11} = A_{22} - \frac{A_{12}^2}{A_{11}},\ K_{12} = A_{26} - \frac{A_{12}A_{16}}{A_{11}} = K_{21},\ K_{13} = 2K_{12}\frac{A_c}{\beta} \qquad (A1\text{-}3)$$

$$K_{14} = B_{22} - \frac{A_{12}B_{12}}{A_{11}} = K_{41},\ K_{22} = A_{66} - \frac{A_{16}^2}{A_{11}},\ K_{23} = 2K_{22}\frac{A_c}{\beta} \qquad (A4\text{-}6)$$

$$K_{24} = B_{26} - \frac{A_{16}B_{12}}{A_{11}} = K_{42},\ K_{43} = 2K_{24}\frac{A_c}{\beta},\ K_{44} = D_{22} - \frac{B_{12}^2}{A_{11}} \qquad (A7\text{-}9)$$

$$K_{51} = B_{26} - \frac{B_{16}A_{12}}{A_{11}},\ K_{52} = B_{66} - \frac{B_{16}A_{16}}{A_{11}},\ K_{53} = 2K_{52}\frac{A_c}{\beta},\ K_{54} = D_{26} - \frac{B_{12}B_{16}}{A_{11}} \qquad (A10\text{-}13)$$

where A_{ij}, B_i, and D_{ij} denote, respectively, the stretching, bending-stretching and bending stiffness quantities associated with the entire structure, where the structure consists of $N = \boldsymbol{r} + p$ host and piezoactuator layers.

The stiffness and mass coefficients have the form

$$a_{11} = \oint K_{11}ds,\ a_{14} = a_{41} = -\oint K_{12}mds,\ a_{22} = \oint \left(K_{11}^2 + 2xK_{14}\ell + K_{44}\ell^2\right)ds \qquad (A14\text{-}16)$$

$$a_{33} = \oint \left(K_{11}y^2 + 2yK_{14}m + K_{44}m^2\right)ds,\ a_{37} = a_{73} = \oint \left(yK_{13} + K_{43}m\right)ds \qquad (A17,18)$$

$$a_{44} = \oint \left(K_{22}m^2 + A_{44}\ell^2\right)ds,\ a_{55} = \oint \left(K_{22}\ell^2 + A_{44}m^2\right)ds \qquad (A19,20)$$

$$a_{56} = a_{65} = -\oint \left(F_\omega K_{21}\ell + K_{24}a\ell\right)ds \qquad (A21)$$

$$a_{66} = \oint \left(K_{11}F_\omega^2 + 2K_{14}F_\omega a + K_{44}a^2\right)ds,\ a_{77} = \oint 2\frac{A_c}{\beta}K_{23}ds \qquad (A22,23)$$

$$(b_1, b_4, b_5, b_{10}) = \oint m_0\left(1,\ y^2,\ x^2,\ F_\omega^2,\right)\ ds,\ (b_{14}, b_{15}, b_{18}) = \oint m_2\left(m^2, \ell^2, a^2\right)ds \qquad (A24,25)$$

where

$$(m_0, m_2) = \sum_{k=1}^{N}\int_{h_{(k-1)}}^{h_{(k)}} \rho_{(k)}\left(1, n^2\right)dn \qquad (A26)$$

FIGURE CAPTIONS

Fig. 1- The Thin-Walled Cantilever Beam

Fig. 2- Displacement Field and Coordinate Systems

Fig. 3- Circumferentially Antisymmetric Stiffness Configuration, $\theta(y) = -\theta(-y)$

Fig. 4- First Normalized Eigenfrequency ($\overline{\omega}_1 = \omega_1/\omega_N$) Versus the Feedback Gain Using $CL1$ for Various Ply Angles
($\omega_N = 44$ rad/s, corresponding to $k_p = 0$ and $\theta = 0$)

Fig. 5- Three Normalized Bending-Twist Coupled Eigenfrequencies ($\overline{\omega}_i = \omega_i/\omega_N$) Versus the Ply Angle for No Control and One Feedback Gain Using $CL1$
($\omega_N = 44$ rad/s, corresponding to $k_p = 0$ and $\theta = 0$)

Fig. 6- First Normalized Mode for Three Feedback Gains Using $CL1$; $\theta = 0$

Fig. 7- First Normalized Coupled Eigenfrequency ($\overline{\omega}_1 = \omega_1/\omega_N$) versus Feedback Gain Using $CL2$ for Several Values of θ; $\omega_N = 44$ rad/s

Fig. 8- Three Normalized Coupled Eigenfrequencies ($\overline{\omega}_i = \omega_i/\omega_N$) for Various Ply Angles and No Control and One Feedback Gain Using $CL2$; $\omega_N = 44$ rad/s

Fig. 9a- The Divergence Speed Parameter Versus the Ply Angle for No Control and One Feedback Gain Using $CL1$; $\Lambda = 0$

Fig. 9b- The Divergence Speed Parameter Versus the Ply Angle for No Control and One Feedback Gain Using $CL1$; $\Lambda = -30°$

Fig. 10a- The Normalized Effective Angle of Attack as a Function of the Position Along the Wing Span for Three Sweep Angles; $k_p = 0$, $\theta = 45°$, $135°$ $\left(q_{\text{flight}} = 2\text{psi}\right)$

Fig. 10b- The Normalized Effective Angle of Attack as a Function of the Position Along the Wing Span for Three Sweep Angles Using $CL1$; $k_p = 0.25$, $\theta = 45°$, $135°$ $\left(q_{\text{flight}} = 2\text{psi}\right)$

Fig. 11- The Normalized Effective Angle of Attack as a Function of the Position Along the Wing Span for Various Feedback Gains Using $CL1$; $\Lambda = -15°$, $\theta = 45°$ $\left(q_{\text{flight}} = 2\text{psi}\right)$

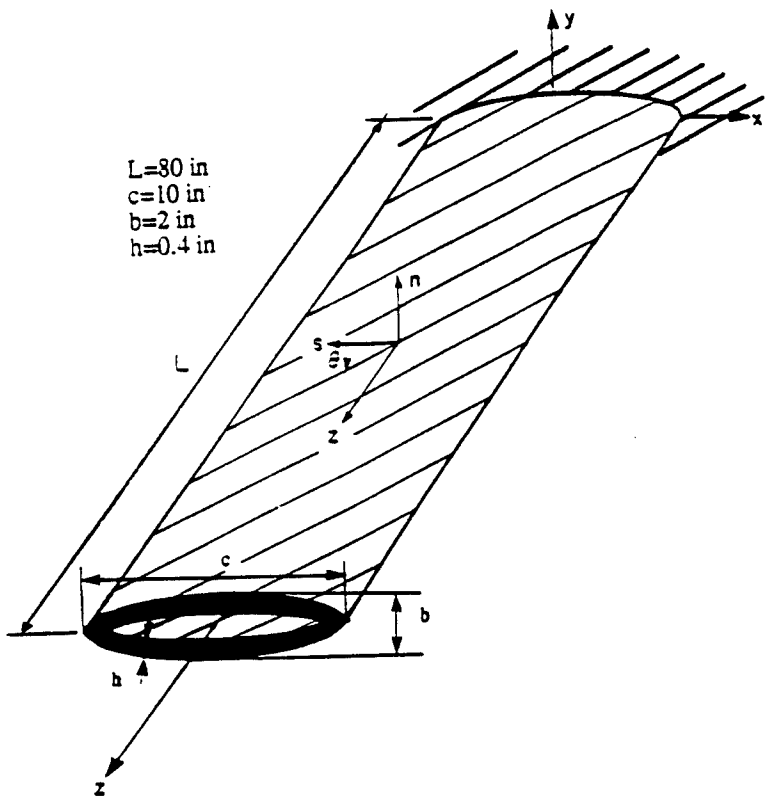

Fig. 1- The Thin-Walled Cantilever Beam

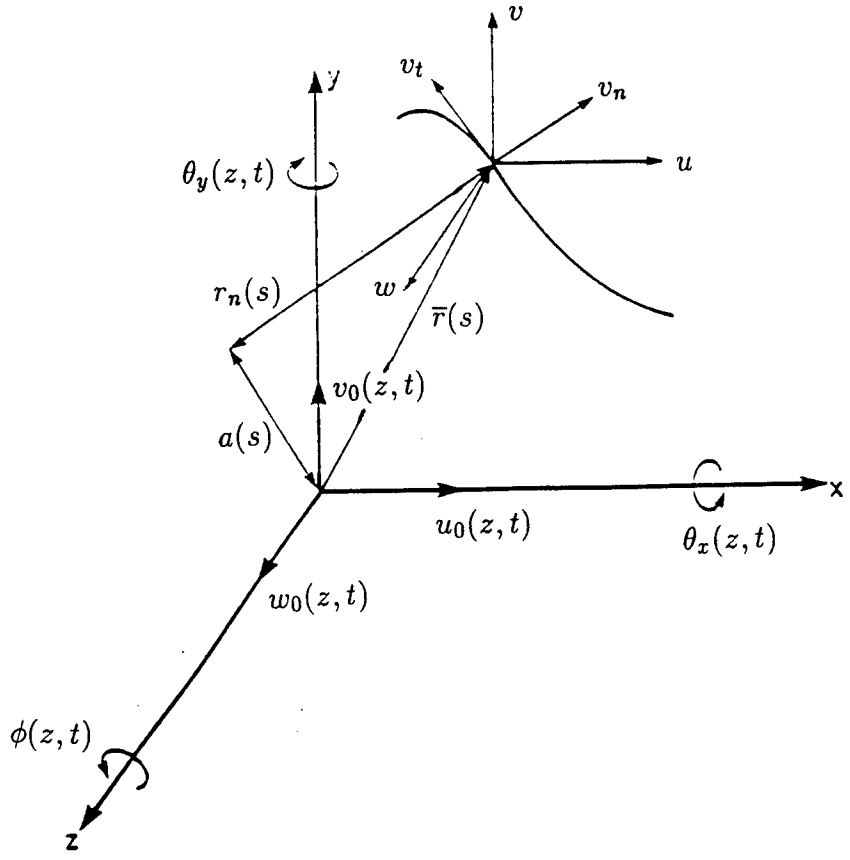

Fig. 2- Displacement Field and Coordinate Systems

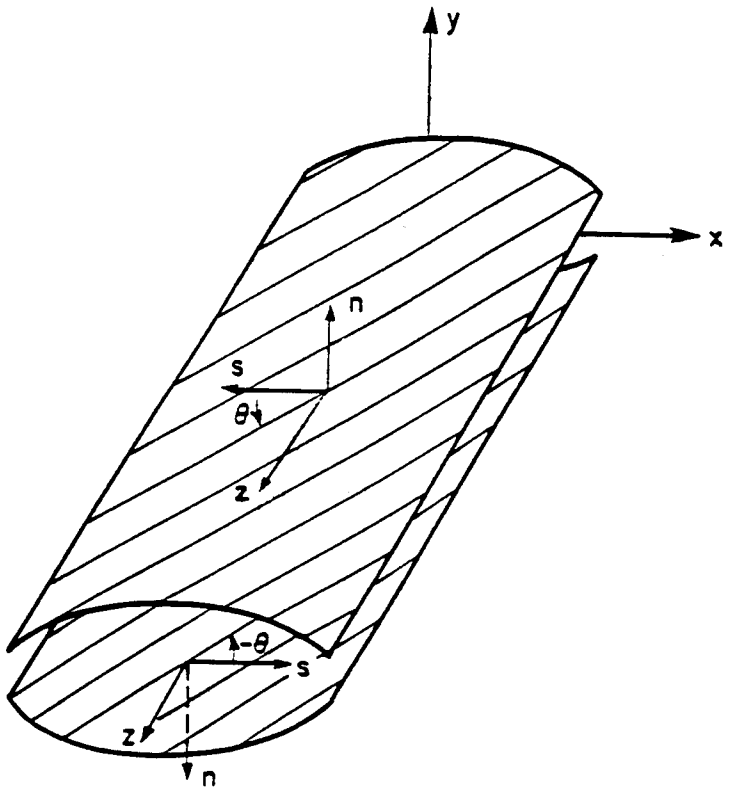

Fig. 3 - Circumferentially Antisymmetric Stiffness Configuration, $\theta(y) = -\theta(-y)$

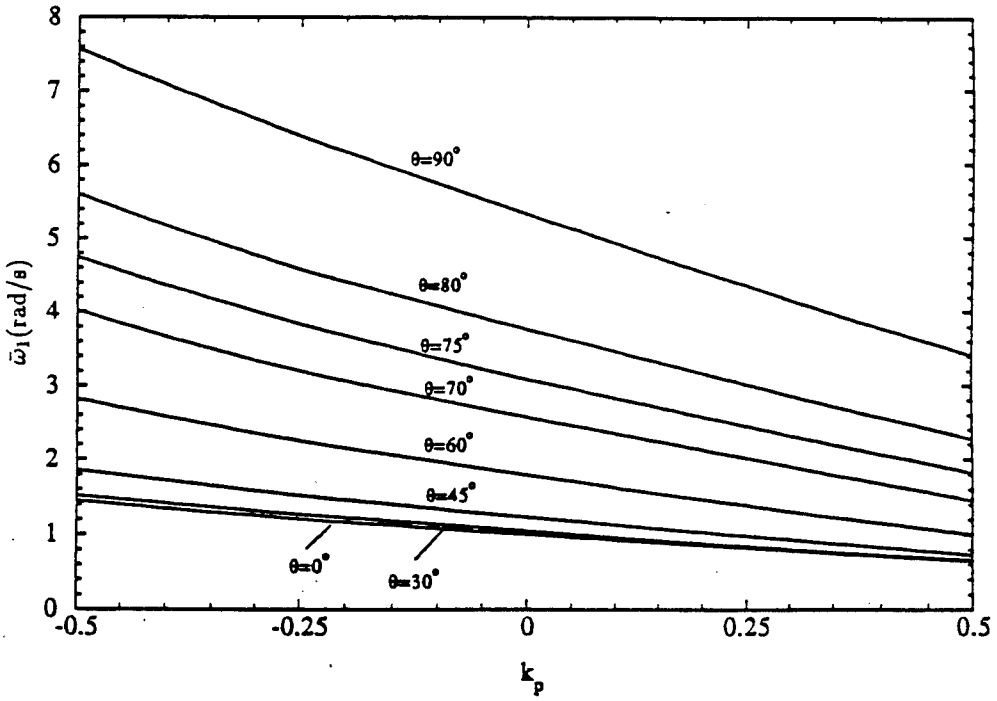

Fig. 4- First Normalized Eigenfrequency ($\overline{\omega}_1 = \omega_1/\omega_N$) Versus the Feedback Gain Using $CL1$ for Various Ply Angles
($\omega_N = 44$ rad/s, corresponding to $k_p = 0$ and $\theta = 0$)

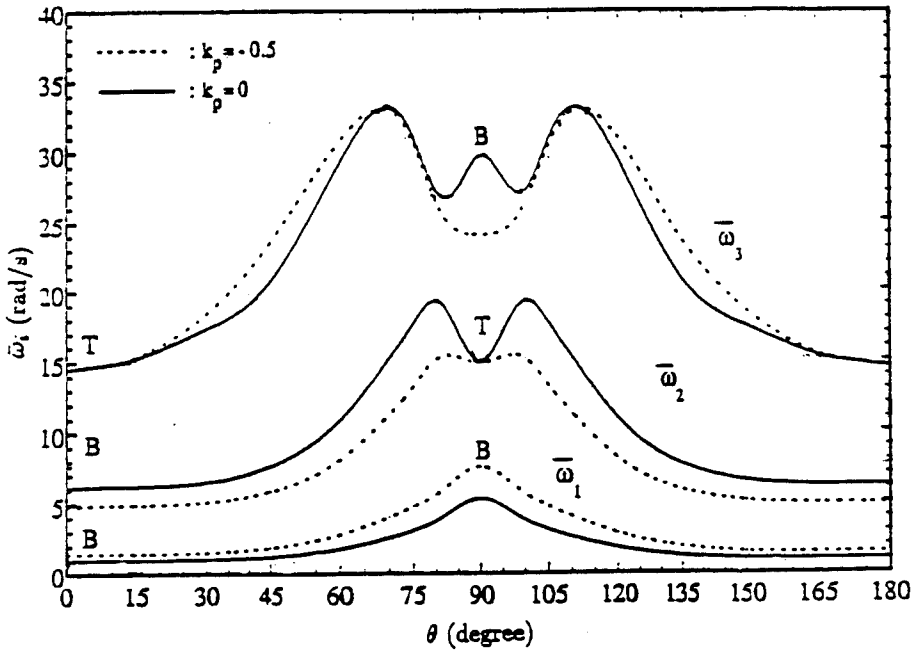

Fig. 5- Three Normalized Bending-Twist Coupled Eigenfrequencies ($\overline{\omega}_i = \omega_i/\omega_N$) Versus the Ply Angle for No Control and One Feedback Gain Using $CL1$ ($\omega_N = 44$ rad/s, corresponding to $k_p = 0$ and $\theta = 0$)

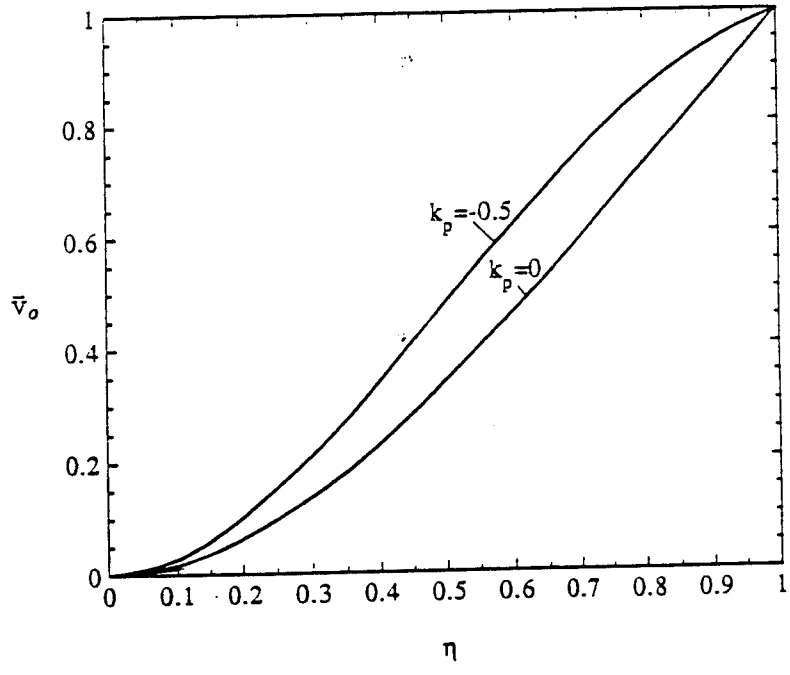

Fig. 6- First Normalized Mode for Three Feedback Gains Using $CL1$; $\theta = 0$

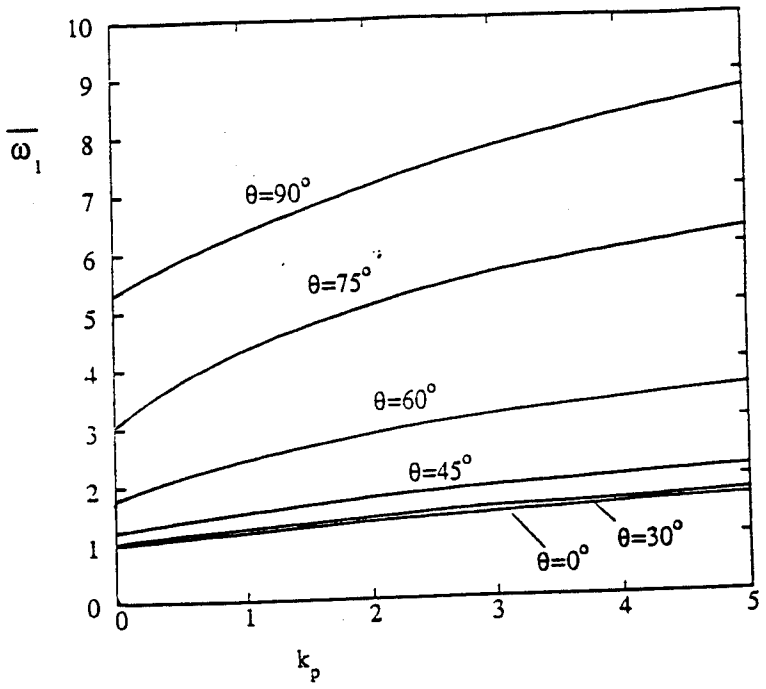

Fig. 7- First Normalized Coupled Eigenfrequency ($\overline{\omega}_1 = \omega_1/\omega_N$) versus Feedback Gain Using $CL2$ for Several Values of θ; $\omega_N = 44$ rad/s

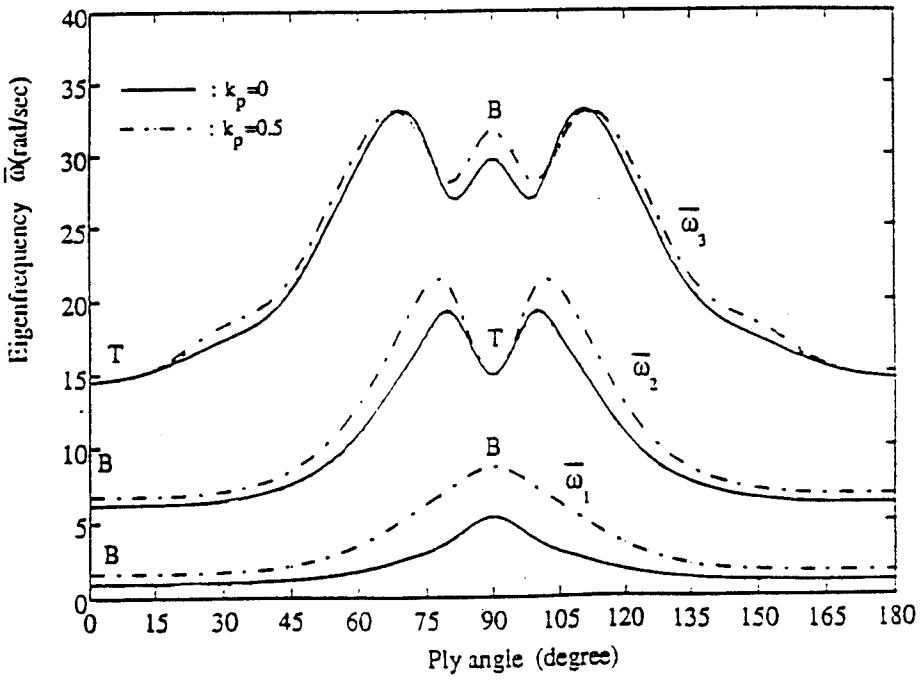

Fig. 8- Three Normalized Coupled Eigenfrequencies ($\overline{\omega}_i = \omega_i/\omega_N$) for Various Ply Angles and No Control and One Feedback Gain Using $CL2$; $\omega_N = 44$ rad/s

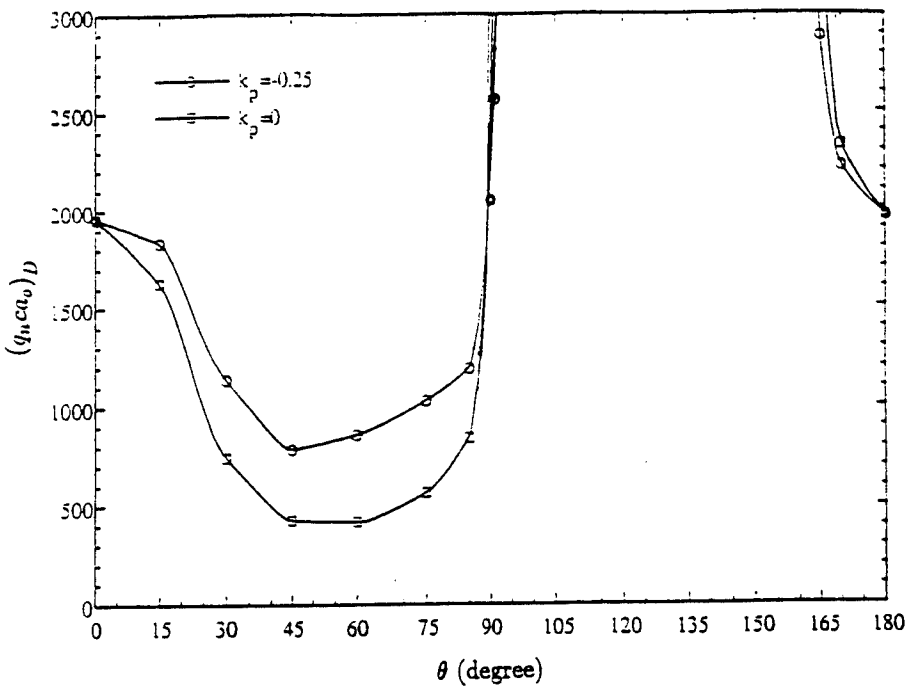

Fig. 9a- The Divergence Speed Parameter Versus the Ply Angle for No Control and One Feedback Gain Using $CL1$; $\Lambda = 0$

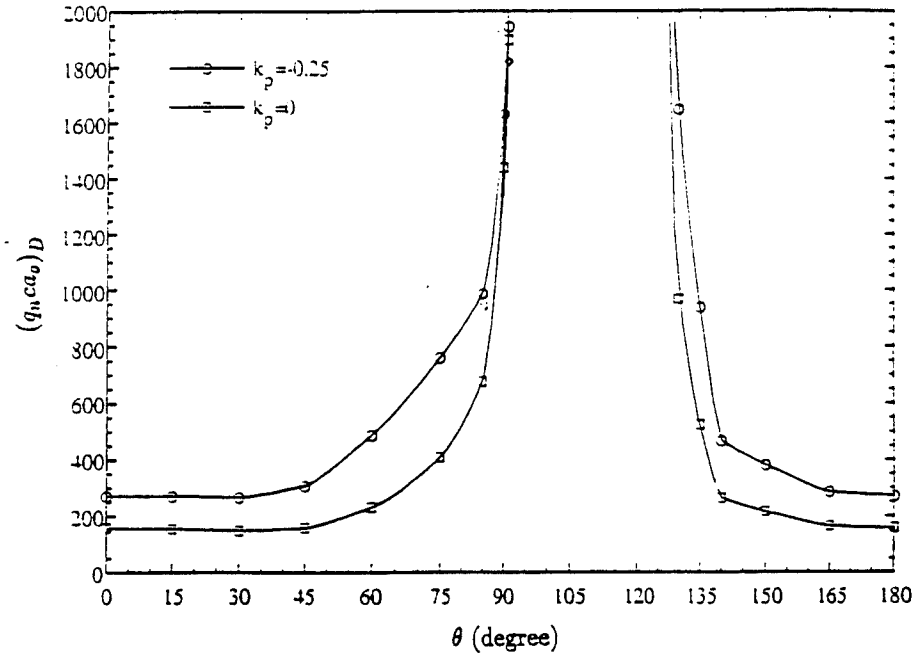

Fig. 9b- The Divergence Speed Parameter Versus the Ply Angle for No Control and One Feedback Gain Using $CL1$; $\Lambda = -30°$

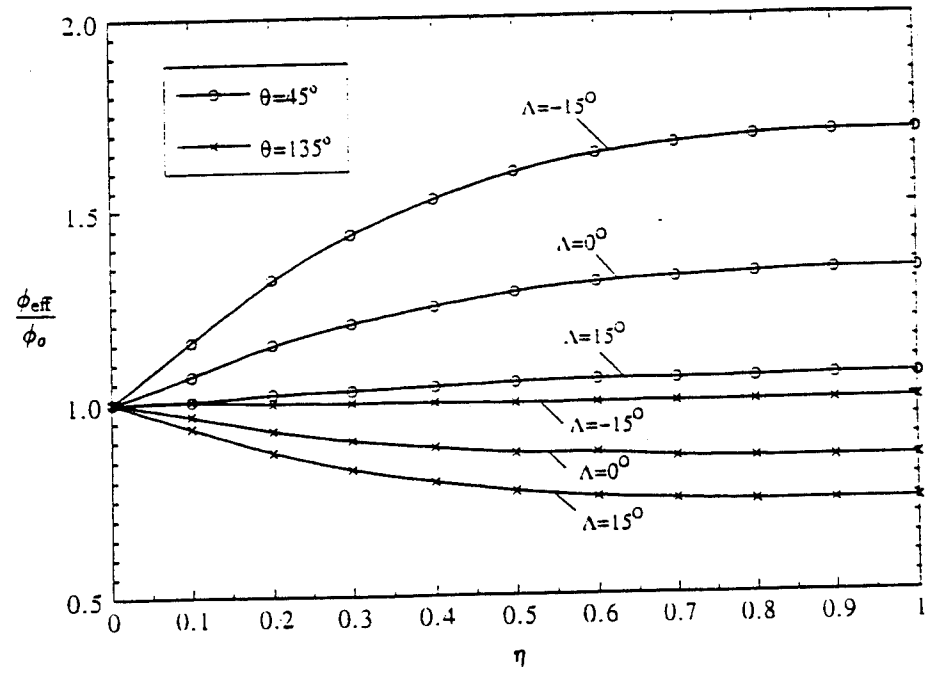

Fig. 10a- The Normalized Effective Angle of Attack as a Function of the Position Along the Wing Span for Three Sweep Angles; $k_p = 0$, $\theta = 45°$, $135°$ $\left(q_{\text{flight}} = 2\text{psi}\right)$

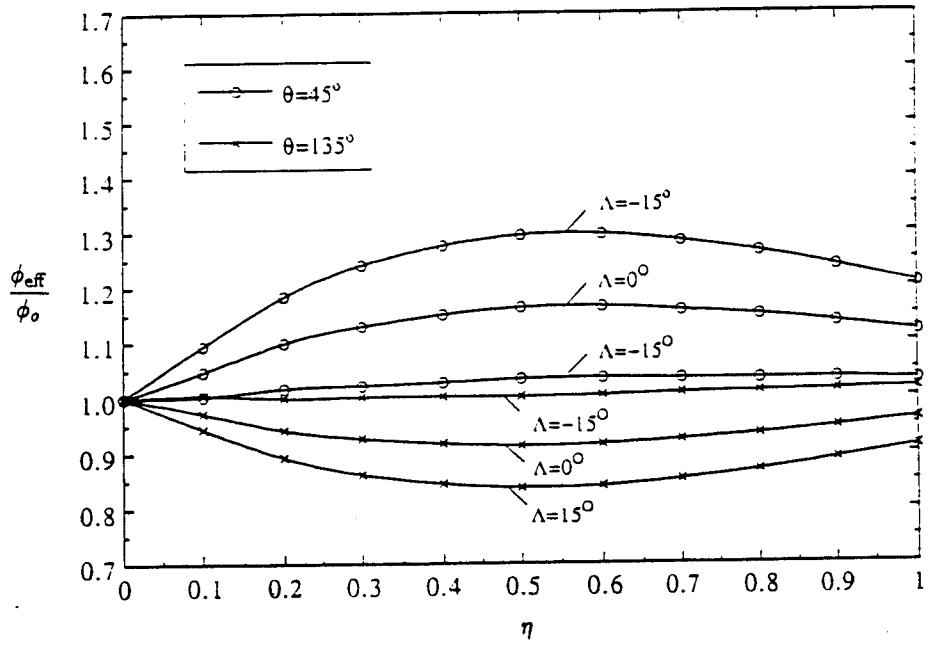

Fig. 10b- The Normalized Effective Angle of Attack as a Function of the Position Along the Wing Span for Three Sweep Angles Using $CL1$; $k_p = 0.25$, $\theta = 45°$, $135°$ $\left(q_{\text{flight}} = 2\text{psi}\right)$

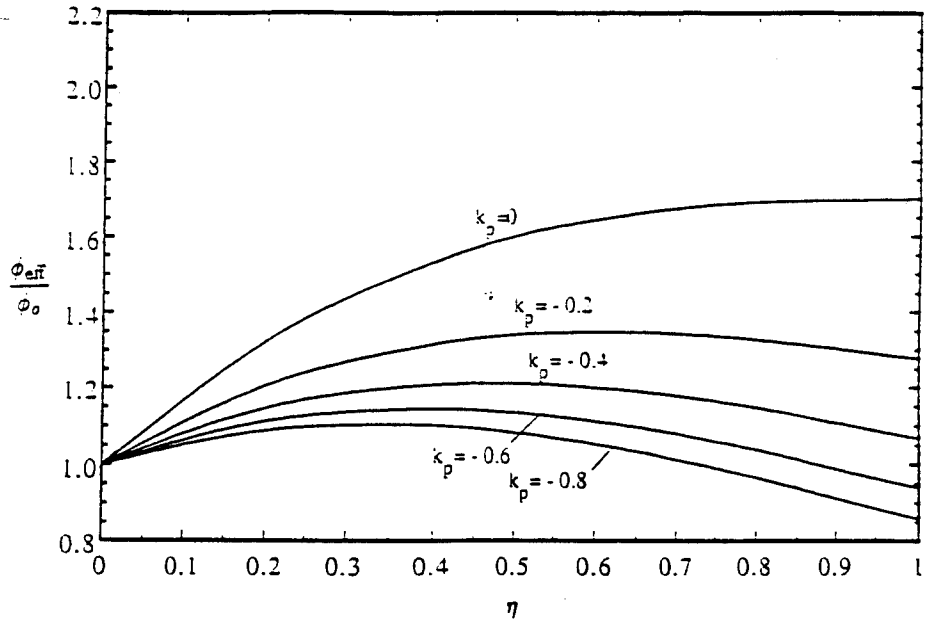

Fig. 11- The Normalized Effective Angle of Attack as a Function of the Position Along the Wing Span for Various Feedback Gains Using $CL1$; $\Lambda = -15°$, $\theta = 45°$ $\left(q_{\text{flight}} = 2\text{psi}\right)$

STRUCTURAL MODELING OF LOW-ASPECT RATIO COMPOSITE WINGS*

L. Meirovitch[1] and T. J. Seitz[2]
Department of Engineering Science and Mechanics
Virginia Polytechnic Institute and State University
Blacksburg, VA 24061

SUMMARY

This paper is concerned with the aeroelastic tailoring of a structural model consisting of a rigid fuselage and a low-aspect ratio wing made of composite materials. The wing is modeled as a trapezoidal plate with root and tip chords parallel to the flow and with general sweep. The fuselage is capable of plunge and pitch and the elastic wing model includes shear deformations but ignores rotatory inertia.

1. INTRODUCTION

Recently, and particularly in the past decade, solutions to the flutter problem based on anisotropic wings made of composite materials have been presented by many authors. Much of this work refined the concept of "composite tailoring" first put forth by Krone[1]. During the same time frame, many researchers have come to the conclusion that the divergence problem associated with forward swept wings is in fact a body-freedom flutter phenomenon. Body-freedom flutter is the coupling of a flexible aircraft mode with a rigid-body mode due to interaction with aerodynamic loads. One common example of this, and the one receiving attention here, is the coupling of flexible wing bending and rigid-body pitch. Work by Weisshaar et al.[2] leads to the conclusion that a clamped wing model generally predicts larger improvements in the instability speed for composite tailoring than for models that include rigid body motions. An accurate prediction of the critical speed in the presence

* Supported by the AFOSR Research Grant 91-0351 monitored by Dr. Spencer T. Wu. The support is greatly appreciated.

[1] University Distinguished Professor. Fellow AIAA.

[2] Graduate Research Assistant. Currently Senior Engineer, Cessna Aircraft Company, Wichita, Kansas 67215. Senior Member AIAA.

of structural parameter variations must be a part of any structural model aiming to model general planforms accurately.

The requirements of modern wing planforms place additional constraints on structural models. In particular, many wings of practical interest are of too low an aspect ratio to be approximated by a beam model. Similarly, the sweep angle should not be confined to aft only, particularly for an optimization problem. Two-dimensional models capable of accepting fiber directional information is suggested in this case, but examples of such models in the literature concerned with this application are rare[3,4].

The structural model suggested by the above physical requirements is a two-dimensional anisotropic plate consisting of several variable thickness layers of generally orthotropic material. Because the interest lies in composite materials, it is also important to include shear deformability in the model. Fuselage rigid-body degrees of freedom must also be included. Two compromises on generality contribute to the goal of low computational effort without significantly affecting the desire to include all the relevant physical effects. Realistic amounts of airfoil camber have little effect on displacements from unsteady pressure loading, suggesting that camber may be omitted for aeroelastic problems. Similarly, the conclusion that rotatory inertia terms for wings of practical thickness can be ignored is supported by the text by Librescu[5].

The interest lies in a structural model that includes the essential physical characteristics required for flutter analysis of modern low-aspect ratio composite wings. The model should be sufficiently accurate to account for all important structural parameters and yet sufficiently simple so as not to be computationally intensive. From the foregoing considerations, a structural model satisfying the imposed requirements has emerged. The model is a trapezoidal plate with root and tip chords parallel to the flow. There are 2k symmetrically stacked, variable thickness, generally orthotropic laminae in the laminate (Figs. 1 and 2). Mindlin shear deformability[6] is included with a shear correction factor of 1.0. The wing is attached to a rigid fuselage capable of pitch and plunge. This is the simplest model retaining the

essential physical characteristics of low-aspect ratio composite wings with general sweep. It is still an involved formulation, including three displacement variables and natural boundary conditions complicated by the sweep angles. To produce a reasonably accurate solution with as few terms as possible, the series solution is in terms of quasi-comparison functions, which guarantees fast convergence[7].

2. DEFINITION OF DISPLACEMENTS AND BOUNDARY CONDITIONS

The mathematical model under consideration consists of a rigid fuselage attached to a flexible wing. The fuselage is assumed to undergo two rigid-body displacements, namely, plunge and pitch. On the other hand, the wing is assumed to act as an elastic plate clamped at the root and free at the the other three boundaries (Fig. 1). The transverse displacement of a typical point in the fuselage has the form

$$w_f(t) = w_C(t) + (x - x_C)\psi_C(t) \tag{1a}$$

where $w_C(t)$ is the plunge, defined as the transverse displacement of the system (fuselage and wing) mass center C and ψ_C is the pitch, defined as the rotation of the system about an axis parallel to y and passing through C, and x_C is the distance from the origin of xyz to point C. Moreover, the displacements of a typical point in the plate are as follows:

$$u(x,y,z,t) = u_0(x,y,t) + z\psi_x(x,y,t) \tag{1b}$$

$$v(x,y,z,t) = v_0(x,y,t) + z\psi_y(x,y,t) \tag{1c}$$

$$w_p(x,y,t) = w_C(t) + (x - x_C)\psi_C(t) + w(x,y,t) \tag{1d}$$

where u_0 and v_0 are midplane elastic deflections in the x and y directions, respectively, ψ_x and ψ_y are angular displacements of a line normal to the nominal plane of the plate due to elasticity and w is the elastic part of the transverse displacement.

Because the wing is attached to a fuselage assumed to be rigid, $w = 0$, $\psi_x = 0$ and $\psi_y = 0$ along $y = 0$. These are the only geometric boundary conditions of the problem.

3. THE EXTENDED HAMILTON'S PRINCIPLE

The dynamical problem can be formulated by means of the extended Hamilton's principle, which can be written in the form[8]

$$\int_{t_1}^{t_2} \left(\delta T - \delta V + \overline{\delta W}_{nc}\right) dt = 0,\ \delta w_C = \delta \psi_C = \delta w = \delta \psi_x = \delta \psi_y = 0 \quad \text{at} \quad t = t_1, t_2 \tag{2}$$

where T is the kinetic energy, V is the potential energy and $\overline{\delta W}_{nc}$ is the virtual work performed by the nonconservative forces.

The kinetic energy arises from two sources, the motion of fuselage and of the wing, and has the expression

$$\begin{aligned} T =& T_f + T_w = \frac{1}{2}\int \left[\dot{w}_C + (x - x_C)\,\dot{\psi}_C\right]^2 dm_f + \frac{1}{2}\int_0^s \int_{LE}^{TE} m\dot{w}_p^2 dxdy \\ =& \frac{1}{2}\left(M_C \dot{w}_C^2 + I_C \dot{\psi}_C^2\right) + \dot{w}_C \int_0^s \int_{LE}^{TE} m\dot{w} dxdy \\ &+ \dot{\psi}_C \int_0^s \int_{LE}^{TE} m\,(x - x_C)\,\dot{w} dxdy + \frac{1}{2}\int_0^s \int_{LE}^{TE} m\dot{w}^2 dxdy \end{aligned} \tag{3}$$

where M_C is the mass of the system and I_C is the pitch mass moment of inertia of the system about the mass center C.

The potential energy is assumed to be entirely due to the strain energy. In view of the lay-up symmetry, it is reasonable to assume that u_0 and v_0 are zero so that the strain-displacement relations assume the simple form

$$\epsilon_x = z\psi_{x,x}, \quad \epsilon_y = z\psi_{y,y}, \quad \epsilon_z = 0 \tag{4a,b,c}$$

$$\gamma_{yz} = \psi_y + w_{,y},\ \gamma_{xz} = \psi_x + w_{,x},\ \gamma_{xy} = z\,(\psi_{x,y} + \psi_{y,x}) \tag{4d,e,f}$$

where the shear strains are recognized as engineering shear strains. Moreover, the symbols $,x$ and $,y$ in the subscripts denote derivatives with respect to x and y, respectively.

For the jth generally orthotropic layer with principal axes 1 and 2, the constitutive equations take the form

$$\begin{bmatrix} \sigma_1 \\ \sigma_2 \\ \tau_{23} \\ \tau_{13} \\ \tau_{12} \end{bmatrix}^j = [Q]^j \begin{bmatrix} \epsilon_1 \\ \epsilon_2 \\ \gamma_{23} \\ \gamma_{13} \\ \gamma_{12} \end{bmatrix}^j \tag{5}$$

The elements of $[Q]^j$ are related to material properties of the jth layer by

$$Q^j_{11} = \frac{E^j_1}{1-\nu^j_{12}\nu^j_{21}}, \quad Q^j_{12} = \frac{\nu^j_{12}E^j_2}{1-\nu^j_{12}\nu^j_{21}} \tag{6a,b}$$

$$Q^j_{22} = \frac{E^j_2}{1-\nu^j_{12}\nu^j_{21}}, \quad Q^j_{44} = G^j_{23} \tag{6c,d}$$

$$Q^j_{55} = G^j_{13}, \qquad Q^j_{66} = G^j_{12} \tag{6e,f}$$

where E_i, G_{im} and ν_{im} are Young's moduli, shear moduli and Poisson's ratios, respectively. The stress, engineering strain and constitutive relationships for the jth layer can be written as follows:

$$\sigma'_j = [T_j]^{-1}\sigma''_j, \ \epsilon'_j = [T_j]^{-1}\epsilon''_j, \ \sigma'_j = [\overline{Q}_j]\epsilon'_j \tag{7a,b,c}$$

where

$$[T_j] = \begin{bmatrix} \cos^2\theta_j & \sin^2\theta_j & 0 & 0 & \sin 2\theta_j \\ \sin^2\theta_j & \cos^2\theta_j & 0 & 0 & -\sin 2\theta_j \\ 0 & 0 & \cos\theta_j & -\sin\theta_j & 0 \\ 0 & 0 & \sin\theta_j & \cos\theta_j & 0 \\ -\frac{1}{2}\sin 2\theta_j & \frac{1}{2}\sin 2\theta_j & 0 & 0 & \cos 2\theta_j \end{bmatrix} \tag{8a}$$

$$\left[\overline{Q}_j\right] = [T_j]^{-1}\,[Q_j]\,[T_j]^{-T} \tag{8b}$$

$$\sigma'_j = [\sigma_x \ \ \sigma_y \ \ \tau_{yz} \ \ \tau_{xz} \ \ \tau_{xy}]^T, \ \sigma''_j = [\sigma_1 \ \ \sigma_2 \ \ \tau_{23} \ \ \tau_{13} \ \ \tau_{12}]^T \tag{8c,d}$$

$$\epsilon'_j = \left[\epsilon_x \ \ \epsilon_y \ \ \frac{\gamma_{yz}}{2} \ \ \frac{\gamma_{xy}}{2} \ \ \frac{\gamma_{xy}}{2}\right], \ \epsilon''_j = \left[\epsilon_1 \ \ \epsilon_2 \ \ \frac{\gamma_{23}}{2} \ \ \frac{\gamma_{13}}{2} \ \ \frac{\gamma_{12}}{2}\right]^T \tag{8e,f}$$

in which the conversion to engineering strain was taken into account. The angle θ_j is from the plate axis x to the material axis $(1)_j$.

Next, we propose to derive the laminate strain energy. The laminate consists of $2k$ symmetrically-stacked layers of variable thickness. Each layer height, t_j, is a continuous function of x and y (Fig. 2). The strain energy density for a single layer j or its counterpart below the midplane is

$$\hat{V}_j = \frac{1}{2}\int_{t_{j-1}}^{t_j} \sum_{i=1}^{5} \sigma^j_i \epsilon^j_i \, dz \tag{9}$$

where $i = x, y, yz, xz, xy$. Summation over all the layers and integration over the domain of the plate leads to the total strain energy

$$V = \frac{1}{2}\int_0^s \int_{LE}^{TE} \left\{ \sum_{j=-k}^{k} \left[\int_{t_{j-1}}^{t_j} \sum_{i=1}^{5} \sigma^j_i \epsilon^j_i \, dz \right] \right\} dx dy \tag{10}$$

where s is the wing span, $LE = LE(y)$ the wing leading edge and $TE = TE(y)$ the wing trailing edge. Substituting the strain-displacement relations, Eqs. (4), and the constitutive relations, Eq. (7c), into Eq. (10) and integrating over the layer thicknesses, we obtain the total strain energy expression

$$\begin{aligned} V=&\frac{1}{2}\int_0^s \int_{LE}^{TE} \sum_{j=-k}^{k} \left\{ \frac{1}{3}\left(t_j^3 - t_{j-1}^3\right) \left[\psi_{x,x}^2 \overline{Q}_{11}^j + \psi_{y,y}^2 \overline{Q}_{22}^j \right.\right. \\ &+ \left(\psi_{x,y} + \psi_{y,x}\right)^2 \overline{Q}_{66}^j + 2\psi_{x,x}\psi_{y,y}\overline{Q}_{12}^j + 2\psi_{x,x}\left(\psi_{x,y} + \psi_{y,x}\right)\overline{Q}_{16}^j \\ &\left. +2\psi_{y,y}\left(\psi_{x,y} + \psi_{y,x}\right)\overline{Q}_{26}^j \right] + \left(t_j - t_{j-1}\right)\left[\left(\psi_x + w_{,x}\right)^2 \overline{Q}_{55}^j \right. \\ &\left.\left. + \left(\psi_y + w_{,y}\right)^2 \overline{Q}_{44}^j + 2\left(\psi_x + w_{,x}\right)\left(\psi_y + w_{,y}\right)\overline{Q}_{45}^j \right] \right\} dxdy \end{aligned} \tag{11}$$

It must be recognized here that $t_j = t_j(x,y)$. The summation can be eliminated from the strain energy expression by considering the total laminate extensional and bending stiffness coefficients A_{ab} and D_{ab} defined as

$$A_{ab} = \sum_{j=-k}^{k} \left(t_j - t_{j-1}\right)\overline{Q}_{ab}^j, D_{ab} = \frac{1}{3}\sum_{j=-k}^{k}\left(t_j^3 - t_{j-1}^3\right)\overline{Q}_{ab}^j \tag{12}$$

and we observe that, because the thickness of the various layers is variable, $A_{ab} = A_{ab}(x,y)$ and $D_{ab} = D_{ab}(x,y)$. Using Eqs. (12), the total laminate strain energy can now be expressed in the compact form

$$V = \frac{1}{2}\int_0^s \int_{LE}^{TE} \left(\psi_D^T D \psi_D + \psi_A^T A \psi_A\right) dxdy \tag{13}$$

where

$$\psi_D = \begin{bmatrix} \psi_{x,x} \\ \psi_{y,y} \\ \psi_{x,y} + \psi_{y,x} \end{bmatrix}, \quad \psi_A = \begin{bmatrix} \psi_y + w_{,y} \\ \psi_x + w_{,x} \end{bmatrix} \tag{14a,b}$$

$$D = \begin{bmatrix} D_{11} & D_{12} & D_{16} \\ D_{12} & D_{22} & D_{26} \\ D_{16} & D_{26} & D_{66} \end{bmatrix}, \quad A = \begin{bmatrix} A_{44} & A_{45} \\ A_{45} & A_{55} \end{bmatrix} \tag{14c,d}$$

It remains to derive an expression for $\overline{\delta W}_{nc}$. Under consideration is a wing in the form of a trapezoidal planform, and in particular one characterized by low aspect ratio and/or forward swept configuration. The most important speed regime for such a wing is undoubtedly

supersonic. The main reason for including the aerodynamics is to demonstrate the usefulness of the structural model. A complete investigation of a wing would require appropriate aerodynamic theories for subsonic, transonic, supersonic and perhaps hypersonic speed regimes. The usefulness of this model can be demonstrated with supersonic aerodynamics, chosen for relevancy and for relative ease of application. For large Mach numbers, $M^2 >> 1$, there is a weak memory effect, in addition to weak three-dimensional effects. This opens up the prospect of a point-function relation between the pressure difference $p_u - p_\ell$ and the displacement w of the wing, which makes it both convenient and useful. The structural model is suitable for wings of any aspect ratio. While piston theory is used to demonstrate this model, it must be understood that, because it is a strip theory, it is not as suitable for very low aspect ratios as more sophisticated theories. This point function property allows the writing of an explicit aerodynamic operator operating on the vertical displacement of the wing, so that the force density can be written in the form[9]

$$A_{11} w_p = -C(x) \left(\frac{\partial}{\partial x} + \frac{1}{U} \frac{\partial}{\partial t} \right) w_p \tag{15}$$

where

$$C(x) = \frac{4q}{M} \left[1 + \frac{\gamma + 1}{2} M \frac{dt_N}{dx} \right] \tag{16}$$

in which M is the Mach number, q the dynamic pressure, t_N the wing half thickness, U the free stream airspeed and γ the ratio of specific heats.

The nonconservative virtual work is due to the aerodynamic forces. The distributed force, Eq. (15), multiplied by the corresponding virtual displacement yields the nonconservative virtual work density. Then, using Eqs. (1d) and (15) and integrating over the domain of the wing, we obtain the nonconservative virtual work

$$\overline{\delta W}_{nc} = \int_0^s \int_{LE}^{TE} A_{11} w_p \delta w_p dx dy = W_C \delta w_C + \Psi_C \delta \psi_C + \int_0^s \int_{LE}^{TE} \hat{W} \delta w dx dy \tag{17}$$

where

$$W_C = - \int_0^s \int_{LE}^{TE} C(x) \Big\{ \psi_C + w_{,x} + \frac{1}{U} \left[\dot{w}_C + (x - x_C) \dot{\psi}_C + \dot{w} \right] \Big\} dx dy \tag{18a}$$

is a resultant aerodynamic force,

$$\Psi_C = -\int_0^s \int_{LE}^{TE} C(x) \left\{ \psi_C + w_{,x} + \frac{1}{U} \left[\dot{w}_C + (x - x_C)\dot{\psi}_C + \dot{w} \right] \right\} (x - x_C)\, dx dy \qquad (18b)$$

is a resultant aerodynamic moment about an axis parallel to y and passing through C and

$$\hat{W} = -C(x) \left\{ \psi_C + w_{,x} + \frac{1}{U} \left[\dot{w}_C + (x - x_C)\dot{\psi}_C + \dot{w} \right] \right\} \qquad (18c)$$

is an aerodynamic force density.

4. THE EIGENVALUE PROBLEM

Inserting Eqs. (3), (13) and (16) into the extended Hamilton's principle and following the usual steps,[8] we can obtain the boundary-value problem for the system. The boundary-value problem consists of two ordinary differential equations for $w_0(t)$ and $\psi_C(t)$ and three partial differential equations for $w(x,y,t)$, $\psi_x(x,y,t)$ and $\psi_y(x,y,t)$, together with appropriate boundary conditions.

The differential eigenvalue problem can be obtained from the boundary-value problem by assuming that the displacements vary exponentially with time. The state of the art does not permit a closed-form solution of the differential eigenvalue problem, so that one must be content with an approximate solution, which amounts to spatial discretization of the problem through a series expansion. As a result, the original differential eigenvalue problem is replaced by an algebraic eigenvalue problem. It turns out that, in deriving the algebraic eigenvalue problem, it is more efficient to use directly the extended Hamilton's principle, Eq. (2). To this end, we assume a solution of the form

$$w_C(t) = q_1(t), \ \psi_C(t) = q_2(t) \qquad (19a,b)$$

$$w(x,y,t) = \sum_{i=3}^{n+2} \phi_i(x,y) q_i(t) \qquad (19c)$$

$$\psi_x(x,y,t) = \sum_{i=n+3}^{2n+2} \phi_i(x,y) q_i(t) \qquad (19d)$$

$$\psi_y(x,y,t) = \sum_{i=2n+3}^{3n+2} \phi_i(x,y) q_i(t) \qquad (19e)$$

where ϕ_i are space-dependent trial functions and q_i are time-dependent generalized coordinates. Inserting Eqs. (19) into Eq. (3) and omitting the integral limits for brevity, we can write the kinetic energy in the discretized form

$$T = \frac{1}{2}\left(M_C\dot{w}_C^2 + I_C\dot{\psi}_C^2\right) + \dot{w}_C \iint m\dot{w}dxdy + \dot{\psi}_C \iint m\left(x - x_C\right)\dot{w}dxdy + \frac{1}{2}\iint m\dot{w}^2 dxdy = \frac{1}{2}\dot{\mathbf{q}}^T M\dot{\mathbf{q}} \tag{20}$$

where $\mathbf{q}$ is a $3n$-vector of amplitudes and M is the symmetric mass matrix having the components

$$M_{11} = M_C,\ M_{12} = 0 \tag{21a,b}$$

$$M_{1j} = \iint m\phi_j dxdy,\ 3 \le j \le n+2 \tag{21c}$$

$$M_{1j} = 0,\ j > n+2 \tag{21d}$$

$$M_{21} = 0,\ M_{22} = I_C \tag{21e,f}$$

$$M_{2j} = \iint m(x - x_C)\phi_j dxdy,\ 3 \le j \le n+2 \tag{21g}$$

$$M_{2j} = 0,\ j > n+2 \tag{21h}$$

$$M_{ij} = \iint m\phi_i\phi_j dxdy, 3 \le i,j \le n+2 \tag{21i}$$

$$M_{ij} = 0,\ i,j > n+2 \tag{21j}$$

Moreover, introducing Eqs. (19c-e) into Eq. (13) and considering Eqs. (14), we obtain the discretized potential energy

$$V = \frac{1}{2}\iint \left(\psi_D^T\psi_D + \psi_A^T A\psi_A\right) dxdy = \frac{1}{2}\mathbf{q}^T K\mathbf{q} \tag{22}$$

where K is the symmetric stiffness matrix having the entries

$$K_{ij} = 0,\ i = 1,2 \text{ and } 1 \le j \le 3n+2 \tag{23a}$$

$$K_{ij} = \iint \left[\phi_{i,x}\phi_{j,x}A_{55} + \left(\phi_{i,y}\phi_{j,x} + \phi_{i,x}\phi_{j,y}\right)A_{45} + \phi_{i,y}\phi_{j,y}A_{44}\right] dxdy,\ 3 \le i,\ j \le n+2 \tag{23b}$$

$$K_{ij} = \iint \left(\phi_{i,x}\phi_j A_{55} + \phi_{i,y}\phi_j A_{45}\right) dxdy,$$

$$3 \le i \le n+2,\ n+3 \le j \le 2n+2 \tag{23c}$$

$$K_{ij} = \iint \left(\phi_{i,x}\phi_j A_{45} + \phi_{i,y}\phi_j A_{44}\right) dxdy,$$

$$3 \le i \le n+2,\ 2n+3 \le j \le 3n+2 \tag{23d}$$

$$K_{ij} = \iint \left[\phi_i\phi_j A_{55} + \phi_{i,x}\phi_{j,x} D_{11} + \phi_{i,y}\phi_{j,y} D_{66}\right.$$

$$\left. + \left(\phi_{i,y}\phi_{j,x} + \phi_{i,x}\phi_{j,y}\right) D_{16}\right] dxdy,\ n+3 \le i,j \le 2n+2 \tag{23e}$$

$$K_{ij} = \iint \left(\phi_i\phi_j A_{45} + \phi_{i,x}\phi_{j,x} D_{16} + \phi_{i,y}\phi_{j,x} D_{66} + \phi_{i,x}\phi_{j,y} D_{12}\right.$$

$$\left. + \phi_{i,y}\phi_{j,y} D_{26}\right) dxdy,\ n+3 \le i \le 2n+2,\ 2n+3 \le j \le 3n+2 \tag{23f}$$

$$K_{ij} = \iint \left[\phi_i\phi_j A_{44} + \phi_{i,x}\phi_{j,x} D_{66} + \phi_{i,y}\phi_{j,y} D_{22}\right.$$

$$\left. + \left(\phi_{i,y}\phi_{j,x} + \phi_{i,x}\phi_{j,y}\right) D_{26}\right] dxdy,\ 2n+3 \le i,j \le 3n+2 \tag{23g}$$

Finally, inserting Eqs. $(19c-e)$ into Eq. (17) and considering Eqs. (18), we can write the discretized virtual work due to aerodynamic forces in the form

$$\overline{\delta W}_{nc} = W_C \delta w_C + \Psi_C \delta\psi_C + \iint \hat{W}\delta w dxdy = -\delta\mathbf{q}^T \left(K_A\mathbf{q} + \frac{1}{U} H\dot{\mathbf{q}}\right) \tag{24}$$

where the entries of the nonsymmetric matrix K_A are

$$K_{A1j} = 0,\ j = 1,2,\ldots,n+2 \tag{25a}$$

$$K_{A21} = \iint C dxdy \tag{25b}$$

$$K_{A22} = \iint C\left(x - x_C\right) dxdy \tag{25c}$$

$$K_{A2j} = \iint C\phi_j dxdy,\ 3 \le j \le n+2 \tag{25d}$$

$$K_{Ai1} = \iint C\phi_{i,x} dxdy,\ 3 \le i \le n+2 \tag{25e}$$

$$K_{Ai2} = \iint C\left(x - x_C\right)\phi_{i,x} dxdy,\ 3 \le i \le n+2 \tag{25f}$$

$$K_{Aij} = \iint C\phi_{i,x}\phi_j dxdy,\ 3 \le i,j \le n+2 \tag{25g}$$

$$K_{Aij} = 0,\ 1 \le i \le n+2,\ j > n+2 \tag{25h}$$

$$K_{Aij} = 0,\ i > n+2 \tag{25i}$$

and those of the symmetric matrix H are

$$H_{11} = \iint C dxdy, H_{12} = \iint C\left(x - x_C\right) dxdy \tag{26a,b}$$

$$H_{1j} = \iint C\phi_j dxdy,\ 3 \le j \le n+2 \tag{26c}$$

$$H_{22} = \iint C\,(x - x_C)^2\, dxdy \tag{26d}$$

$$H_{2j} = \iint C\,(x - x_C)\,\phi_j dxdy, 3 \le j \le n+2 \tag{26e}$$

$$H_{ij} = \iint C\phi_i\phi_j dxdy,\ 3 \le i,j \le n+2 \tag{26f}$$

$$H_{ij} = 0,\ 1 \le i \le n+2,\ j > n+2 \tag{26g}$$

$$H_{ij} = 0,\ i > n+2 \tag{26h}$$

Introducing Eqs. (20), (22) and (24) into Eq. (2), integrating by parts with respect to time and invoking the arbitrariness of $\delta\mathbf{q}$, we obtain a set of simultaneous ordinary differential equations, which can be written in the compact form

$$M\ddot{\mathbf{q}} + \frac{1}{U}H\dot{\mathbf{q}} + (K + K_A)\,\mathbf{q} = \mathbf{0} \tag{27}$$

Then, letting

$$\mathbf{q}(t) = \mathbf{a}e^{\lambda t} \tag{28}$$

we obtain the desired algebraic eigenvalue problem

$$\left(\lambda^2 M + \frac{\lambda}{U}H + K + K_A\right)\mathbf{a} = \mathbf{0} \tag{29}$$

and we note that the problem is nonself-adjoint due to the presence of the aerodynamic matrices H and K_A.

The solution of the eigenvalue problem (29) requires that it be cast in state form. To this end, we introduce the state vector $\mathbf{x} = \begin{bmatrix}\mathbf{a}^T & \lambda\mathbf{a}^T\end{bmatrix}^T$. Then, adjoining the identity $\lambda\mathbf{a} = \lambda\mathbf{a}$, Eq. (29) can be rewritten in the state form

$$A\mathbf{x} = \lambda B\mathbf{x} \tag{30}$$

where

$$A = \begin{bmatrix} 0 & I \\ -(K + K_A) & -H/U \end{bmatrix},\ B = \begin{bmatrix} I & 0 \\ 0 & M \end{bmatrix} \tag{31a,b}$$

Because the matrix B is singular, some of the eigenvalues are infinite. Numerical solutions for this type of eigenvalue problems can be obtained by an algorithm described in Ref. 10.

5. APPROXIMATE SOLUTIONS IN TERMS OF QUASI-COMPARISON FUNCTIONS

In Sec. 4, we derived a discretized model for our system by assuming an approximate solution in the form of a linear combination of trial functions. The accuracy of the approximate solution and the computational time depend on the nature of the trial functions. To examine the nature of the trial functions, a brief discussion of the various classes of functions should prove beneficial.

Exact, closed-form solutions of differential eigenvalue problems represent the class of eigenfunctions. Clearly, they satisfy both the differential equations and all the boundary conditions of the problem. In most practical problems closed-form solutions do not exist. They certainly do not exist in the problem at hand. Approximate solutions generally fail to satisfy the differential equations. Functions satisfying certain differentiability conditions and all the boundary conditions, but not necessarily the differential equations, are called *comparison functions.*[8] In many problems, including that under consideration, comparison functions are difficult to generate. In the case of self-adjoint systems, it is often advantageous to formulate the eigenvalue problem by a variational approach, which amounts to rendering Rayleigh's quotient stationary. In this case, the trial functions need satisfy reduced differentiability conditions and the geometric boundary conditions alone. Such functions are known as *admissible functions.*[8] It has been demonstrated in Ref. 7 that solutions in terms of admissible functions can at times converge very slowly. To improve convergence, a new class of functions was created in Ref. 11, namely the class of *quasi-comparison functions.* The quasi-comparison functions are linear combinations of admissible functions capable of satisfying all the boundary conditions of the problem. Quasi-comparison functions can be generated by combining several families of admissible functions chosen so as to permit the satisfaction of the natural boundary conditions. It turns out that solutions in terms of quasi-comparison

functions tend to satisfy not only the natural boundary conditions but also the differential equations much more accurately than solutions in terms of mere admissible functions. In fact, solutions in terms of quasi-comparison functions can at times be more accurate than solutions in terms of comparison functions, because combinations of functions from several families with different characteristics permit better approximations of the solution throughout the interior of the domain than combinations of functions from a single family.[7,11] In Refs. 12 and 13, it was demonstrated that solutions in terms of quasi-comparison functions exhibit the same superior convergence characteristics in the case of nonself-adjoint systems as well.

In view of the above discussion, we propose to choose the trial functions in Eqs. $(19c-e)$ from the class of quasi-comparison functions. These functions must depend on both x and y and are assumed to have the form of products of chordwise functions $X_{k_f}(x)$ and spanwise functions $Y_{\ell_f}(y)$.

The eigenvalue problem is defined in terms of trial functions ϕ_i and ϕ_j $(i,j = 1,2,3,\ldots, 3n+2)$, where n is the number of trial functions for each of the three displacements w, ψ_x and ψ_y. There are additionally two rigid-body modes, namely, $\phi_1 = 1$ and $\phi_2 = 1$.

Let the same set of trial functions be used for each of the displacements w, ψ_x and ψ_y. The undetermined coefficients, of course, are not the same. Then, for $i = 3,4,5,\ldots,3n+2$,

$$\phi_f(x,y) = X_{k_f}(x)\,Y_{\ell_f}(y)\,,\ 1 \le f \le n \tag{32a}$$

where

$$f = i - 2 - n \cdot \mathrm{INT}\left(\frac{i-2}{n}\right) \tag{32b}$$

Similarly, for the companion set of trial functions

$$\phi_g = X_{k_g}(x)Y_{\ell_g}(y),\ 1 \le g \le n \tag{32c}$$

in which

$$\text{for}\quad g = j - 2 - n \cdot \mathrm{INT}\left(\frac{j-2}{n}\right) \tag{32d}$$

where INT( ) implies truncation to the corresponding integer value.

The functions X_{k_f} and Y_{ℓ_f} are each chosen from two different families. The indices k_f and ℓ_f determine the order of combination of functions X_{k_f} and Y_{ℓ_f} into ϕ_f, and hence they depend on f, which in turn depends on i according to Eq. (32b). Because the interest is in low-aspect ratio wings, the dependence of k_f and ℓ_f on f is such that the spanwise and chordwise functions are about equal in number or

$$\ell_f = f - \frac{1}{2}\left(d^2 - d\right) \qquad f = 1, 2, 3, \ldots, \frac{n}{2} \tag{33a}$$

$$\ell_f = \frac{1}{2}\left(2f - n - d^2 + d\right) \qquad f = \frac{n}{2} + 1, \frac{n}{2} + 2, \ldots, n \tag{33b}$$

$$k_f = 1 - d - \ell_f \qquad f = 1, 2, 3, \ldots, n \tag{33c}$$

where

$$d = \text{NINT}\sqrt{2f} \qquad f = 1, 2, 3, \ldots, \frac{n}{2} \tag{34a}$$

$$d = \text{NINT}\sqrt{2f - n} \qquad f = \frac{n}{2} + 1, \ \frac{n}{2} + 2, \ldots, n \tag{34b}$$

and NINT( ) implies rounding to the nearest integer value. It is assumed in Eqs. (33) and (34) that n is an even integer.

The chordwise functions $X_{k_f}(x)$ are segments of a sine function with an appropriate number of zero crossings. Accounting for wing sweep and the variable limits of x, X_{k_f} actually become functions of both x and y. The first family of chordwise function are chosen as

$$X_{k_f}(x, y) = \sin\left\{\frac{3\pi}{4} + \pi\left(k_f - \frac{3}{2}\right)\left[\frac{x - y\tan\eta_L}{r - y(\tan\eta_L - \tan\eta_T)}\right]\right\} \qquad LE \le x \le TE \tag{35}$$

The spanwise functions $Y_{\ell_f}(y)$ are also appropriate segments of a sine function with an appropriate number of zero crossings, or

$$Y_{\ell_f}(y) = \frac{y}{s}\sin\left[\frac{(2\ell_f - 1)\pi}{2s}y\right], \ 0 \le y \le s \tag{36}$$

The second family of functions X_{k_f} consists of terms from a power series, except that the functions alternate direction between the leading edge and the trailing edge. The wing sweep

requires shifting and scaling as before, resulting in

$$X_{k_f}(x,y) = \left\langle \left\{ r\left[1+(-1)^{k_f}\right] - (-1)^{k_f} x + \left[1+(-1)^{k_f}\right](\tan\eta_T - \tan\eta_L)\, y \right\} / 2\,[r + (\tan\eta_T - \tan\eta_L)\, y] \right\rangle^{\mathrm{INT}\left(\frac{k_f+3}{2}\right)}, \quad LE \le x \le TE \tag{37}$$

where INT( ) implies truncation to the corresponding integer value. Equation (37) appears complicated but it merely represents a power series shifted, scaled, and alternating in direction so as to accomodate the swept boundaries. The second family of spanwise functions is simply

$$Y_{\ell_f}(y) = \left(\frac{y}{s}\right)^{\left(\frac{\ell_f+3}{2}\right)} \quad 0 \le y \le s \tag{38}$$

The algebraic eigenvalue problem is assembled inside a double loop for f and g from 1 to n. The entries of the matrices M, K, K_A and H are given by Eqs. (21,) (23), (25) and (26), respectively.

The complete set of two-dimensional quasi-comparison functions is expressed in terms of f through ℓ_f and k_f as follows:

$$\phi_f = \frac{y}{s}\sin ay, \quad f = 3,4,\ldots,\frac{n+2}{2}, \quad k_f = 1 \tag{39a}$$

$$\phi_f = \frac{xy}{rs}\sin ay, \quad f = 3,4,\ldots,\frac{n+2}{2}, \quad k_f = 2 \tag{39b}$$

$$\phi_f = \frac{y}{s}\sin ay \ \sin\frac{b+cx+dy}{r+ey}, \quad f = 3,4,\ldots,\frac{n+2}{2}, \quad k_f \ge 3 \tag{39c}$$

$$\phi_f = \left(\frac{y}{s}\right)^N, \quad f = \frac{n+4}{2},\ldots,n \quad k_f = 1 \tag{40a}$$

$$\phi_f = \frac{x}{r}\left(\frac{y}{s}\right)^N, \quad f = \frac{n+4}{2}\ldots,n, \quad k_f = 2 \tag{40b}$$

$$\phi_f = My^N\left[\frac{1}{2}(1-Q) + Q\frac{x+yp}{r+ye}\right]^s, \quad f = \frac{n+4}{2},\ldots,n, \quad k_f \ge 3 \tag{40c}$$

where

$$b = \frac{3r\pi}{4}, \quad e = \tan\eta_T - \tan\eta_L \tag{41a,b}$$

$$p = -\tan\eta_L, \quad a = \frac{\left(2\ell_f - 1\right)\pi}{2s} \tag{41c,d}$$

$$c = \pi\left(k_f - \frac{3}{2}\right),\ d = \pi\left[\frac{3}{4}e + \left(k_f - \frac{3}{2}\right)p\right] \qquad (41e,f)$$

$$M = \left(\frac{1}{s}\right)^N,\ N = \frac{\ell_f + 3}{2} \qquad (41g,h)$$

$$Q = -(-1)^{k_f},\ s = \mathrm{INT}\left(\frac{k_f + 1}{2}\right) \qquad (41i,j)$$

Similar series can be written for ϕ_g by replacing f by g and i by j. The simpler forms for ϕ_f when $k_f = 1, 2$ are due to the simple form of the rigid chordwise shape functions corresponding to the first two terms in $X_{k_f}(x)$, as mentioned previously. An example of the series $\phi_f(x,y)$ for $n = 6$ should prove helpful. The six terms consist of three terms from each of the two families, or

$$\phi_1 = \frac{y}{s}\sin\frac{\pi}{2s}y,\ \phi_2 = \frac{xy}{rs}\sin\frac{\pi}{2s}y,\ \phi_3 = \frac{y}{s}\sin\frac{3\pi}{2s}y \qquad (42a,b,c)$$

$$\phi_4 = \left(\frac{y}{s}\right)^2,\ \phi_5 = \frac{x}{r}\left(\frac{y}{s}\right)^2,\ \phi_6 = \left(\frac{y}{s}\right)^{2.5} \qquad (42d,e,f)$$

6. NUMERICAL RESULTS

In presenting numerical results, it is useful to define several dimensionless quantities. The frequency can be nondimensionalized as follows:

$$\Omega = \omega A\left[\frac{\rho_{\mathrm{ref}}}{E_{\mathrm{ref}}t_{\mathrm{ref}}^2}\right]^{1/2} \qquad (43)$$

Similarly, a speed parameter can be defined, yielding the dimensionless dynamic pressure

$$\lambda_a = \frac{2qA^2}{E_{\mathrm{ref}}t_{\mathrm{ref}}^4} = \frac{\rho_{\mathrm{air}}U^2A^2}{E_{\mathrm{ref}}t_{\mathrm{ref}}^4} \qquad (44)$$

The quantities $(\ )_{\mathrm{ref}}$ are reference values. The quantities E_{ref} and ρ_{ref} are E_2 and ρ for the main structural material, t_{ref} is the total thickness at the wing root and leading edge intersection. Other dimensionless parameters are taper ratio TR and the aspect ratio AR. Extensive vibration and flutter results can and have been generated with this model. The intent here is to develop and present the formulation, so that the presented results are merely a summary.

i. Convergence and accuracy

The convergence of the free-vibration eigenvalues of an anisotropic low aspect ratio wing is considered in Fig. 3. The convergence rate of the first five nonzero eigenvalues is depicted as the frequency parameter Ω versus the number of terms in the approximating series. The first two eigenvalues have zero value and correspond to rigid-body modes, which converge immediately; they are not shown in Fig. 3. It should be pointed out here that a linear combination of admissible functions must possess a minimum number of terms before it qualifies as a quasi-comparison function. The number must be such as to permit satisfaction of all natural boundary conditions. As soon as this number of terms has been reached, convergence of the computed eigenvalues to the actual ones is relatively rapid.

The two flutter mechanisms of most concern are the bending-torsion mode and the body-freedom mode. The body-freedom flutter mode occurs instead of the divergence mode when the pitch degree of freedom is introduced. Reasonably accurate representations of the pitch mode and the first two flexible modes, as well as fairly accurate representation of the third flexible mode, are required to capture these two mechanisms. The indications from Fig. 3 are that 20 terms are sufficient for this purpose, certainly for establishing a trend.

Convergence of the flutter dynamic pressure parameter for a forward swept anisotropic wing is shown in Fig. 4. The flutter mechanism acting is body-freedom flutter. Reasonable convergence has been achieved with 20 terms.

Figure 5 shows three frequencies corresponding to an isotropic plate of aspect ratio 5; the computed values are compared with the exact values given in Table 11.4 of Ref. 14. The plate is 1/2 inch steel and is fixed on a short side. The remaining three edges are free. The clamped condition is simulated with the present model by taking very large values for fuselage mass and pitch inertia. The results are quite acceptable. As expected from the discussion of quasi-comparison functions the matching is poor for small numbers of terms but begins to converge quite rapidly when a certain critical number of terms is reached.

The accuracy of the flutter analysis is checked through a comparison with results obtained

in Ref. 15 by Rossettos and Tong, which is one of the few works available on the flutter of a plate with free edges in the supersonic region. Their model consists of a single layer, constant thickness, square composite plate clamped at one edge and subjected to supersonic flow on the upper surface. The aerodynamics is based on a variant of the piston theory that converges to Eq. (15) for sufficiently high Mach numbers and with flow over both surfaces. Comparison is for a square composite plate with a fiber orientation of 24°. The model derived here predicted on the average flutter speeds 6% higher than those of Ref. 15.

ii. Free vibration results

The interest in the free vibration case is mainly for its relation to the flutter results. The two flutter mechanisms, body-freedom and bending-torsion, dictate that concentration is on the pitch mode and the first two flexible modes, although the first few flexible modes above these will also have some influence. The convergence of the rigid-body modes, pitch and plunge, is not an issue.

For body-freedom flutter, the most critical parameter is geometrical. If the wing is not swept forward or nearly so then this flutter mechanism cannot arise. Work by a number of authors demonstrate a surprising influence of a tailoring layer swept just a few degrees off nominal. Body-freedom flutter can be eliminated, or pushed up to significantly higher speeds, if a percentage of the spanwise plies are reoriented 10° forward. Two factors are at work in this case and both are free vibration matters. When an orthotropic layer for which $E_1 >> E_2$ is reoriented, bending begins to occur in the direction normal to E_1. The result is an effective rotation of the elastic axis in the direction opposite to the reorientation of the tailoring ply. The other factor at work is the necessary reduction of spanwise bending stiffness that must accompany the reorienting of plies away from the midchord. This second factor eventually overpowers the first, so that ply reorientations are most effective when they are small.

Figure 6 shows the frequency parameter of the first flexible mode varying with the sweep angle of a tailoring layer. The results for three wings are shown. An interesting phenomenon

is observed in Fig. 6 for the low-aspect ratio wing. This wing has its highest bending stiffness associated with a significantly aft swept tailoring layer, $\theta = 10°$. The implication is that tailoring plies might not be as effective for low-aspect ratio wings. This trend, shown to be true in the next subsection, was not previously discovered due to inherent limitations of the one-dimensional models commonly used.

Much has been said about the benefits of using the anisotropicity of a composite layup to tailor the response of a wing. Such discussion has been limited almost entirely to ply orientation. The dominant use of one-dimensional structural models nas forced this limitation on the current investigation. One can easily suppose that distribution of the tailoring material in both the spanwise and chordwise directions might significantly affect the response. These trends are readily investigated with the current plate model. As ply distribution for a low-aspect ratio anisotropic wing is varied from a concentration near the trailing edge to the leading edge, there is a change in frequency of the natural modes. The associated frequency parameters increase by 8%, 6% and 3%, respectively, for the first three flexible modes. The bending-torsion separation increases by 5%. For a similar spanwise variation from wing tip concentration to wing root, frequencies again vary. In this case, the increases are 34%, 14% and 12%, respectively, for the first three flexible modes. For bending-torsion separation, the change is slight at 2.5%. This reflects the increase in bending stiffness, which occurs when material is shifted near the wing root. Clearly, the two-dimensional nature of this material distribution has an effect on the free vibration outcome. It seems reasonable to expect that the flutter response will also be affected, allowing a refinement of the concept of tailoring with composites.

iii. Flutter analysis results

Two flutter mechanisms are of primary concern for a symmetric model of a wing with forward or aft sweep. The first is the classical bending-torsion flutter that can occur for a wing of any sweep when the frequencies of these two modes begin to coalesce as the speed increases. One mode, the torsion mode, turns downward toward a very stable condition just

as the bending mode heads for instability. The two frequencies coalesce as the instability approaches. Complete coalescence does not occur when the fuselage is capable of rigid-body motions. The rigid-body pitch frequency assumes a nonzero value, which rises as the speed increases. Without a tailored layup, the pitch and bending modes would surely combine to cause body-freedom flutter before the bending-torsion coupling could arise. Recall that bending-torsion flutter is unlikely at any speed for a significant forward sweep angle. It is seen then that the same tailoring which eliminates body-freedom flutter by apparent aft sweeping of the elastic axis also makes bending-torsion flutter possible. A trade-off is implied and caution must be exercised when contemplating a tailored composite design solution.

Next, the characteristics of body-freedom flutter are considered. For a swept forward orthotropic wing, the flutter mode will be body-freedom flutter, or divergence if clamped. The bending-torsion case occurs at a much higher speed or may not occur at all for a large forward sweep angle. The pitch mode is characteristically very lightly damped and will move toward instability as the bending mode moves away from the imaginary axis. The pitch and bending frequencies coalesce eventually with increasing dynamic pressure rather than separating, as would be the case for bending-torsion flutter.

Weisshaar et al.[2] have reported a trend in the ratio $\Omega_{\text{flutter}}/\Omega_{\text{fundamental}}$ for the two flutter mechanisms just presented. In a particular case in Ref. 5, the ratio is equal to 0.26 for a body-freedom flutter and to 3.40 for a bending-torsion flutter. The ratios for comparable cases in this work are 0.42 and 2.64, respectively.

The effect of tailoring plies, particularly on divergence or body-freedom flutter has received a great deal of attention. Figure 7 shows the flutter dynamic pressure versus the tailoring ply angle for two orthotropic wings ($AR = 3$ and $AR = 6$) and one isotropic wing ($AR = 8$). In all three cases, body-freedom flutter is critical and small negative ply angles are expected to be effective. There is an implication in Fig. 6 that the low-aspect ratio wing does not realize much benefit, because its maximum bending stiffness occurs for a somewhat more aft swept configuration than the other higher-aspect ratio cases. This fact,

demonstrated in Fig. 7, has important design implications for the design of low-aspect ratio wings. If the model used does not account for low-aspect ratios, then this phenomenon will be entirely missed.

Figure 7 shows the interesting and somewhat surprising result that flutter dynamic pressure is strongly affected by very small changes in the layer orientation in the vicinity of 0°. Virtually all the analytical and experimental work on tailoring forward swept wings to date does not consider low-aspect ratio wings.

Finally, the distribution of tailoring plies over the wing planform is considered. The present model is ideally suited to investigation of parameters such as layer thicknesses, which are free to vary in both chordwise and spanwise directions. Such distribution investigations are likely to result in lower structural weight or higher flutter speeds, so that they must be included in any search for an optimal wing design. The present model can be used to conduct such investigations with ease. The results are impressive. In the chordwise direction, a flutter dynamic pressure increase of 25% or decrease of 25% is observed, depending on whether the leading or trailing edge is favored for a linear material distribution, respectively. Similarly, in the spanwise direction, the flutter dynamic pressure increases 29% if the wing root is favored, but drops 35% if the plies are concentrated near the tip. These results are for an orthotropic wing of aspect ratio 6 and a forward sweep angle of 20°. The tailoring layer is swept 10° forward of the midchord line. These new results go a long way toward justifying this more sophisticated model.

7. SUMMARY AND CONCLUSIONS

At the outset, the goal was to develop a structural model representing a modern aircraft wing sufficiently well and one that is sufficiently simple to be used in a multidisciplinary optimization problem. This goal has been accomplished with the development of a plate model that accounts for shear deformation, variable layer thickness and orientation, fuselage degrees of freedom and chordwise flexibility. Consistent with conclusions reached by previous investigators, certain factors such as wing camber, unsymmetric ply stacking and rotatory

inertia are sufficiently small for the problem at hand that they can be ignored.

The algebraic eigenvalue problem was formulated directly from the extended Hamilton principle. In solving the algebraic eigenvalue problem, the recently developed quasi-comparison functions were relied upon to guarantee rapid convergence.

The numerical results obtained by means of the current model confirmed various trends established by earlier investigators. They demonstrate that there is a very wide array of interrelated parameters affecting the instability speed. The most clear outcome is a demonstration of the necessity of a formal optimization approach to bring consistency to the investigation of all the pertinent parameters.

The numerical results are limited to demonstration of the various features of the model and opening forays into regions of investigation previously closed to simpler models. Nevertheless, several previously unreported trends having significant bearing on the design of modern wings were revealed. These initial inquiries open the door to further research and refinement of the concept of composite tailoring. The results indicate that composite tailoring of forward swept wings may not be nearly as effective for low-aspect ratio wings as for high-aspect ratio wings. This is an important result which virtually mandates a structural model of at least the level of sophistication used here to accomplish optimal design of a low-aspect ratio forward swept wing.

A second and also important new finding pertaining to two-dimensional models is the merit of tailoring ply distributions. Beyond finding the optimum angle of orientation of a tailoring ply, significant improvements in the flutter speed are left undiscovered if the distribution is not also subjected to scrutiny. The results presented here indicate that the tailoring plies are most effective when the distribution favors the leading edge and the wing root. This result is also unobtainable with more conventional models and points once again to the need of sufficient sophistication in modeling. Optimization methods are dictated by a large number of interacting parameters, but such effort is wasted if the physical system is not modeled with sufficient accuracy.

8. REFERENCES

1. Krone, N. J., Jr., "Divergence Elimination with Advanced Composites," AIAA Paper 75-1009, *The AIAA Aircraft Systems and Technology Meeting*, Los Angeles, CA, Aug. 1975.
2. Weisshaar, T. A., Zeiler, T. A., Hertz, T. J. and Shirk, M. H., "Flutter of Forward Swept Wings, Analysis and Tests," *Proceedings of the AIAA/ASME/ASCE/AHS 23rd Structures, Structural Dynamics and Materials Conference*, New Orleans, LA, 1982, pp. 111-121.
3. Giles, G. L., "Equivalent Plate Analysis of Aircraft Wing Box Structures with General Planform Geometry," *Journal of Aircraft*, Vol. 23, No. 11, 1986, pp. 859-864.
4. Giles, G. L., "Further Generalization of an Equivalent Plate Representation for Aircraft Structural Analysis," *Journal of Aircraft*, Vol. 26, No. 1, 1989, pp. 67-74.
5. Librescu, L., *Elastostatics and Kinetics of Anisotropic and Heterogeneous Shell-Type Structures*, Noordhoff International Publishing, The Netherlands, 1977.
6. Mindlin, R. D., "Influence of Rotatory Inertia and Shear on Flexural Motions of Isotropic, Elastic Plates," *Journal of Applied Mechanics*, March 1951, pp. 31-38.
7. Meirovitch, L. and Kwak, M. K., "Convergence of the Classical Rayleigh-Ritz Method and the Finite Element Method," *AIAA Journal*, Vol. 28, No. 8, 1990, pp. 1509-1516.
8. Meirovitch, L., *Computational Methods in Structural Dynamics*, Sijthoff & Noordhoff, The Netherlands, 1980.
9. Bisplinghoff, R. L. and Ashley, H., *Principles of Aeroelasticity*, Dover Publications, Inc., New York.
10. Moler, C.B. and Stewart, G.W., "An Algorithm for Generalized Matrix Eigenvalue Problems," *SIAM Journal of Numerical Analysis*, Vol. 10, No. 2, 1973, pp. 241-256.
11. Meirovitch, L. and Kwak, M. K., "Rayleigh-Ritz Based Substructure Synthesis for Flexible Multibody Systems," *AIAA Journal*, Vol. 29, No. 10, 1991, pp. 1709-1719.
12. Hagedorn, P., "Quasi-Comparison Functions in the Dynamics of Elastic Multibody systems," *Proceedings of the Eighth VPI&SU Symposium on Dynamics and Control of Large Structures* (Ed: L. Meirovitch), Blacksburg, VA, May 6-8, 1991, pp. 97-108.
13. Meirovitch, L. and Hagedorn, P., "A New Approach to the Modeling of Nonself-Adjoint Systems," *XVIIIth International Congress of Theoretical and Applied Mechanics*, Haifa, Israel, Aug. 22-28, 1992. To appear in the *Journal of Sound and Vibration.*
14. Blevins, R.D., *Formulas for Natural Frequency and Modeshape*, Van Nostrand Reinhold, New York, 1979.
15. Rossettos, J.N. and Tong, P., "Finite-Element Analysis of Vibration and Flutter of Cantilever Anisotropic Plates,", *Journal of Applied Mechanics*, Vol. 41, No. 4, 1974, pp. 1075-1080.

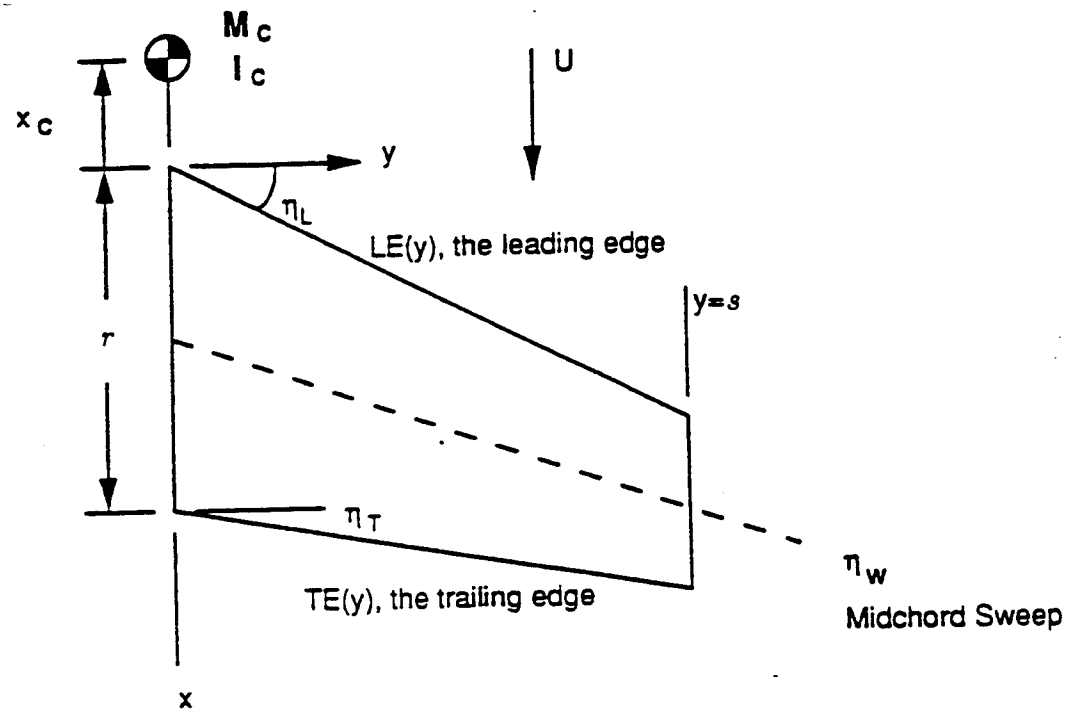

Fig. 1 - Wing Planform

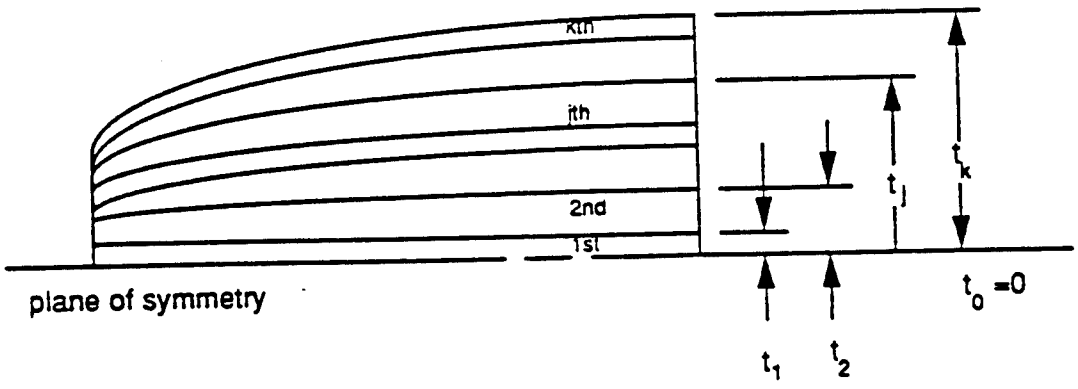

Fig. 2 - The Laminate

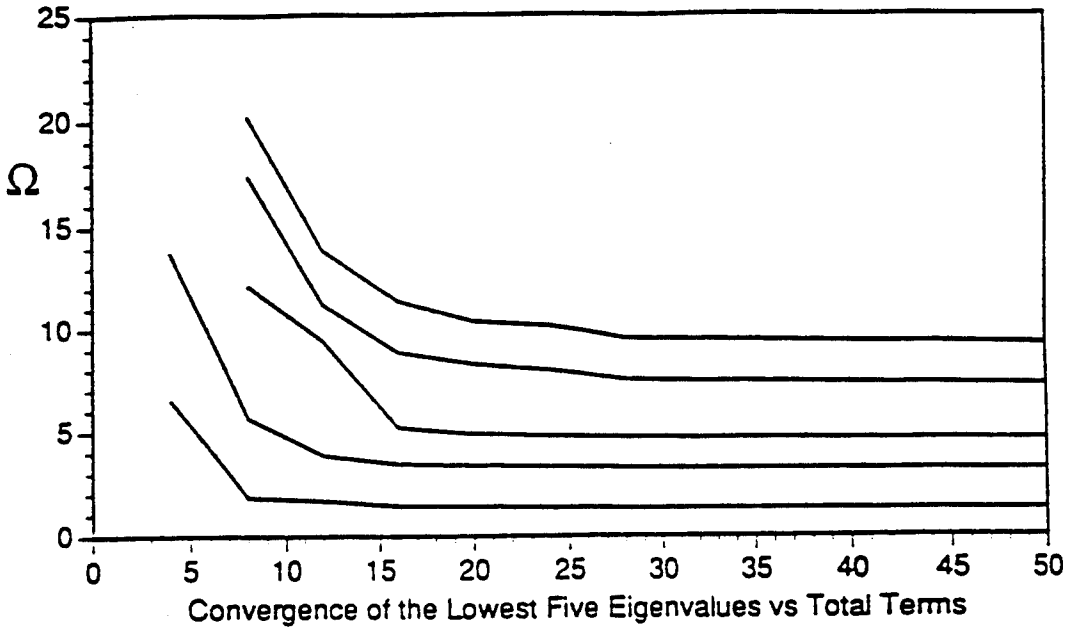

Fig. 3 - Free Vibration Convergence

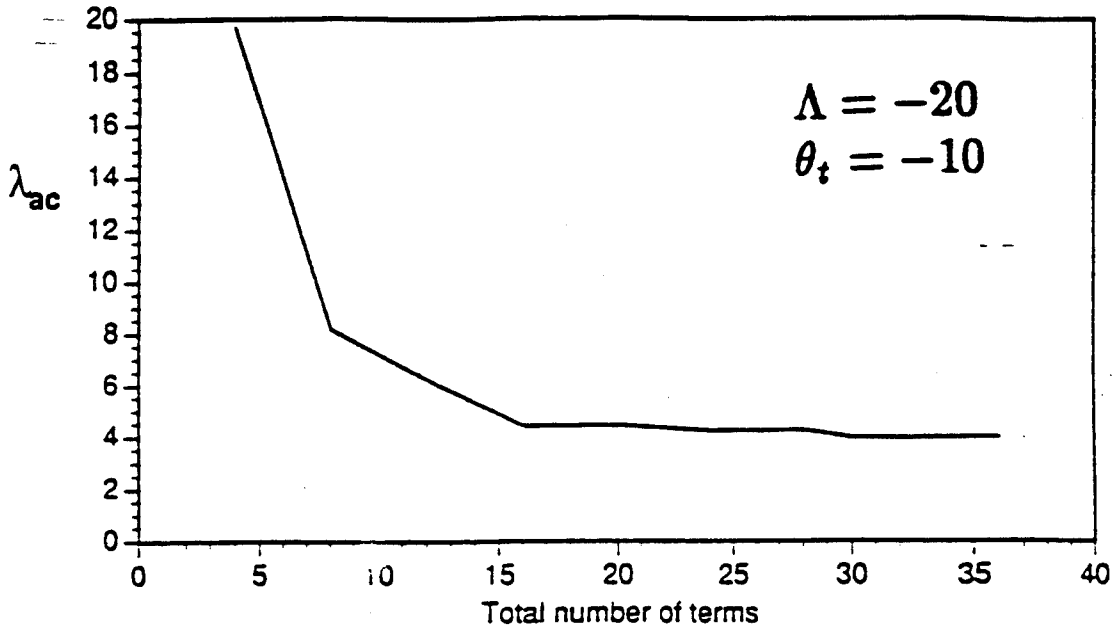

Fig. 4 - Convergence of the Flutter Dynamic Pressure

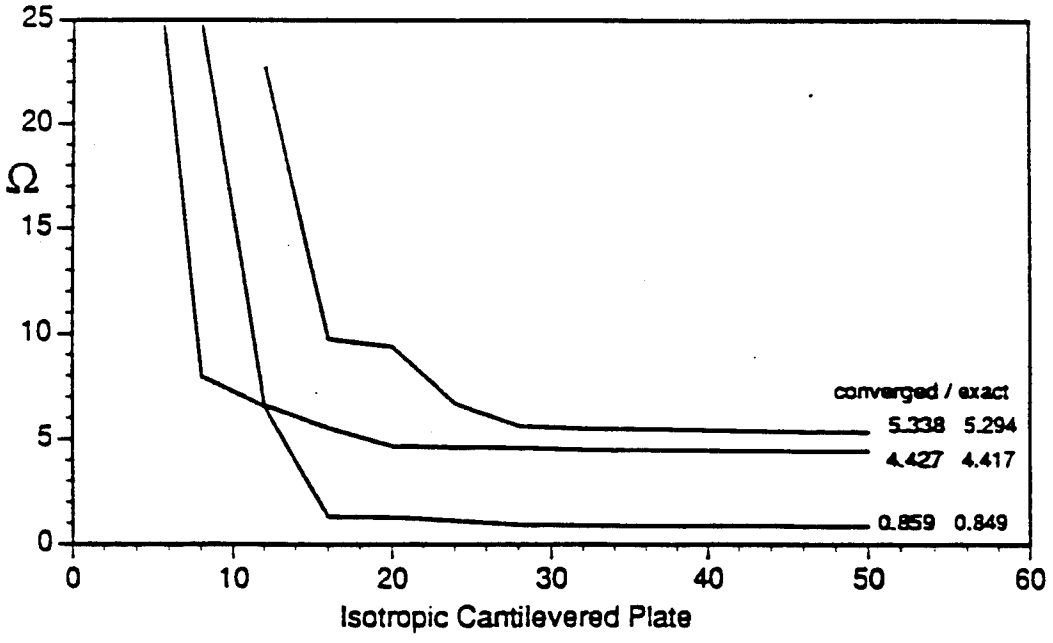

Fig. 5 - Frequency Convergence

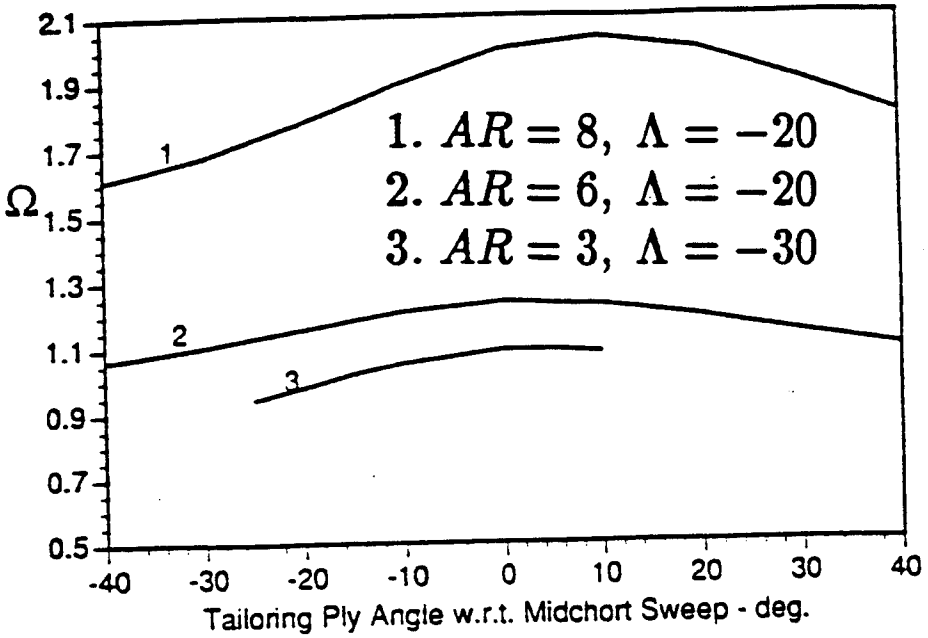

Fig. 6 - Frequency Parameter vs Ply Angle

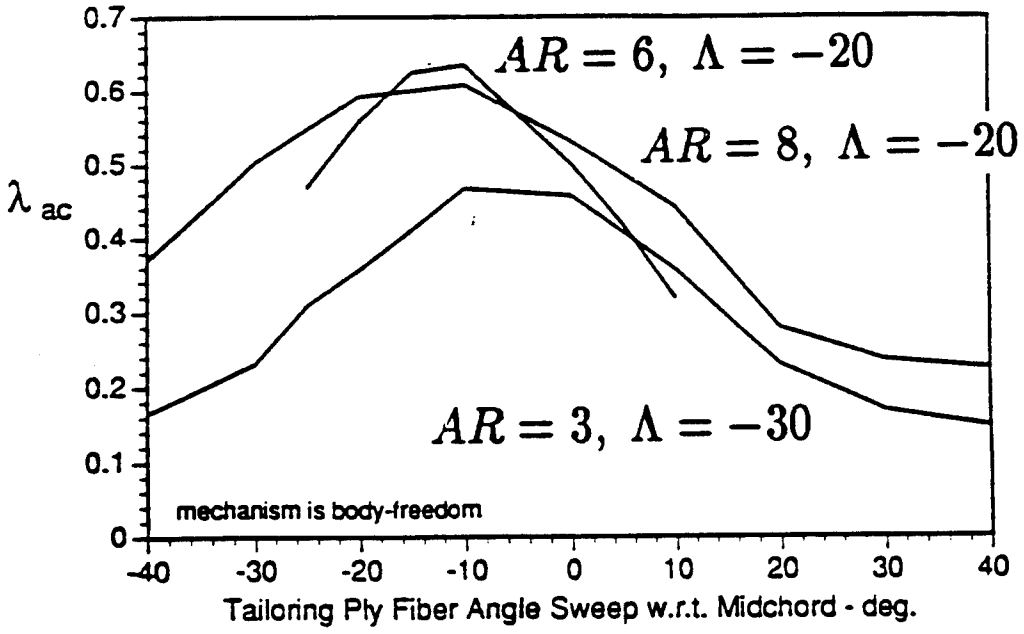

Fig. 7 - Flutter Dynamic Pressure vs Ply Angle

Integrated Structural Design and Vibration Suppression Using Independent Modal Space Control

R. A. Canfield and L. Meirovitch

Reprinted from

AIAA Journal

Volume 32, Number 10, Pages 2053–2060

A publication of the
American Institute of Aeronautics and Astronautics, Inc.
370 L'Enfant Promenade, SW
Washington, DC 20024-2518

AIAA JOURNAL
Vol. 32, No. 10, October 1994

Integrated Structural Design and Vibration Suppression Using Independent Modal Space Control

Robert A. Canfield*
Air Force Institute of Technology, Wright-Patterson Air Force Base, Ohio 45433
and
Leonard Meirovitch†
Virginia Polytechnic Institute and State University, Blacksburg, Virginia 24061

The integrated design of a structure and its control system is treated as a multiobjective optimization problem. Structural mass and a quadratic performance index constitute the vector objective function. The closed-loop performance index is taken as the time integral of the Hamiltonian. Constraints on natural frequencies, closed-loop damping, and actuator forces are also considered. Derivatives of the objective and constraint functions with respect to structural and control design variables are derived for a finite element beam model of the structure and constant feedback gains determined by independent modal space control. Pareto optimal designs generated for a simple beam demonstrate the benefit of solving the integrated structural and control optimization problem.

Introduction

THE fields of structural optimization and optimal control have made significant strides with the advent of the computer age. Each discipline has independently generated useful methods and computational tools for design. Yet, they share an approach in which certain system parameters or design variables are selected so as to optimize an objective function subject to a given set of constraints. In structural optimization, the objective function is often related to the cost of the structure, and it may involve the weight of the structure or the volume of material. The design variables typically characterize the material distribution or geometry of the structure. Any quantity characterizing the response of the structure, such as stress, displacement, or frequency, may be constrained to preclude structural failure. The structural response may be static or dynamic, although time usually plays no particular role in the formulation of the structural optimization problem.[1,2] In contrast, in modern optimal control a control law optimizing some performance index (the objective function) over a given time interval is synthesized. In the linear quadratic regulator (LQR) theory,[3] control gains relating actuator forces to sensor outputs by means of a linear transformation are typical control design variables. The performance index is rendered independent of time by integrating over the control time.

In common design practice, structural design precedes control design. The mathematical model for the structural optimum, or at least the final structural design, constitutes the plant for the control design. The control designer then proceeds to synthesize the optimal control system for the given plant. Uncertainties in structural modeling of the plant are often considered to ensure that the control system is robust with respect to plant errors. The possibility exists that the plant can be altered so as to enhance performance in conjunction with both structural and control optimization. As a result of difficulties in lifting and deploying heavy objects such as space stations, which can contain large solar arrays, antennas and precision laser, or optical systems, the spacecraft structures must be highly flexible. Moreover, stringent performance requirements for pointing accuracy, vibration suppression, shape control, etc., demand active controls to augment any passive damping. The goal of integrated design is to take advantage of any synergistic interaction between the flexible structure and its active control system.

The integrated structural and control design problem was first considered by Hale et al.[4] Messac and Turner[5] emphasized transformation of the state space to modal coordinates and the dependence of the weighting matrices on the modes. In formulating the combined optimization problem Salama et al.[6] established a precedent followed by many others. They eliminated control design variables by considering steady-state (constant) gains and selecting particular weighting matrices (identity) for the quadratic performance index.

Haftka et al.[7] minimized control effort through structural changes while maintaining specified damping ratios. However, the damping ratios of the lower modes decreased, and the frequency response magnitude and decay time increased. In another early study, Venkayya and Tischler[8] reached a different conclusion, namely, that a nominal truss model and a structurally optimal truss had nearly the same control design for regulating a disturbance. They considered a disturbance dominated by the first mode, but both structural designs had the same fundamental eigenvalue, perhaps explaining the similar control designs. Miller and Shim[9] also considered the same class of disturbances, i.e., an initial displacement representing the response to a static load.

Rew and Junkins[10] searched for optimal state and control weighting matrices for the quadratic performance index but did not consider any structural variables. Bodden and Junkins[11] minimized some unspecified robustness measure while placing closed-loop eigenvalues in a desired region. When the structural variables were included, a sequential approach was used. McLaren and Slater[12] employed a similar homotopy continuation method that converged only after about 750 complete analyses for one case, and after 10 h of CPU time on a Cray Y-MP supercomputer for another.

Lust and Schmit[13] searched for structural variables and linear output feedback gains on equal footing for the steady-state response to deterministic harmonic loading. Special attention was paid to developing explicit approximations to the highly nonlinear implicit response functions. Later, Thomas and Schmit[14] extended this formulation to problems with noncollocated actuators and sensors, as well as stability constraints on the complex eigenvalues. Sepulveda et al.[15] extended to complex eigenvalues Canfield's Rayleigh quotient approximation (RQA) for eigenvalues of conservative systems.[16] Based on the complex RQA, Thomas et al.[17] improved the approximations for damping and control forces.

Only Belvin and Park[18] appear to have taken advantage of inde-

Presented as Paper 93-1670 at the AIAA/ASME/ASCE/AHS/ASC 34th Structures, Structural Dynamics, and Materials Conference, La Jolla, CA, April 22, 1993; received June 2, 1993; revision received April 11, 1994; accepted for publication April 12, 1994. This paper is declared a work of the U.S. Government and is not subject to copyright protection in the United States.

*Assistant Professor, Department of Aeronautics and Astronautics. Member AIAA.

†University Distinguished Professor, Department of Engineering Science and Mechanics.

pendent modal space control[3] (IMSC) to treat the integrated structural/control problem. The authors did not claim to have found the integrated optimum, rather they used IMSC to decouple structural and control design by determining the primary influence of the structural design on the control objective.

A novel approach proposed by Messac et al.[19] combined disturbance rejection and command following performance errors in a quadratic performance norm. One of the final designs was characterized as nonintuitive, because the second frequency was reduced by half, whereas in separable design structural optimization would normally stiffen the second mode, increasing its frequency.[18] A comparison of designs obtained for two simple truss structures was made by Rao[20] for various objective functions.

Problem Statement

We are concerned with a linear, time-invariant, distributed-parameter system. Following spatial discretization, the equations of motion are given by

$$M(v_s)\ddot{q}(t) + C(v_s)\dot{q}(t) + K(v_s)q(t) = Du(v_s, v_c, t) \tag{1}$$

where q is the configuration vector, M the mass matrix, C the damping matrix, and K the stiffness matrix, all parameterized by the n_s vector v_s of structural variables. The system is regulated by a vector of control forces $u(v_s, v_c, t)$ which is also parameterized by the n_c-vector v_c of control design variables, and transmitted to the structure according to the load distribution matrix D. The structural, and control vectors can be combined into the complete design vector $v = [v_s^T \; v_c^T]^T$.

Modal Space Control

If the structure is subject to proportional viscous damping, the uncontrolled system can be decoupled by means of the classical modal transformation. By the expansion theorem,[21] this transformation is given by

$$q(t) = \sum_{i=1}^{n_m} \phi_i \eta_i(t) = \Phi\eta \tag{2}$$

where Φ is the classical modal matrix and η the vector of modal coordinates. The eigenvectors are orthogonal with respect to the mass matrix and can be normalized so as to satisfy $\Phi^T M\Phi = I$, $\Phi^T K\Phi = \Omega^2$, where Ω^2 is the diagonal matrix of eigenvalues. Synthesizing a control law is more convenient when the left side of Eq. (1) is transformed to diagonal form. To this end we insert Eq. (2) into Eq. (1), premultiply by Φ^T, assume that damping is of the proportional type,[21] and obtain

$$\ddot{\eta}(t) + 2\zeta\Omega(v_s)\dot{\eta}(t) + \Omega^2(v_s)\eta(t) = \Phi^T(v_s)Du(v_s, v_c, t) = f(t) \tag{3}$$

where ζ is the diagonal matrix of modal damping factors, assumed to be constant for the class of structures under consideration, and $f(t)$ is the modal force vector.

Typically, not all n_m modes need be controlled, so the control design problem can be truncated. To this end, we partition the decoupled equations into n_C equations for the controlled modes and n_R equations for the residual modes. Consistent with this, the modal matrix, the modal coordinate vector, and the modal force vector have the partitioned forms $\Phi = [\Phi_C \; \Phi_R]$, $\eta = [\eta_C^T \; \eta_R^T]^T$, and $f(t) = [f_C(t)^T \; f_R(t)^T]^T$, respectively. The controlled equations in Eq. (3) can be transformed to state space. To this end, we introduce the state vector $x = [\eta_C^T \; \dot{\eta}_C^T]^T$. Then, the state equations for the controlled modes can be written in the matrix form

$$\dot{x} = Ax + Bu \tag{4}$$

where

$$A = \begin{bmatrix} 0 & I \\ -\Omega_C^2 & -2\zeta_C\Omega_C \end{bmatrix}, \qquad B = \begin{bmatrix} 0 \\ \Phi_C^T D \end{bmatrix} \tag{5}$$

are coefficient matrices. For linear feedback of the controlled modes, the control law is

$$f_C(t) = \Phi_C^T Du(t) = -G\eta_C - H\dot{\eta}_C \tag{6}$$

where the modal control gain matrices G and H are constant in the steady-state case. To implement modal feedback control the modal displacements and velocities must be extracted from the system outputs. Application of the second part of the expansion theorem[21] provides the transformation of physical to modal coordinates

$$\eta_C(t) = \Phi_C^T Mq(t) \tag{7a}$$

$$\dot{\eta}_C(t) = \Phi_C^T M\dot{q}(t) \tag{7b}$$

in which the $q(t)$ are deterministic physical coordinates. State estimation is not considered here; however, if at least as many sensed outputs are available as controlled modes, modal state estimation is not an obstacle.[3] Meirovitch et al.[22] successfully demonstrated the use of modal filters based on Eqs. (7) for control of an experimental beam by means of IMSC.

Although they are not controlled, the residual modes receive the excitation

$$f_R(t) = \Phi_R^T Du(t) \tag{8}$$

The closed-loop system is described by

$$\dot{x} = A_c x \tag{9}$$

where

$$A_c = \begin{bmatrix} 0 & I \\ -\bar{G} & -\bar{H} \end{bmatrix} \tag{10}$$

is the closed-loop plant matrix, in which

$$\bar{G} = \Omega_C^2 + G, \qquad \bar{H} = 2\zeta_C\Omega_C + H \tag{11}$$

Independent Modal Space Control

The general idea of the IMSC method is that the control force for a given mode depends only on the modal displacement and velocity of that mode. Hence, the independence of open-loop modal equations is preserved for the closed-loop equations. For self-adjoint systems, the $2n_C \times 2n_C$ matrix Riccati equation for linear optimal control reduces to a series of n_C independent 2×2 matrix equations for each of the controlled modes. It follows that, in the case of IMSC, the modal gain matrices G and H in Eq. (6) are diagonal. Equation (6) yields the modal control forces, from which we obtain the actuator forces

$$u(t) = (\Phi_C^T D)^{-1} f_C(t) \tag{12}$$

When the number of controlled modes and actuators is not the same, the exact inverse $(\Phi_C^T D)^{-1}$ in Eq. (12) can be replaced by a pseudoinverse, but the modal forces will be only approximately independent, depending how close $\Phi_C^T D$ is to a square matrix.

In optimal IMSC, the weighting matrices for the modal space quadratic performance index are assumed to be diagonal, so that the performance index for the steady-state case can be expressed as the sum of independent modal performance indices in the form

$$J = \frac{1}{2}\int_0^\infty (x^T Qx + f_C^T R f_C)\, dt$$

$$= \frac{1}{2}\sum_{r=1}^{n_C}\int_0^\infty (\dot{\eta}_r^2 + \omega_r^2\eta_r^2 + r_r f_r^2)\, dt \tag{13}$$

As a result, the $2n_C \times 2n_C$ matrix algebraic Riccati equation reduces to n_C independent 2×2 matrix algebraic Riccati equations. The latter have the analytic solution

$$g_r = \omega_r\sqrt{\omega_r^2 + r_r^{-1}} - \omega_r^2$$
$$h_r = \sqrt{r_r^{-1} + 2g_r}, \qquad r = 1, 2, \ldots, n_C \tag{14}$$

One choice of control design variables is the modal control force weighting factors $v_c = [r_1 r_2 \ldots r_{n_C}]^T$, because they determine the modal gains for IMSC optimal control uniquely. Alternatively, all of the r_r could be eliminated by using Eqs. (14) to solve for each h_r in terms of g_r, or vice versa. In the former case,

$$h_r(g_r, \omega_r) = \sqrt{r_r^{-1} + 2g_r}, \qquad r_r^{-1} = \left(\frac{g_r + \omega_r^2}{\omega_r}\right)^2 - \omega_r^2 \tag{15}$$

whereas in the latter case,

$$g_r(h_r, \omega_r) = \left[\sqrt{4 + \left(\frac{h_r}{\omega_r}\right)^2} - 2\right]\omega_r^2 \tag{16}$$

Now, either the g_r or the h_r can be taken as control design variables.

Pareto Optimal Solutions

A natural approach to integrating design requirements from two or more disciplines is to optimize a vector of cost functions. Ideally, all of the criteria in the vector would be optimized simultaneously. Because all criteria cannot be optimized at once, an understanding of what constitutes a vector optimum is required. Following Koski,[23] we state the multiobjective (multicriteria or vector) optimization problem as

$$F^*(v^*) = \min_{v \in \Omega} F(v) \tag{17a}$$

where $F:\Omega \rightarrow R^m$ is a vector objective function

$$F(v) = \lfloor F_1(v)\ F_2(v)\ \ldots\ F_m(v) \rfloor^T \tag{17b}$$

and its components $F_i:\Omega \rightarrow R$, $i = 1, 2, \ldots, m$ are the criteria. The design variable vector $\boldsymbol{v}$ belongs to the feasible set $\Omega \subset R^n$, defined by the vectors $\boldsymbol{h}$ and $\boldsymbol{g}$ of equality and inequality constraints, respectively, as

$$\Omega = \{v \in R^n \,|\, \boldsymbol{h}(v) = 0,\ \boldsymbol{g}(v) \leq 0\} \tag{17c}$$

where vector inequalities are understood to apply individually to each component of the vector. (Distinction between the vectors $\boldsymbol{g}$ and $\boldsymbol{h}$ for constraint functions and modal gains g_r and h_r should be clear from the context of the equations.) In general, no unique point exists that optimizes all m criteria simultaneously. Pareto defined the vector optimum v^* as that for which there exists no feasible vector v that would decrease some criterion without simultaneously increasing at least one other criterion.

A popular technique for generating Pareto minima is the constraint method.[23] In this method the vector optimization is replaced by

$$F_k^*(v^*) = \min_{v \in \Omega \cap \Omega_k(\varepsilon)} F_k(v) \tag{18a}$$

where

$$\Omega_k(\varepsilon) = \{v : F_i(v) \leq \varepsilon_i,\ i \neq k\} \tag{18b}$$

and

$$\varepsilon \in E_k = \{\lfloor \varepsilon_1 \varepsilon_2 \ldots \varepsilon_{k-1} \varepsilon_{k+1} \ldots \varepsilon_m \rfloor^T\} : \Omega(\varepsilon) \neq \emptyset \tag{18c}$$

One criterion is taken as a scalar objective function whereas the remaining are constrained by a set of constants ε_i such that a feasible solution exists. Again, parametric variation of the ε_i generates a set of Pareto minima. An important implication for the problem under consideration is that any single objective function may be minimized whereas the others are treated as constraints. The choice of criterion is at our discretion. The same Pareto optimal designs should be generated by minimizing either structural weight or the quadratic performance index, for example, while constraining the other. Of course, this assumes that each scalar optimization finds the global minimum or that the same set of local minima will be found for each choice of objective function. The constraint method is the basis for seeking Pareto optimal solutions of this research. Thus, the focus is on determining efficient methods to solve Eqs. (18) for the integrated structural and control problem.

Theoretical Development

Performance Index for Integrated Structural and Control Design

In using the LQR theory[3] for optimal control, one determines a control law that minimizes a quadratic performance index for a given positive semidefinite state weighting matrix Q and a positive definite control weighting matrix R. The choice of weighting matrices is otherwise at the discretion of the control designer. Each choice produces a different optimal control. In practice, the designer alters Q and R to balance system performance and control effort. As an example, one particular choice might result in saturation of an actuator in some simulation. Then, the designer might increase the weighting factor(s) associated with that actuator. In this sense, the performance index is not used to compare candidate control laws. Instead, other criteria are used as a basis for comparison in the simulations. The dilemma is compounded in integrated structural and control design, in which performance for different plants and control laws must be compared. Therefore, the question of an appropriate performance measure for controls is a critical one. We propose here that the time integral of the total system energy be used as the single, unique, and physically meaningful performance measure. The total system energy consists of the kinetic and elastic potential energy and the energy expended by the control system. As mentioned in the literature review, the structural energy has been used frequently to define a unique state weighting matrix Q. Defining the control weighting matrix R is more arbitrary. Two interpretations of "control effort" are considered next.

The control effort in the performance index is taken to represent the energy expended by the control system, which is often assumed to be proportional to the square of the control inputs. When the input represents an actuator force, the energy to actuate certain mechanical systems might be proportional to the square of each actuator's force. In this case, we expect the energy expended by each actuator to be independent of the others, in which case R is diagonal. Assuming that the proportionality factors of each actuator are known a priori, we consider a performance measure for the system defined by Eq. (1) in the form

$$J = \frac{1}{2}\int_0^\infty \left(\begin{Bmatrix} \boldsymbol{q} \\ \dot{\boldsymbol{q}} \end{Bmatrix}^T \begin{bmatrix} K_s & 0 \\ 0 & M \end{bmatrix} \begin{Bmatrix} \boldsymbol{q} \\ \dot{\boldsymbol{q}} \end{Bmatrix} + \boldsymbol{u}^T R \boldsymbol{u} \right) dt \tag{19}$$

where R is a unique weighting matrix of factors for the control energy.

Before proceeding any further, let us consider alternative measures for the control effort. The weighting matrix $R = D^T K^{-1} D$ was proposed by Venkayya and Tischler[8] and employed by Rao[20] and Belvin and Park.[18] This weighting matrix provides a quasistatic measure of the energy imparted to the structure by the control system. It can be derived by assuming that the forces are applied quasistatically to the structure by the control $\boldsymbol{Du}(t)$. The elastic energy imparted to the structure has the expression

$$(1/2)[\boldsymbol{Du}(t)]^T \tilde{\boldsymbol{q}}(t) = (1/2)\,[\boldsymbol{Du}(t)]^T K^{-1} \boldsymbol{Du}(t)$$
$$= (1/2)\,\boldsymbol{u}^T(t) R \boldsymbol{u}(t) \tag{20}$$

where $\tilde{\boldsymbol{q}}(t)$ represents the static displacement due to the quasi-static force $\boldsymbol{Du}(t)$. However, one could as well consider the energy imparted to the structure by the control force vector $\boldsymbol{Du}(t)$ applied impulsively. Both are approximate measures of the actual energy used by the control system to do work on the structure.

Next, we consider the actual work done by the actuator forces, or

$$W = \int_0^t \dot{\boldsymbol{q}}^T F(t)\,dt = \int_0^t \dot{\eta}^T \boldsymbol{f}(t)\,dt = W_C + W_R \tag{21}$$

where

$$W_C = \int_0^t \dot{\eta}_C f_C(\tau)\,dt, \qquad W_R = \int_0^t \dot{\eta}_R f_R(\tau)\,dt \tag{22}$$

are the work done by the controlled modes and by the residual modes, respectively. At this point, we define the useful work as the work done by the actuator forces on the controlled modes, i.e., W_C, and note that for IMSC we can evaluate W_C analytically. Because the modal forces are linear in the state variables, we assume that the integral has a quadratic form, or

$$\int_0^t \dot{\eta}_C^T(\tau) f_C(\tau)\,d\tau = \boldsymbol{x}^T(t) R \boldsymbol{x}(t) \tag{23}$$

in which $\boldsymbol{x} = [\eta_C^T \;\; \dot{\eta}_C^T]^T$ is the modal state vector. Differentiating both sides of Eq. (23) with respect to time, we have

$$\dot{\eta}_C^T(t) f_C(t) = \dot{\boldsymbol{x}}^T(t) R \boldsymbol{x}(t) + \boldsymbol{x}^T(t) R \dot{\boldsymbol{x}}(t) \tag{24}$$

Substituting $\boldsymbol{x} = [\eta_C^T \;\; \dot{\eta}_C^T]^T$ and Eq. (6) into the left side of Eq. (24) and Eq. (9) into the right side, we obtain

$$\boldsymbol{x}^T \begin{bmatrix} 0 & -(1/2)G \\ -(1/2)G & -H \end{bmatrix} \boldsymbol{x} = \boldsymbol{x}^T [A_c^T R + R A_c] \boldsymbol{x} \tag{25}$$

Equation (25) will be satisfied for an arbitrary state only if the matrices in brackets are equal. Because for IMSC the various submatrices are diagonal, insertion of Eq. (10) into Eq. (25) yields

$$R = \frac{1}{2} \begin{bmatrix} \bar{G}\bar{H}^{-1} H - G & 0 \\ 0 & \bar{H}^{-1} H \end{bmatrix} \tag{26}$$

where $\bar{G}$ and $\bar{H}$ are defined by Eqs. (11). When no natural damping is present $\bar{H} = H$ and Eq. (26) reduces to

$$R = \frac{1}{2} \begin{bmatrix} \Omega_C^2 & 0 \\ 0 & I \end{bmatrix} \tag{27}$$

which is precisely equal to the modal state weighting matrix Q rendering $(1/2)\boldsymbol{x}^T Q \boldsymbol{x}$ the sum of kinetic and strain energy. This result is to be expected, because for a conservative structural system the change in energy from the initial time to a quiescent state at the final time must be dissipated entirely by the control system. Hence, if we define control effort as the useful work done by the control system, it is sufficient to merely include the state weighting matrix in the performance index. It is important to stress here that Eq. (19) with $R = 0$ represents a performance index for comparing two systems and not a performance index used to derive LQR control gains.

In summary, in seeking an appropriate and physically meaningful control performance measure we arrived at two alternatives. One employs the unique matrix R in Eq. (19) yielding the energy expended by the actuators over time, assuming that such a characterization of the control system is available. In the absence of knowledge about R, the second alternative is to consider the useful work done by the control system over a given time interval. For a conservative plant the useful work is simply the change in internal energy of the plant. Therefore, when comparing two systems, it is sufficient to use the unique state weighting matrix that produces the total structural energy and let $R = 0$ when comparing two systems. Of course, the second choice ignores control spillover, which must be small for any feasible system. We also assumed the control gains were such that the actuators did not reach saturation. Next, we derive the time-invariant form of the performance index and formulate constraints for the actuator forces.

Independent Model Space Control Time-Invariant System Energy

We wish to minimize the time integral of the system energy, Eq. (19), as a function of the vector of structural parameters ν_s determining the natural frequencies and the vector of control parameters ν_c determining the control gains. Because the plant and control are taken to be time invariant, the performance index can be expressed without regard to time, assuming that the closed-loop system is stable. The performance index, Eq. (19), can be written in the partitioned modal state space form

$$J = \begin{Bmatrix} \eta_C(0^+) \\ \dot{\eta}_C(0^+) \end{Bmatrix}^T \begin{bmatrix} P_{11} & P_{12} \\ P_{12}^T & P_{22} \end{bmatrix} \begin{Bmatrix} \eta_C(0^+) \\ \eta_C(0^+) \end{Bmatrix} \tag{28}$$

The positive definite symmetric coefficient matrix P is a solution to the Lyapunov equation

$$Q_c + A_c^T P + P A_c = 0 \tag{29}$$

for

$$Q_c = \begin{bmatrix} \Omega^2 & 0 \\ 0 & I \end{bmatrix} + [G_\eta \;\; H_\eta]^T R [G_\eta \;\; H_\eta] \tag{30}$$

where G_η and H_η relate the actuator forces to modal coordinates according to

$$u(t) = -G_\eta \eta_C - H_\eta \dot{\eta}_C \tag{31}$$

The use of IMSC in formulating Eqs. (28–30) has significant implications. First, the actuator gains can be synthesized from the modal control gains by means of Eq. (6) or

$$G_\eta = (\Phi_C^T D)^{-1} G, \qquad H_\eta = (\Phi_C^T D)^{-1} H \tag{32}$$

As a result, even if R is diagonal in Eq. (30), the modes recouple Eq. (29) via Eqs. (32). However, choosing $R = 0$ becomes quite attractive when using IMSC. Then Q_c becomes diagonal, thus decoupling Eq. (29) and permitting an analytical determination of the diagonal partition matrices of P. Indeed, inserting

$$P = \begin{bmatrix} P_{11} & P_{12} \\ P_{12}^T & P_{22} \end{bmatrix} \tag{33}$$

and Eqs. (10), (11), and (30) in to Eq. (29), we obtain

$$p_{11_i} = \frac{\omega_i^2 (2\zeta_i \omega_i + h_i)}{2(\omega_i^2 + g_i)} + \frac{2\omega_i^2 + g_i}{2(2\zeta_i \omega_i + h_i)} \tag{34a}$$

$$p_{12_i} = \frac{\omega_i^2}{2(\omega_i^2 + g_i)} \tag{34b}$$

$$p_{22_i} = \frac{2\omega_i^2 + g_i}{2(\omega_i^2 + g_i)(2\zeta_i \omega_i + h_i)}, \qquad i = 1, 2, \ldots, n_C \tag{34c}$$

A critical assumption must be examined for properly minimizing the integrated objective function, Eq. (28). An arbitrary external disturbance for a fixed plant is often assumed to induce an arbitrary initial state of unknown direction but constant magnitude. Minimizing Eq. (28) for this case is then shown to be equivalent to

$$\min J \Leftrightarrow \min [\mathrm{tr}(P)] \tag{35}$$

In earlier approaches to the integrated problem, this assumption has often been made in a casual manner. However, if design of the plant itself is under consideration, the initial state depends on the structural properties. Indeed, an arbitrary external disturbance of given magnitude produces a corresponding initial state depending on the as yet undetermined stiffness and mass of the structure. Therefore, the sensitivity of the initial state $\partial x_0/\partial v_{si}$ cannot be ignored. Calculating $\partial x_0/\partial v_{si}$ involves the assumption of a certain disturbance, e.g., an impulsive force of given magnitude or at least assumed statistics governing the nature of the disturbance. The same assumptions apply to calculating actuator forces, as well. For a given disturbance, the derivative of the performance index, Eq. (28), with respect to structural and control variables is

$$\frac{\partial J}{\partial v_i} = x_0^T \frac{\partial P}{\partial v_i} x_0 + 2 x_0^T P \frac{\partial x_0}{\partial v_i} \tag{36}$$

Sensitivity of the first term requires differentiation of Eq. (29). The second term in Eq. (36) involves structural variables only. Both terms are included in the following derivation for the IMSC performance index.

Consider an impulsive disturbance represented by the force vector $\hat{Q}\delta(t)$ where $\hat{Q}$ is the intensity vector and $\delta(t)$ is the Dirac delta function. Solution of the modal counterpart to Eq. (1) with the right side replaced by the impulsive force $\hat{Q}\delta(t)$ results in the initial modal velocities

$$\dot{\eta}(0^+) = \Phi^T(v_s)\hat{Q} \tag{37}$$

By substitution of Eq. (37) into Eq. (28), the performance index can be simplified to

$$J = \dot{\eta}^T(0^+) P_{22} \dot{\eta}^T(0^+) = (\Phi_C^T \hat{Q})^T P_{22} (\Phi_C^T \hat{Q})$$

$$= \hat{\Phi}^T P_{22} \hat{\Phi} = \sum_{i=1}^{n_C} p_{22_i} \hat{\phi}_i^2 \tag{38}$$

where $\hat{\phi}_i$ is the ith component of the vector $\hat{\Phi} \equiv \Phi_C^T \hat{Q}$, so that the control objective represented by Eq. (38) a simple weighted sum of the diagonal elements of $P_{22}(v_s, v_c)$. It should be pointed out here that an initial condition due to an impulse is more realistic than a static preload and applies to unconstrained as well as to constrained structures. Sensitivity of the integrated IMSC performance index for an impulsive disturbance, Eq. (38), is considered in the next section.

Independent Modal Space Control Performance Index Derivatives

Differentiation of Eq. (38) with respect to the structural variables leads to

$$\frac{\partial J}{\partial v_{sk}} = \sum_{i=1}^{n_C} \left(2 p_{22_i} \hat{\phi}_i \frac{\partial \hat{\phi}_i}{\partial v_{sk}} + \frac{\partial p_{22_i}}{\partial v_{sk}} \hat{\phi}_i^2 \right) \tag{39}$$

The partial derivative term $\partial \hat{\phi}_i / \partial v_{sk}$ in Eq. (39) requires natural eigenvector derivatives. An explicit expression for the partial derivative term

$$\frac{\partial p_{22_i}}{\partial v_{sk}} = \frac{h_i}{4(\omega_i^2 + g_i)^2 \sqrt{4 + h_i^2/\omega_i^2}} \frac{\partial \omega_i^2}{\partial v_{sk}} \tag{40}$$

was derived by differentiating Eq. (34c). The structural frequency derivative in Eq. (40) is well known.[1] Note that its coefficient on the right side of Eq. (40) is positive,

$$\frac{\partial p_{22_i}}{\partial \omega_i^2} > 0 \tag{41}$$

so that, ignoring the modal sensitivity appearing in Eq. (39), we conclude that a reduction of the performance index implies a reduction of structural frequencies, i.e., a softening of the structure. This result is in opposition to the heuristic conclusion reached by Belvin and Park,[18] but agrees with the observation of Messac et al.[19]

Differentiation of Eq. (38) with respect to the control design variables leads to

$$\frac{\partial J}{\partial v_{ck}} = \frac{\partial p_{22_k}}{\partial v_{ck}} \hat{\phi}_k^2 \tag{42}$$

The partial derivative with respect to a control design variable is the partial derivative with respect to the IMSC modal rate gain, $v_{ck} = h_k$. Hence, by differentiating Eq. (34c) and using Eq. (16) for optimal IMSC gains, the partial derivative on the right side of Eq. (42) can be shown to have the form

$$\frac{\partial p_{22_i}}{\partial h_i} = \frac{-\omega_i^2}{2(\omega_i^2 + g_i)^2 \sqrt{4 + h_i^2/\omega_i^2}} - \frac{\omega_i^2 + g_i/2}{h_i^2 (\omega_i^2 + g_i)} \tag{43}$$

and note that $\partial p_{22_i}/\partial h_i < 0$ so that decreasing the performance index implies increasing the modal gains, as expected. However, the modal gains will be prevented from becoming infinitely large by constraints on the actuator forces posed in the next section.

Actuator Force Constraints

Actuator forces are constrained to be smaller than some maximum magnitude for all time. To create a finite number of constraints for the integrated optimization, the actuator inputs (forces) can be evaluated at only a few peak times. Peak actuator forces occur either at $t = 0$ or when the derivative of the force with respect to time vanishes. In the first case, the peak inputs for each actuator are easily determined from $u(0^+) = -\hat{G}x_0$. Inserting Eqs. (6) and (37) into Eq. (12), the initial IMSC actuator forces corresponding to an initial velocity caused by an impulse of intensity $\hat{Q}$ are

$$u(0^+) = -(\Phi_C^T D)^{-1} H \Phi_C^T \hat{Q} \tag{44}$$

Subsequent peak inputs first require determination of the peak times from the transcendental equation resulting from differentiating the scalar form of Eq. (12)

$$0 = \left. \frac{\partial u_j(t)}{\partial t} \right|_{\hat{t}} = -\hat{G}_j A_c x(\hat{t}) , \qquad \forall \in N_u \tag{45}$$

where $\hat{G}_j$ represents the jth row of the gain matrix $\hat{G}$. Solution of Eq. (45) generates a set of p_j peak times $T_j = \{\hat{t}_1, \ldots, \hat{t}_{pj}\}$ for each of the n_u inputs. For IMSC the modal states are known explicitly in terms of the design variables and time.[24]

Actuator Force Derivatives

Consider first the actuators forces at time $t = 0^+$ due to an impulse. The initial state vector

$$x(0^+) = \begin{Bmatrix} 0 \\ \Phi_C^T \hat{Q} \end{Bmatrix} \tag{46}$$

does not vary with time or control variables, only with structural variables. Therefore, we divide the possible derivatives into those that depend on structural variables v_s and those that depend on control variables v_c. Differentiating Eq. (44) with respect to struc-

tural variables first and noting that H does not depend explicitly on v_{sk}, we have

$$\frac{\partial u(0^+)}{\partial v_{sk}} = -(\Phi_C^T D)^{-1}\left[H\frac{\partial(\Phi_C^T\hat{Q})}{\partial v_{sk}} - \frac{\partial \Phi_C^T}{\partial v_{sk}} D(\Phi_C^T D)^{-1} H(\Phi_C^T\hat{Q})\right] \tag{47}$$

$$k = 1, \ldots, n_s$$

where the modal gradients $\partial\Phi_C/\partial v_{sk}$ were first encountered in Eq. (39). Differentiation of Eq. (44) with respect to control variables yields

$$\frac{\partial u(0^+)}{\partial v_{ck}} = -(\Phi_C^T D)^{-1}\frac{\partial H}{\partial v_{ck}}(\Phi_C^T\hat{Q}), \qquad k = 1, \ldots, n_c \tag{48}$$

The modal rate gains along the diagonal H are themselves the control design variables, so that $\partial H_C/\partial v_{ck}$ is a matrix of all zeros, except for entry in the kth row and column which is equal to one. Actuator force derivatives at subsequent peak times can also be derived,[24] but were not considered in the examples to follow.

Example: Simply Supported Beam with Three Actuators

The performance index, Eq. (38), was minimized for the purpose of designing the IMSC modal gains for a uniform beam with three actuators, described in Ref. 3 (Fig. 1). The material properties are given in unspecified consistent units such that $EI/(mL^4) = 1$. The disturbance was a unit impulse at $0.43L$. The force actuators were located $0.15L$, $0.55L$, and $0.73L$ of the span. Coupled control to damp out the first eight modes produced a maximum actuator force of magnitude 3.8 units.[3] The first 12 modes were used to simulate the closed-loop response of the beam to the unit impulse. Time histories of the midspan deflection of the beam and the corresponding actuator forces appear in Fig. 2 for three cases using IMSC, described next.

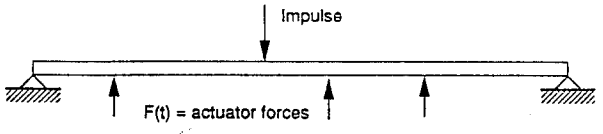

Fig. 1 Simply supported beam with three actuators.

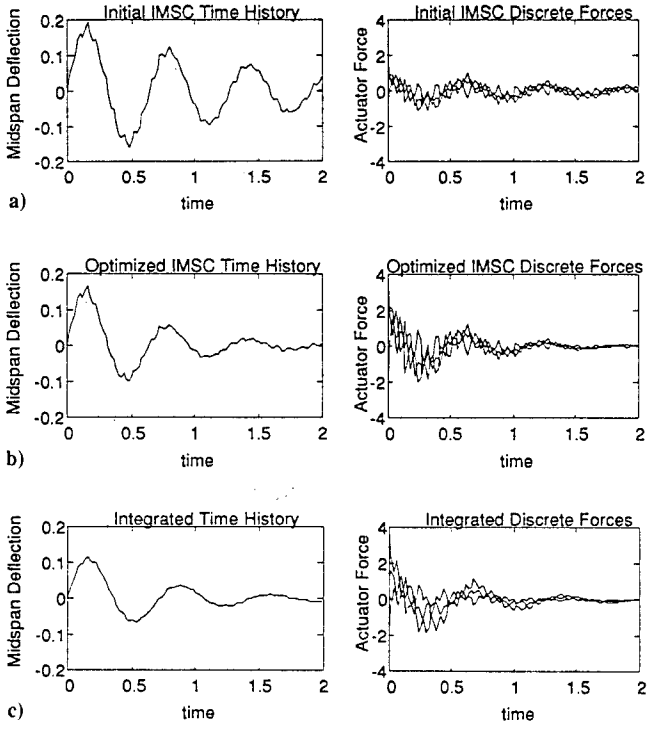

Fig. 2 Time histories of beam with three actuators.

Table 1 Independent modal space control gains for simply supported beam

Case	Mode i	ρ_i	g_i	h_i	ζ_i
Initial	1	1.0	0.4987	1.4133	0.0714
IMSC	2	1.0	0.4999	1.4142	0.0179
	3	1.0	0.5000	1.4142	0.0080
Optimized	1	0.1769	2.7874	3.3510	0.1674
IMSC	2	0.1391	3.5909	3.7910	0.0480
	3	0.1639	3.0500	3.4930	0.0197
Optimized	1	0.1955	2.517	3.186	0.1782
structure	2	0.0989	5.045	4.494	0.0614
and IMSC	3	0.1505	3.322	3.646	0.0199

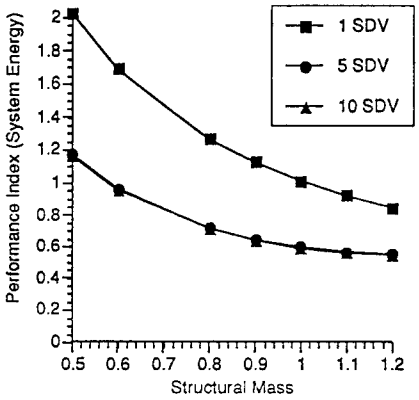

Fig. 3 Pareto optima for simply supported beam.

IMSC was used to control only the first three modes. For unit values of the modal control weighting factors r_r in Eq. (13), actuator forces were lower and their time history smoother than for coupled control, but at the expense of decreased damping. Next, IMSC modal gains were treated as design variables and Eq. (28) was minimized subject to constraints on each actuator force. The upper limit on the actuator forces, 3.8 units, was taken as the maximum value from the original example. Only a single call to an IMSL nonlinear optimization subroutine was needed. Results in Fig. 2b demonstrate higher damping and a 14% reduction in the maximum deflection without saturating the actuators. The modal control weighting factors and IMSC modal gains for each case are given in Table 1. This case represents the best performance possible by optimizing control gains alone without design structural variables. In other words, it is the optimal control for a fixed structure.

Next, structural design variables were introduced. To establish the relationship between bending and inertia properties (i.e., EI and mL), a particular cross-sectional shape was specified. A circular tube of outer radius $R = L/100$ and thickness $t = R/10$ was considered. Thickness was selected as the structural design variable while the outside radius remained fixed. The minimum thickness allowed was $t_{\min} = R/40$, whereas the maximum thickness was $t_{\max} = R/5$. To approximate the continuous distribution of material along the span, an Euler-Bernoulli beam was modeled using 100 finite elements. Each structural design variable controlled the thickness of a group of elements located symmetrically about the midspan. The performance index, Eq. (38), was minimized while requiring no increase in total mass and limiting the actuator forces. Also, the fundamental natural frequency was constrained to be at least 80% of its initial value. The integrated optimization problem may be stated as minimizing the system energy

$$\min_{v_c, v_s} J(v_c, v_s) \tag{49a}$$

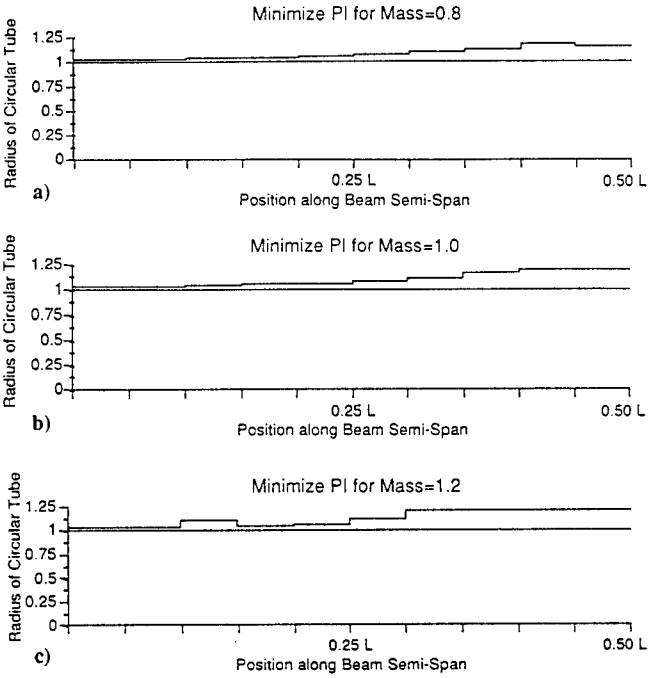

Fig. 4 Optimum beam profiles for 10 structural design variables.

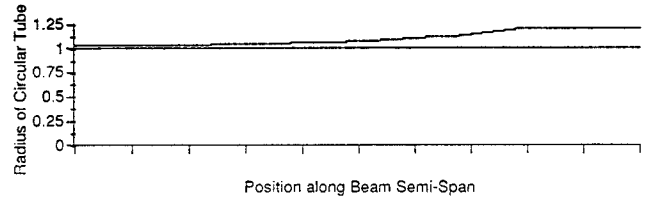

Fig. 5 Optimum beam profile for 50 structural design variables.

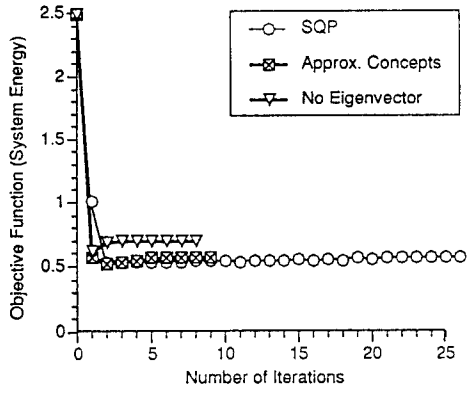

Fig. 6 Iteration histories for mass = 1.

subject to behavior constraints on nondimensional mass, fundamental frequency, and actuator constraints,

$$m(v_s) \le 1 \tag{49b}$$

$$\omega_1^2(v_s) \ge 0.8\,(\omega_1^2)_0 \tag{49c}$$

$$u_j(v_c, v_s, t) \le 3.8, \qquad j = 1, 2, 3 \tag{49d}$$

as well as side constraints

$$R/40 \le v_{sk} \le R/5, \qquad k = 1, 2, \ldots, 10 \tag{49e}$$

$$0 < v_{ck}, \qquad k = 1, 2, 3 \tag{49f}$$

Structural design variables v_s (tube thickness) and control design variables v_c (modal gains) were determined simultaneously. The time history in Fig. 2c indicates a 29% reduction in maximum amplitude without loss of damping or exceeding the actuator limit. This third case demonstrates the benefit of multiobjective optimization. Performance improvement over Fig. 2b was achieved by simultaneously determining control design variables and structural design variables.

Pareto optimal solutions were generated by parametrically varying the mass constraint. The resulting Pareto optimal sets in Fig. 3 show that not many structural design variables (SDV) were needed to approximate the Pareto optimal objective function values. Results for more than 10 structural design variables were not shown because they were indistinguishable from the curve for 10 variables. The same Pareto curves were generated by minimizing the mass subject to a constrained performance index. The resulting beam profiles in Fig. 4 for minimizing the performance index with 10 structural design variables were identical to those found by minimizing mass. Of course, the true optimum structural design entails a continuously varying cross section, simulated in Fig. 5 by using 50 structural design variables for mass constrained to unity (a refinement of Fig. 4b).

The effect of the eigenvector derivative terms appearing in Eq. (42) is demonstrated by the iteration histories given in Fig. 6. The curve labeled "SQP" represents a solution of the integrated optimization problem using sequential quadratic programming to solve Eqs. (49) directly. The curve labeled "Approx. Concepts" is a more efficient solution in which all structural and control functions are approximated by first- or second-order Taylor series.[24] The resulting approximate subproblem was solved iteratively until it converged to the exact solution found by SQP. The third curve, labeled "No Eigenvector," was an attempt to solve the integrated problem while ignoring the first term in the summation of Eq. (42). Without the eigenvector sensitivity, the solution converged to a distinctly different nonoptimal design with higher system energy. This alternate design was achieved only when using approximation concepts. The direct SQP algorithm failed to converge at all when eigenvector derivatives were ignored.

Conclusion

The integrated structural and control design problem was posed as a multiobjective optimization problem. The total energy integrated over time was identified as the performance index for constant feedback gain closed-loop control. Independent modal space control enabled a closed-form solution of the system energy as a function of open-loop frequencies, modal damping, and modal gains. Peak actuator forces were constrained to be within prescribed limits. Pareto optima for the multiobjective optimization problem were generated using the constraint method. The resulting scalar optimization problem was efficiently solved by forming an explicit approximate subproblem. Results revealed that eigenvector sensitivity was important to converging to the integrated optimum. More importantly, an integrated design approach clearly improved the performance of the closed-loop system without an increase in structural mass. Once the superiority of the integrated approach was established, Pareto optimal curves were developed to illustrate the extent to which structural mass changes could affect the closed-loop performance index.

Several important insights were gained from this research. First, a unique and physically meaningful performance index such as the total system energy lends itself to a fair comparison among candidate structural and control systems. Furthermore, IMSC offered the advantage not only of computational efficiency, but more importantly, it permitted the derivation of explicit expressions for the performance index and its derivatives. We infer from these derivatives that the total energy in the system imparted by an impulsive disturbance is reduced by softening the structure, i.e., by reducing its natural frequencies. Moreover, the eigenvector derivatives account for the effect structural changes have on the initial condition resulting from fixed external disturbances. The open-loop modes also determine the effectiveness of actuators. Thus, structural changes may help satisfy constraints on actuator forces.

Explicit actuator force constraints were incorporated as the physical means by which control gains were bounded. This approach of minimizing the system energy and structural mass subject to constraints on frequencies and actuator forces made integrated structural and control design a tractable problem. The use of IMSC and the selection of modal gains as the control design variables were the key to producing computational solutions for Pareto optimal designs, thus demonstrating the tradeoff between structural and control objectives.

Acknowledgment

This work was supported in part by the Air Force Office of Scientific Research AFOSR Grant 91-0351, monitored by Spencer T. Wu. The support is greatly appreciated.

References

[1]Fox, R. L., *Optimization Methods for Engineering Design*, Addison-Wesley, Reading, MA, 1971.

[2]Vanderplaats, G. N., *Numerical Optimization Techniques for Engineering Design: With Applications*, McGraw-Hill, New York, 1984, pp. 1–21.

[3]Meirovitch, L., *Dynamics and Control of Structures*, Wiley, New York, 1990, pp. 305–333.

[4]Hale, A. L., Lisowski, R. J., and Dahl, W. E., "Optimal Simultaneous Structural and Control Design of Maneuvering Flexible Spacecraft," *Journal of Guidance, Control, and Dynamics*, Vol. 8, No. 1, 1984, pp. 86–93.

[5]Messac, A., and Turner, J., "Dual Structural-Control Optimization of Large Space Structures," AIAA Paper 84-1042, May 1984.

[6]Salama, M., Garba, J., Demsetz, L., and Udwadia, F., "Simultaneous Optimization of Controlled Structures," *Computational Mechanics*, Vol. 3, 1988, pp. 275–282.

[7]Haftka, R. T., Martinovic, Z. N., and Hallauer, W. L.,"Enhanced Vibration Controllability by Minor Structural Modifications," *AIAA Journal*, Vol. 23, No. 8, 1985, pp. 1260–1266.

[8]Venkayya, V. B., and Tischler, V. A., "Frequency Control and Its Effect on the Dynamic Response of Flexible Structures," *AIAA Journal*, Vol. 23, No. 11, 1985, pp. 1768–1774.

[9]Miller, D. F., and Shim, J., "Gradient-Based Combined Structural and Control Optimization," *Journal of Guidance, Control, and Dynamics*, Vol. 10, No. 3, 1987, pp. 291–298.

[10]Rew, D. W., and Junkins, J. L., "In Search of the Optimal Quadratic Regulator," *Dynamics and Control of Large Structures*, Virginia Polytechnic Inst. and State Univ./AIAA, Blacksburg, VA, 1985, pp. 109–123.

[11]Bodden, D. S., and Junkins, J. L., "Eigenvalue Optimization Algorithms for Structure/Controller Design Iterations," *Journal of Guidance, Control, and Dynamics*, Vol. 8, No. 6, 1985, pp. 697–706.

[12]McLaren, M. D., and Slater, G. L., "A Covariance Approach to Integrated Control/Structure Optimization," *Proceedings of the AIAA Dynamics Specialist Conference* (Long Beach, CA), AIAA, Washington, DC, 1990, pp. 189–205.

[13]Lust, R. V., and Schmit, L. A., "Control Augmented Structural Synthesis," *AIAA Journal*, Vol. 26, No. 1, 1988, pp. 86–95.

[14]Thomas, H. L., and Schmit, L. A., "Control-Augmented Structural Synthesis with Dynamic Stability Constraints," *AIAA Journal*, Vol. 29, No. 4, 1991, pp. 619–626.

[15]Sepulveda, A. E., Thomas, H. L., and Schmit, L. A., "Improved Transient Response Approximations for Control Augmented Structural Optimization," *Proceedings of the 2nd Pan-American Congress of Applied Mechanics*, Valparaiso, Chile, 1991, pp. 611–614.

[16]Canfield, R. A., "High Quality Approximation of Eigenvalues in Structural Optimization," *AIAA Journal*, Vol. 28, No. 6, 1990, pp. 1116–1122.

[17]Thomas, H. L., Sepulveda, A. E., and Schmit, L. A., "Improved Approximations for Control Augmented Structural Synthesis," *AIAA Journal*, Vol. 30, No. 1, 1992, pp. 171–179.

[18]Belvin, W. K., and Park, K. C., "Structural Tailoring and Feedback Control Synthesis: An Interdisciplinary Approach," *Journal of Guidance, Control, and Dynamics*, Vol. 13, No. 3, 1990, pp. 424–429.

[19]Messac, A., Gueler, R., and Malek, K., "Control-Structure Integrated Design: A Computational Approach," *Proceedings of the AIAA/ASME/ASCE/AHS 32nd Structures, Structural Dynamics, and Materials Conference* (Baltimore, MD), AIAA, Washington, DC, April 1991, pp. 553–568 (AIAA Paper 91-1161).

[20]Rao, S. S., "Combined Structural and Control Optimization of Flexible Structures," *Engineering Optimization*, Vol. 13, 1988, pp. 1–16.

[21]Meirovitch, L., *Computational Methods in Structural Dynamics*, Sijthoff and Noordhoff, Alphen aan den Rijn, The Netherlands, 1980, pp. 60–62, 210–212.

[22]Meirovitch, L., Baruh, H., Montgomery, R. C., and Williams, J. P.,"Nonlinear Natural Control of an Experimental Beam," *Journal of Guidance, Control, and Dynamics*, Vol. 7, No. 4, 1984, pp. 437–442.

[23]Koski, J., "Multicriterion Optimization in Structural Design," *New Directions in Optimum Structural Design*, edited by E. Atrek, R. H. Gallagher, K. M. Ragsdell, and O. C. Zienkiewicz, Wiley, New York, 1984, pp. 483–503.

[24]Canfield, R. A., *Integrated Structural Design, Vibration Control, and Aeroelastic Tailoring by Multiobjective Optimization*, Ph.D. Dissertation, Dept. of Engineering Science and Mechanics, Virginia Polytechnic Institute and State Univ., Blacksburg, VA, Dec. 1992.

AIAA-94-1491

Vibration and Static Aeroelastic Instability of Nonuniform, Thin-Walled Beam Composite Wings

L. Librescu, L. Meirovitch and O. Song
Department of Engineering Science and Mechanics
Virginia Polytechnic Institute and State University
Blacksburg, VA 24061

AIAA/ASME/ASCE/AHS/ASC
35th Structures, Structural Dynamics, and Materials Conference
April 18-20, 1994
Hilton Head, SC

Vibration and Static Aeroelastic Instability of Nonuniform, Thin-Walled Beam Composite Wings†

L. Librescu*, L. Meirovitch** and O. Song***
Department of Engineering Science and Mechanics
Virginia Polytechnic Institute and State University
Blacksburg, VA 24061

Abstract

The equations of motion for a nonuniform, anisotropic thin-walled beam are derived and applied to the study of vibration and static aeroelastic instability of slender tapered aircraft wings made of advanced composite materials. Numerical results illustrate the effects of anisotropy, transverse shear flexibility, primary and secondary warping, as well as of wing taper ratio, and the implications of these effects on the vibrational and divergence instability characteristics are discussed.

Introduction

The demands on advanced flight vehicles to achieve the highest performance possible over the broadest range of missions has stimulated a great deal of research lately. Improvement of flight vehicle structural efficiency can be achieved by reducing weight, controling wing deformations, as well as the aeroelastic load distribution, increasing the flutter speed, increasing control effectiveness, etc. Through the use of advanced composite materials, the designer acquires a great deal of freedom in carrying out structural and aeroelastic tailoring. This amounts to taking advantage of the light weight and the cross-couplings of composite materials to optimize the response characteristics.

To permit results useful in the design of advanced flight vehicles, the structural models must be as comprehensive as possible, which implies that they must include all the essential characteristics of real aircraft structures. To meet this requirement, in a number of recent studies[1-5], a refined wing structural model of advanced flight vehicles, including many effects unexplored heretofore, was developed and the implications of the newly introduced effects were revealed.

One factor that has not received sufficient attention to date is the *nonuniformity* of the wing cross section. It seems that for composite aircraft wings modeled as *solid beams*, the only results for nonuniform wings were presented in Refs. 3 and 6. However, there appears to be no investigation of wing structures modeled as *nonuniform thin-walled beams*. It is one of the goals of this paper to develop a tapered thin-walled beam model for slender swept wings.

Due to renewed interest in flight vehicles operating at supersonic and hypersonic speeds, a biconvex cross-section profile of the wing will be considered. In addition to cross-sectional nonuniformity, the thin-walled wing model will also incorporate anisotropy and heterogeneity of the composite structure, transverse shear flexibility of the constituent materials and primary and secondary warping effects. Based on the anisotropy of the material, the ply angles inducing the most favorable elastic cross-couplings from the point of view of aeroelastic and dynamic response characteristics will be implemented.

The equations of motion and associated boundary conditions for wing structure models as described above, and permitting study the static aeroelastic behavior and vibrational response, are derived by means of the extended Hamilton's principle. Upon solving the related eigenvalue problems, the influence of the cross-sectional nonuniformity and of other nonclassical features is investigated.

Basic Assumptions

Under consideration is a structural model consisting of a thin-walled beam and intended to simulate the lifting surface of advanced flight vehicles. The cross-sectional contour has a biconvex profile, with geometrical characteristics varying linearly along the wing span. (see Fig. 1). The model incorporates the following nonclassical features (some of them used in Ref. 5):

i) Anisotropy of constituent materials,

ii) Transverse shear flexibility,

iii) Primary and secondary warping effects and

iv) A tapered wing surface with geometrically similar cross sections at all spanwise stations.

The latter requires the following linear distribution along the span of the chord $c(\eta)$, height $b(\eta)$ of the midline cross-section profile and of the offset $e(\eta)$ between

† Supported by the AFOSR Rsearch Grant 91-0351 monitored by Dr. Spencer T. Wu and Dr. Walter F. Jones. The support is greatly appreciated.
The authors are listed in alphabetical order.
* Professor.
** University Distinguished Professor. Fellow AIAA.
*** Post-Doctoral Research Associate

the aerodynamic and reference axes

$$\begin{Bmatrix} c(\eta) \\ b(\eta) \\ e(\eta) \end{Bmatrix} = [1-\eta(1-\sigma)] \begin{Bmatrix} c_R \\ b_R \\ e_R \end{Bmatrix} \tag{1}$$

where $\sigma \equiv c_T/c_R$ defines the taper ratio, $\eta \equiv z/L$ is the dimensionless spanwise coordinate, where L denotes the wing semi-span, and the subscripts R and T refer to the root and tip wing sections. Moreover,

$$R(\eta) = [1-\eta(1-\sigma)]\, R_R \tag{2}$$

in which $R(\eta)$ is the radius of curvature of the circular arc associated with the midline contour at section η, R_R is the radius of curvature of the root section of the wing. Note that points on the beam cross sections are identified by the *global* coordinates x, y, while z is the spanwise coordinate. The assumption of in-plane nondeformability of the beam cross section is also adopted.

Due to the geometrical similarity of the cross sections, the angles Θ between the axis y and the radii R taken at points $c_R/2$, $c/2$ and $c_T/2$ are equal, i.e. $\Theta_R = \Theta_T = \Theta \equiv \Theta_o$.

Kinematical Equations

In view of features iii) and iv), the primary warping function F_ω becomes a function of both s and η, i.e.,

$$F_\omega \equiv F_\omega(s,\eta) = \int_0^s [r_n(\bar{s}) - \psi]\, d\bar{s} \tag{3a}$$

where

$$\psi \equiv \psi(\eta) = \frac{2A_c(\eta)}{\beta(\eta)} \tag{3b}$$

denotes the torsional function, in which $A_c(\eta) \equiv \oint r_n(\bar{s},\eta)\, d\bar{s}$ is the cross-sectional area of the beam bounded by the midline contour at η, $s(\eta)$ denotes the arc-length measured along the circumferential coordinate (whose origin is arbitrarily but conveniently chosen), $\bar{s}$ is a dummy coordinate associated with the s-coordinate, $\oint(\cdot)ds$ denotes the integral along the closed midline contour, $r_n(s,\eta) = x(s,\eta)\frac{dy}{ds} - y(s,\eta)\frac{dx}{ds}$ denotes a geometric quantity (see Ref. 5) and $\beta(\eta) = \oint d\bar{s}(\eta)$ is the circumferential contour length at η. After lengthy calculations one obtains

$$\psi(\eta) = R(\eta)\left(1 - \frac{\sin 2\Theta_o}{2\Theta_o}\right) \tag{4a}$$

$$A_c(\eta) = R^2(\eta)(2\Theta_o - \sin 2\Theta_o) \tag{4b}$$

$$\beta(\eta) = 4R(\eta)\Theta_o \tag{4c}$$

As readily seen, in the case of the nonuniform thin-walled beam theory, ψ, A_c, β, F_ω, r_n and a are functions not only of the circumferential coordinate s but also of the spanwise coordinate z. As a result, free warping is precluded for the problem at hand.

In accordance with i)–iii), and in order to reduce the three-dimensional elasticity theory of beams to an equivalent one-dimensional one, the components of the displacement vector are expressed as

$$u(x,y,z,t) = u_o(z,t) - y(s,z)\,\phi(z,t) \tag{5a}$$

$$v(x,y,z,t) = v_o(z,t) + x(s,z)\,\phi(z,t) \tag{5b}$$

$$\begin{aligned} w(x,y,z,t) = {} & w_o(z,t) + \theta_x(z,t)\left[y(s,z) - n\frac{dx}{ds}\right] \\ & + \theta_y(z,t)\left[x(s,z) + n\frac{dy}{ds}\right] \\ & - \phi'(z,t)\left[F_\omega(s,z) + na(s,z)\right] \end{aligned} \tag{5c}$$

in which $F_\omega(s,z)$ and $na(s,z)$ are related to the primary and secondary warping functions, respectively, and n denoting the coordinate in the thickness direction. In addition,

$$a(s,z) = -y(s,z)\,dy/ds - x(s,z)\,dy/ds \tag{6a}$$

and

$$\theta_x(z,t) = \gamma_{yz}(z,t) - v_o'(z,t) \tag{6b}$$

$$\theta_y(z,t) = \gamma_{xz}(z,t) - u_o'(z,t) \tag{6c}$$

where $\theta_x(z,t)$ and $\theta_y(z,t)$ denote the rotations about axes x and y, respectively, γ_{xz} and γ_{yz} denote the transverse shear strains in the planes xz and yz, respectively, and primes denote derivatives with respect to z. The quantities $u_o(z,t)$, $v_o(z,t)$ and $u_o(z,t)$ denoting the rigid-body translations along x, y and z axes, respectively, and $\theta_x(z,t)$, $\theta_y(z,t)$ and $\phi(z,t)$ denoting the rotations about x and y axes and the twist about the z-axis, respectively, represent the unknowns of the problem.

Constitutive Equations

Consider the case of composite thin-walled beams consisting of a finite number N of homogeneous layers. It is assumed that the material of each constituent layer is linearly elastic and anisotropic and that the bonding between the layers is perfect. The three-dimensional constitutive equations for a generally orthotropic elastic material can be expressed in the matrix form

$$\begin{bmatrix} \sigma_{ss} \\ \sigma_{zz} \\ \sigma_{nn} \\ \sigma_{zn} \\ \sigma_{ns} \\ \sigma_{sz} \end{bmatrix} = \begin{bmatrix} \bar{Q}_{11} & \bar{Q}_{12} & \bar{Q}_{13} & 0 & 0 & \bar{Q}_{16} \\ \bar{Q}_{12} & \bar{Q}_{22} & \bar{Q}_{23} & 0 & 0 & \bar{Q}_{26} \\ \bar{Q}_{13} & \bar{Q}_{23} & \bar{Q}_{33} & 0 & 0 & \bar{Q}_{36} \\ 0 & 0 & 0 & \bar{Q}_{44} & \bar{Q}_{45} & 0 \\ 0 & 0 & 0 & \bar{Q}_{45} & \bar{Q}_{55} & 0 \\ \bar{Q}_{16} & \bar{Q}_{26} & \bar{Q}_{36} & 0 & 0 & \bar{Q}_{66} \end{bmatrix} \begin{bmatrix} \epsilon_{ss} \\ \epsilon_{zz} \\ \epsilon_{nn} \\ \gamma_{zn} \\ \gamma_{ns} \\ \gamma_{sz} \end{bmatrix} \tag{7}$$

where $\bar{Q}_{ij}$ denote the transformed elastic coefficients associated with the kth layer in the global coordinate system of the structure and $\gamma_{pr} = 2\epsilon_{pr}$, $p \neq r$ and ϵ_{ij} denote the components of the strain tensor. The three-dimensional dependence in Eqs. (7) can be reduced to an equivalent one-dimensional dependence in two steps. The first step, yielding the two-dimensional local constitutive equations, consists of the integration of the original three-dimensional form through the laminate thickness, while the second step, resulting in the one-dimensional form, consists of the integration of the previous form of constitutive equations along the midline contour of the beam cross-section.

In light of i) and ii), and considering Eqs. (5) and (7), the *local constitutive equations* expressed in terms of the strain measures can be shown to consist of *the equations for the stress resultants*

$$\begin{bmatrix} N_{xx} \\ N_{sx} \end{bmatrix} = \begin{bmatrix} K_{11} & K_{12} & K_{13} & K_{14} \\ K_{21} & K_{22} & K_{23} & K_{24} \end{bmatrix} \begin{bmatrix} \epsilon^0_{xx} \\ \tilde{\gamma}_{sx} \\ \phi' \\ \epsilon^n_{xx} \end{bmatrix} \tag{8}$$

the transverse shear stress resultant

$$N_{zn} = A_{44}\gamma_{zn} \tag{9}$$

and *the equations for the stress couples*

$$\begin{bmatrix} L_{xx} \\ L_{sx} \end{bmatrix} = \begin{bmatrix} K_{41} & K_{42} & K_{43} & K_{44} \\ K_{51} & K_{52} & K_{53} & K_{54} \end{bmatrix} \begin{bmatrix} \epsilon^0_{xx} \\ \tilde{\gamma}_{sx} \\ \phi' \\ \epsilon^n_{xx} \end{bmatrix} \tag{10}$$

where K_{ij} denote the modified local stiffness coefficients (see **Appendix**). Consistent with Eqs. (5), the strain components entering into the above constitutive equations are $\epsilon_{xx} = \epsilon^o_{xx} + n\epsilon^n_{xx}$, $\gamma_{sx} = \tilde{\gamma}_{sx} + \bar{\tilde{\gamma}}_{sx}$ and γ_{zn}, where

$$\epsilon^0_{xx}(s,z,t) = w_0' + x(s,z)\theta_y' + y(s,z)\theta_x' - F_\omega(s,z)\phi'' \tag{11a}$$

$$\epsilon^n_{xx}(s,z,t) = \theta_y'\frac{dy}{ds} - \theta_x'\frac{dx}{ds} - a(s,z)\phi'' \tag{11b}$$

$$\tilde{\gamma}_{sx}(s,z,t) = [u_0' + \theta_y]\frac{dx}{ds} + [v_0' + \theta_x]\frac{dy}{ds} \tag{11c}$$

$$\bar{\tilde{\gamma}}_{sx}(s,z,t) = 2\frac{Ac(z)}{\beta(z)}\phi' \tag{11d}$$

$$\gamma_{zn}(s,z,t) = [u_0' + \theta_y]\frac{dy}{ds} - [v_0' + \theta_x]\frac{dx}{ds} \tag{11e}$$

in which ϵ^o_{xx} and ϵ^n_{xx} denote the axial strain components associated with primary and secondary warping, respectively, $\tilde{\gamma}_{sx}$ and $\bar{\tilde{\gamma}}_{sx}$ represent the tangential shear strains in the mid-surface of the beam induced by transverse shear and by the twist, respectively, and γ_{zn} denotes the transverse shear strain component. The stress resultants, the stress couples and the strain measures, Eqs. (8)–(10), exhibit a two-dimensional spatial dependence, the dependence being on s and z. In the dynamical problem, they also depend on time. Moreover, in light of the dependence of A_c and β on z, the stiffness coefficients K_{13}, K_{23}, K_{43}, K_{53} depend on z, as well.

The Boundary-Value Problem

The boundary-value problem, consisting of the differential equations of motion and the boundary conditions, can be derived conveniently by means of the extended Hamilton's principle,[7] which can be stated as follows:

$$\int_{t_1}^{t_2} (\delta T - \delta V + \delta W)\, dt = 0,$$
$$\delta u_0 = \delta v_0 = \delta w_0 = \delta\theta_x = \delta\theta_y = \delta\theta = 0 \text{ at } t = t_1, t_2 \tag{12}$$

where T is the kinetic energy, V the potential energy, which is equal to the strain energy, and δW the virtual work due to nonconservative forces. The kinetic energy has the form

$$T = \frac{1}{2}\int_0^L \oint \sum_{k=1}^{N} \int_{h_{(k)}} \rho^{(k)} \left[\left(\dot{u}_0 - y(s,z)\dot{\phi}\right)^2 + \left(\dot{v}_0 + x(s,z)\dot{\phi}\right)^2 + \left\{ \left(\dot{w}_0 + y(s,z)\dot{\theta}_x + x(s,z)\dot{\theta}_y - F_\omega(s,z)\dot{\phi}'\right) + n\left(\frac{dy}{ds}\dot{\theta}_y - \frac{dx}{ds}\dot{\theta}_x - a(s,z)\dot{\phi}'\right)\right\}^2 \right] dn\,ds\,dz \tag{13}$$

On the other hand, the strain energy can be shown to have the expression

$$V = \frac{1}{2}\int_0^L \oint_c \sum_{k=1}^{N} \int_{h_{(k)}} \left\{ \sigma^{(k)}_{xx}\left[w_0' + x(s,z)\theta_y' + y(s,z)\theta_x' - F_\omega(s,z)\phi'' + n\left(\frac{dy}{ds}\theta_y' - \frac{dx}{ds}\theta_x' - a(s,z)\phi''\right)\right] + \sigma^{(k)}_{sx}\left[(u_0' + \theta_y)\frac{dx}{ds} + (v_0' + \theta_x)\frac{dy}{ds} + \frac{2Ac(z)}{\beta(z)}\phi'\right] + \sigma^{(k)}_{nx}\left[(u_0' + \theta_y)\frac{dy}{ds} - (v_0' + \theta_x)\frac{dx}{ds}\right]\right\} dn\,ds\,dz \tag{14}$$

Moreover, the virtual work of nonconservative forces can be written as

$$\delta W = \int_0^L (p_y\delta v_0 + m_z\delta\phi)\, dz \tag{15}$$

where p_y and m_z denote the lift force per unit length and aerodynamic twist moment (positive nose up) about the elastic axis.

Carrying out integrations with respect to n, s and t, we can write

$$\int_{t_0}^{t_1} \delta T dt = -\int_{t_0}^{t_1} \left[\int_0^L (I_1 \delta u_0 + I_2 \delta v_0 + I_3 \delta w_0 + (I_4 - I_9') \delta\phi + I_5 \delta\theta_y + I_7 \delta\theta_x) dz - I_9 \phi \Big|_0^L \right] dt \quad (16)$$

where I_i denote inertia terms (see **Appendix**), functions of z and t. Upon integration with respect to n and s in Eq. (14), we can write the variation in the potential energy

$$\delta V = -\int_0^L [T_z' \delta w_0 + (M_y' - Q_x)\delta\theta_y + (M_x' - Q_y)\delta\theta_x + (B_\omega'' + M_z')\delta\phi + Q_x' \delta u_0 + Q_y' \delta v_0] dz + [T_z \delta w_0 + M_y \delta\theta_y + M_x \delta\theta_x - B_\omega \delta\phi' + (B_\omega' + M_z)\delta\phi + Q_x \delta u_0 + Q_y \delta v_0] \Big|_0^L \quad (17)$$

where

$$T_z(z,t) = \oint N_{zz} ds \quad (18a)$$

$$Q_x(z,t) = \oint \left(N_{sz} \frac{dx}{ds} + N_{zn} \frac{dy}{ds} \right) ds \quad (18b)$$

$$Q_y(z,t) = \oint \left(N_{sz} \frac{dy}{ds} - N_{zn} \frac{dx}{ds} \right) ds \quad (18c)$$

$$M_x(z,t) = \oint \left(y(s,z) N_{zz} - L_{zz} \frac{dx}{ds} \right) ds \quad (18d)$$

$$M_y(z,t) = \oint \left(x(s,z) N_{zz} + L_{zz} \frac{dy}{ds} \right) \quad (18e)$$

$$M_z(z,t) = 2 \oint N_{sz} \psi(z) ds \quad (18f)$$

$$B_\omega(z,t) = \oint [F_\omega(s,z) N_{zz} + a(s,z) L_{zz}] ds \quad (18g)$$

In Eqs. (18), T_z, Q_x and Q_y denote the axial force and shear forces in the x- and y-directions, M_x, M_y and M_z denote the moments about the x-, y- and z-axes, respectively, and B_ω is the bimoment quantity. Substition of Eqs. (15)–(17) into Eq. (12), followed by the usual steps, results in the boundary-value problem for the most general case of anisotropy. The boundary-value problem consists of six differential equations of motion with variable coefficients for the displacements $u_0, v_0, w_o, \theta_x, \theta_y$ and ϕ, together with the corresponding boundary conditions. Such a set exhibits complete coupling between the various modes, i.e., primary and secondary warping, vertical and lateral bending, twist and transverse shear. It is the principal goal of structural tailoring to select the appropriate fiber orientation so as to produce desired elastic couplings between certain modes. For the problem at hand, the induced elastic couplings must play a decisive role in enhancing the free vibration and aeroelastic response characteristics of the wing structure. In this sense, the bending-twist cross-coupling is the most significant in the design of aircraft wings. The above criteria for selecting fiber orientation, together with ease of implementation in design and manufacturing, result in a ply-angle distribution governed by

$$\theta(y) = -\theta(-y). \quad (19)$$

The ply-configuration is shown in Fig. 3. According to terminology adopted in Refs. 8 and 9, structures displaying this ply-angle distribution are referred to as *circumferentially asymmetric stiffness configuration* and *symmetric configuration*, respectively.

As a result of the ply-angle distribution, Eq. (19), Hamilton's principle, Eq. (12), yields two independent boundary-value problems, referred to here as Problem A and Problem B. Problem A is of eighth order and involves the twist ϕ, the vertical bending v_0 and the vertical transverse shear θ_x. On the other hand, Problem B is of sixth order and involves the extension w_0, the lateral bending u_0 and the lateral transverse shear θ_y. For cantilevered beams, boundary-value Problem A is governed by the differential equations of motion

$$-\underline{(a_{66}\phi'')''} + (a_{73}\theta_x')' + (a_{77}\phi')' + \delta_d m_z = \delta_v(b_4 + b_5)\ddot{\phi} - \delta_v \underline{\left((b_{10} + b_{18})\ddot{\phi}'\right)'} \quad (20a)$$

$$[a_{55}(v_o' + \theta_x)]' + \underline{(a_{56}\phi'')'} + \delta_d p_y = \delta_v b_1 \ddot{v}_o \quad (20b)$$

$$(a_{33}\theta_x')' + (a_{37}\phi')' - a_{55}(v_o' + \theta_x) - \underline{a_{56}\phi''} = \delta_v(b_4 + b_{14})\ddot{\theta}_x \quad (20c)$$

to be satisfied over $0 < z < L$. Moreover, at $z = 0$ the solution of Eqs. (20) must satisfy the boundary conditions

$$\phi = 0,\ v_0 = 0,\ \theta_x = 0,\ \underline{\phi' = 0} \quad (21a-d)$$

and at $z = L$ it must satisfy the boundary conditions

$$\underline{-(a_{66}\phi'')'} + a_{73}\theta_x' + a_{77}\phi' = \underline{-\delta_v(b_{10} + b_{18})\ddot{\phi}'} \quad (22a)$$

$$a_{55}(v_o' + \theta_x) + \underline{a_{56}\phi''} = 0 \quad (22b)$$

$$a_{33}\theta_x' + a_{37}\phi' = 0, \quad \underline{a_{66}\phi'' = 0} \quad (22c,d)$$

Note that the underlined terms in Eqs. (20)–(22) are due to the warping restraint effect. Moreover, to identify the two problems to be studied, namely, the free vibration and the aeroelastic divergence instability, two

tracing quantities, δ_v and δ_d, have been introduced in Eqs. (20)-(22). For Problem A, $\delta_v = 1$ and $\delta_d = 0$, whereas for Problem B, $\delta_d = 1$ and $\delta_v = 0$.

The boundary-value Problem B is governed by the differential equations

$$(a_{41}w_o')' + [a_{44}(u_o' + \theta_y)]' = b_1\ddot{u}_o \quad (23a)$$

$$(a_{11}w_o')' + [a_{14}(u_o' + \theta_y)]' = b_1\ddot{w}_o \quad (23b)$$

$$(a_{22}\theta_y')' - a_{41}w_o' - a_{44}(u_o' + \theta_y) = (b_5 + b_{15})\ddot{\theta}_y \quad (23c)$$

and the boundary conditions

$$u_0 = 0, \quad w_0 = 0, \quad \theta_y = 0 \quad (24a\text{-}c)$$

to be satisfied at $z = 0$, as well as the boundary conditions

$$\begin{aligned} a_{41}w_o' + a_{44}(u_o' + \theta_y) &= 0 \\ a_{11}w_o' + a_{14}(u_o' + \theta_y) &= 0 \\ a_{22}\theta_y' &= 0 \end{aligned} \quad (25)$$

to be satisfied at $z = L$.

In the following, the study of the boundary-value problem A governing the vibrational and aeroelastic response behavior of wing structures will be carried out. It should be mentioned here that the stiffness terms $a_{37} = a_{73}$ and $a_{56} = a_{65}$ appearing in Eqs. (20) and (22) are responsible for the coupling between bending and twist, with the effect of a_{56} expected to be weaker than the effect of a_{37}. The boundary-value problem B involves only a single coupling term, $a_{14} = a_{41}$, coupling the lateral transverse shear and the axial extension motions. The rigidity coefficients a_{ij} and the inertia coefficients b_i appearing in Eqs. (20), (22), (23) and (25) are displayed in the **Appendix**. With the exception of a_{11} and b_1, all the other rigidities a_{ij} and inertia coefficients b_i depend on z.

Structural Tailoring for Improved Vibration and Static Aeroelastic Instability Characteristics

Static aeroelastic instability is an important factor in the design of modern aircraft. The analysis performed here addresses the problem of designing the wing so as to take advantage of structural couplings from a static aeroelastic viewpoint. This is done by using the unique directional properties of advanced composite materials. The same importance should be afforded to the vibrational characteristics, which are basic to determining the dynamic response and flutter instability and to actively controlling the wing structure.

In the case of free vibration, the terms associated with the external loadings are omitted, $\delta_d = 0$ and $\delta_v = 1$, whereas for static aeroelastic problems, the only loading terms to be retained are the ones associated with the aerodynamic lift p_y and the torsional aerodynamic moment m_z, amounting to $\delta_d = 1$ and $\delta_v = 0$. Using strip-theory aerodynamics, we can write[10]

$$p_y(z) = q_n c(z) a_o [\phi_o + \phi - v_o' \tan\Lambda] - NW/2L \quad (25a)$$

$$\begin{aligned} m_z(z) = {} & q_n c(z) a_o e(z) [\phi_o + \phi - v_o' \tan\Lambda] \\ & + q_n c(z)^2 C_{MAC} - NWd/2L \end{aligned} \quad (25b)$$

where $q_n = \frac{1}{2}\rho U_n^2$ denotes the dynamic pressure normal to the leading edge of the swept wing, $c(z)$ the chord of the wing, a_o the "corrected lift" curve slope coefficient, Λ the angle of sweep (considered positive for swept-back), $e(z)$ the offset between the aerodynamic and reference axis, ϕ_o the rigid angle of attack (measured in planes normal to the leading edge), C_{MAC} the wing section pitching moment coefficient (whose influence, as usual, is disregarded), $W/2L$ the wing weight per unit length and N the load factor normal to the wing surface.

Due to the relatively high order of the problem and the fact that the problem is characterized by variable coefficients, the solution tends to be very complex. Towards the goal of solving the two eigenvalue problems a powerful computational methodology based on the extended Galerkin method was devised. For some special cases, the solution accuracy was checked by comparing the results with the exact ones obtained via the Laplace transform method, devised by the same authors, and the agreement was found to be excellent. As a general remark, we observe from Eqs. (25) that for $\Lambda < 0$, i.e., for swept-forward wings, the aeroelastic bending-twist coupling results in an increase in $p_y(z)$ and $m_z(z)$, which in turn reduces dramatically the divergence speed.

The study of the static aeroelastic critical case implies determination of divergence instability conditions. The determination of the divergence speed leads to the solution of an eigenvalue problem, where the divergence speed plays the role of an eigenvalue. Structural tailoring applied to the vibration of wing structures must result in an increase in the eigenfrequencies without weight penalties. The determination of natural frequencies requires the solution of an eigenvalue problem as well.[7]

Uncoupled Cases for Divergence Instability

In two uncoupled cases, closed-form solutions for the divergence instability can be obtained. They correspond to a) pure bending divergence of swept wings infinitely rigid in transverse shear and b) pure torsional divergence. In the former case, eliminating $a_{56}\phi''$ from the Eqs. (20b,c), assuming a very large

torsional stiffness, letting $\theta_x \rightarrow -v_o'$ and $\delta_v = 0$, $\delta_d = 1$ and implementing a Rayleigh-quotient procedure to the resulting equation, the expression for the obtained divergence speed can be shown to be

$$(q_n)_D = \frac{-2\int_0^L a_{33}(z)\,(v_o'')^2\,dz}{a_o\,\tan\Lambda\int_o^L c(z)\,(v_o^2)'\,dz} \qquad (26)$$

This equation reveals that only a swept-forward wing ($\Lambda \rightarrow -\Lambda$) can exhibit divergence instability in pure bending. This result constitutes an extension to the case of wings modeled as thin-walled beams of that obtained in Ref. 3 for solid beams.

In the pure torsional case, assuming that the bending stiffness is large and implementing a Rayleigh quotient procedure in conjunction with Eq. (20a), one obtains

$$(q_n)_D \equiv q_D = \frac{\int_0^L \underline{(a_{66}(z))\,(\phi'')^2}\,dz + \int_0^L (a_{77}(z))\,(\phi')^2\,dz}{a_o\int_0^L c(z)e(z)\phi^2 dz} \qquad (27)$$

in which the underscored term is connected with the warping inhibition. As in the case of solid beams,[3] Eq. (27) reveals that pure torsional divergence can occur for straight wings only.

From Eq. (26), we conclude that, to increase as much as possible $(q_n)_D$, the wing structure in pure bending should be designed so that $K_{14} \rightarrow 0$, a condition resulting in an increase of the overall bending stiffness a_{33}.

Closed-Form Solution for the Divergence of Swept Forward Wings

Having the conditions corresponding to decoupled divergence in bending and torsion, Eqs. (26) and (27), respectively, a closed-form solution for the coupled divergence of swept forward wings can be established. Although approximate, for the case of solid beams,[1] the solution was shown to provide results in excellent agreement with the exact ones.

The solution for the divergence of swept forward wings is based on a linear algebraic relationships of the two decoupled expressions of the divergence instability. The linear relationship yields the expression for the divergence in the form

$$(q_n)_D = \frac{1}{a_o c_R L^2}\frac{U}{S} \qquad (28)$$

where

$$U = \frac{\int_0^1 \left[\frac{A_{66}}{L^2}\frac{a_{66}(z)}{a_{77}(z)}\left(\frac{d^2\phi}{d\eta^2}\right)^2 + A_{77}\left(\frac{d\phi}{d\eta}\right)^2\right]d\eta}{\int_0^1 CE\phi^2 d\eta} \qquad (29a)$$

and

$$S = \frac{e_R}{(a_{77})_R} - \frac{UL\tan\Lambda\int_0^1 C\frac{d\,(v_o^2)}{d\eta}d\eta}{2\,(a_{33})_R\int_0^1 A_{33}\left(\frac{d^2 v_o}{d\eta^2}\right)^2 d\eta} \qquad (29b)$$

In Eqs. (29), $A_{66} = a_{66}/(a_{66})_R$, $A_{77} = a_{77}/(a_{77})_R$ and $A_{33} = a_{33}/(a_{33})_R$ are normalized stiffness quantities while $C = c(z)/c_R$ and $E = e(z)/e_R$ denote the normalized chord and distance between aerodynamic line and reference axis, respectively. It should be mentioned that in Eqs. (28), (29) the warping restraint effect was included but the effect of transverse shear flexibility was not. Equation (28) represents the counterpart for thin-walled beams of the expression for the divergence obtained in Ref. 3 for solid beams.

Numerical Results and Discussions

The wing structure, whose geometrical characteristics are depicted in Fig. 1, is assumed to be made of graphite-epoxy material with the following elastic properties:

$E_1 = 30 \times 10^6$ psi, $E_2 = E_3 = 0.75 \times 10^6$ psi
$G_{13} = G_{23} = 0.37 \times 10^6$ psi, $G_{12} = 0.45 \times 10^6$ psi
$\mu_{12} = \mu_{23} = \mu_{13} = 0.25$, $\rho = 14.3 \times 10^{-5}$ lb sec^2/in^4

The eigenvalue problem was solved for a variety of cases and the results are presented in the following. Figures 3 and 4 show the first three eigenfrequencies versus the ply angle for various values of the taper ratio. Figures 5 and 6 display the first four uncoupled eigenfrequencies versus the taper ratio for $\theta = 0°$ and $\theta = 90°$ and Fig. 7 presents the first four coupled eigenfrequencies for $\theta = 45°$. Figures 8 and 9 show the distribution of the normalized vertical displacement and twist in the lowest three modes for $\theta = 45°$ and for different values of taper ratio. Figure 10 displays the divergence speed versus the taper ratio for a swept back wing with $\Lambda = 5°$ and with ply angles $\theta = 0°$ and $90°$. Finally, Figs. 11 and 12 display the distribution along the wing span of the normalized bending and torsional stiffness. The figures reveal that the linear variation along the span of the chord and height of the cross-section profile induces a parabolic distribution for these stiffness quantities.

In all the plots presented, the significant effects of the taper ratio on the vibration and static aeroelastic instability characteristics of aircraft wings have been demonstrated. As shown, an increase in the taper ratio results in a decay in the vibrational and static aeroelastic properties of the wing structure. This trend can be reversed by implementation of tailoring techniques. This amounts to proper selection of the ply angle so as to reduce negative effects of wing taper. Hence, tailoring permits exploitation of advantages offered by wing taper.

References

1. Weisshaar, T. A., "Aeroelastic Tailoring of Forward Swept Composite Wings," *Journal of Aircraft*, Vol. 18, Aug. 1981, pp. 669–676.
2. Weisshaar, T. A. and Foist, B. L., "Vibration Tailoring of Advanced Composite Lifting Surfaces," *Journal of Aircraft*, Vol. 22, No. 2, Feb. 1985, pp. 141–147.
3. Librescu, L. and Simovich, J., "General Formulation for the Aeroelastic Divergence of Composite Swept Forward Wing Structures," *Journal of Aircraft*, Vol. 25, April 1988, pp. 364–371.
4. Librescu, L. and Thangjitham, S., "Analytical Studies on Static Aeroelastic Behavior of Forward-Swept Composite Wing Structures," *Journal of Aircraft*, Vol. 27, Nov. 1990, pp. 151–157.
5. Librescu, L., Meirovitch, L. and Song, O., "A Refined Structural Model of Composite Aircraft Wings for the Enhancement of Vibrational and Aeroelastic Response Characteristics," AIAA Paper, 93-1536 CP, *Proceedings of the AIAA/ASME/ ASCE/AHS/ASC 34th SDM Structures, Structural Dynamics, and Materials Conference*, April 1993, La Jolla, CA, pp. 3457-3464.
6. Weisshaar, T. A., "Divergence of Forward Swept Composite Wings," *Journal of Aircraft*, Vol. 17, June 1980, pp. 442-448.
7. Meirovitch, L., *Computational Methods in Structural Dynamics*, Sijthoff & Noordhoff International Publishers, The Netherlands, 1980.
8. Rehfield, L. W. and Atilgan, A. R., "Toward Understanding the Tailoring Mechanisms for Thin-Walled Composite Tubular Beames," *Proceedings of the First U.S.S.R.-U.S.A. Symposium on Mechanics of Composite Materials, ASME 1989*, Riga, Lituania, May 23–26, 1989, pp. 187-196.
9. Smith, E. C. and Chopra, I., "Formulation and Evaluation of an Analytical Model for Composite Box-Beams," *Journal of the American Helicopter Society*, Vol. 36, 1991, pp. 23–35.
10. Bisplinghoff, R. L. and Ashley, H., *Principles of Aeroelasticity*, Wiley, New York, 1962.

APPENDIX

The *modified local stiffness coefficients* are given by

$$
\begin{aligned}
&K_{11} = A_{22} - \frac{A_{12}^2}{A_{11}},\ K_{12} = A_{26} - \frac{A_{12}A_{16}}{A_{11}} = K_{21}\\
&K_{13}(z) = 2K_{12}\frac{A_c(z)}{\beta(z)},\ K_{14} = B_{22} - \frac{A_{12}B_{12}}{A_{11}} = K_{41}\\
&K_{22} = A_{66} - \frac{A_{16}^2}{A_{11}},\ K_{23}(z) = 2K_{22}\frac{A_c(z)}{\beta(z)}\\
&K_{24} = B_{26} - \frac{A_{16}B_{12}}{A_{11}} = K_{42}\\
&K_{43}(z) = 2K_{24}\frac{A_c(z)}{\beta(z)},\ K_{44} = D_{22} - \frac{B_{12}^2}{A_{11}}\\
&K_{51} = B_{26} - \frac{B_{16}A_{12}}{A_{11}},\ K_{52} = B_{66} - \frac{B_{16}A_{16}}{A_{11}}\\
&K_{53}(z) = 2K_{52}\frac{A_c(z)}{\beta(z)},\ K_{54} = D_{26} - \frac{B_{12}B_{16}}{A_{11}}
\end{aligned}
\tag{A.1}
$$

where A_{ij}, B_{ij} and D_{ij} denote local stretching, stretching-bending coupling and bending rigidity quantities, respectively. The dependence on the z-coordinate of various coefficients components K_{ij} is indicated explicitly.

The *inertia terms* are as follows:

$$
\begin{aligned}
I_1(z) &= \oint \left[\ddot{u}_0 - y(z)\ddot{\phi}\right] m_0 ds\\
I_2 &= \oint \left[\ddot{v}_0 + x(z)\ddot{\phi}\right] m_0 ds\\
I_3(z) &= \oint \left[\ddot{w}_0 + x(z)\ddot{\theta}_y + y(z)\ddot{\theta}_x - F_\omega(s,z)\ddot{\phi}'\right] m_0 ds,\\
I_4(z) &= \oint [(x^2(z) + y^2(z))\ddot{\phi} - y(z)\ddot{u}_0 + x(z)\ddot{v}_0] m_0 ds\\
I_5(z) &= \oint [x(z)\ddot{w}_0 + x^2(z)\ddot{\theta}_y\\
&\quad + x(z)y(z)\ddot{\theta}_x - x(z)F_\omega(s,z)\ddot{\phi}'] m_0 ds\\
&\quad + \oint \left(\frac{dy}{ds}\frac{dy}{ds}\ddot{\theta}_y - \frac{dx}{ds}\frac{dy}{ds}\ddot{\theta}_x - \frac{dy}{ds}a(s,z)\ddot{\phi}'\right) m_2 ds\\
I_7(z) &= \oint [y(z)\ddot{w}_0 + y^2(z)\ddot{\theta}_x\\
&\quad + x(z)y(z)\ddot{\theta}_y - y(z)F_\omega(s,z)\ddot{\phi}'] m_0 ds\\
&\quad + \oint \left[\frac{dx}{ds}\frac{dx}{ds}\ddot{\theta}_x - \frac{dx}{ds}\frac{dy}{ds}\ddot{\theta}_y + \frac{dx}{ds}a(s,z)\ddot{\phi}'\right] m_2 ds\\
I_9(z) &= \oint [-F_\omega(s,z)\ddot{w}_0 - x(z)F_\omega(s,z)\ddot{\theta}_y\\
&\quad - y(z)F_\omega(s,z)\ddot{\theta}_x + F_\omega(s,z)^2\ddot{\phi}'] m_0 ds
\end{aligned}
\tag{A.2}
$$

$$+\oint\left[\frac{dx}{ds}a(s,z)\ddot{\theta}_x-\frac{dy}{ds}a(s,z)\ddot{\theta}_y+a^2(s,z)\ddot{\phi}'\right]m_2ds$$

where

$$(m_0,m_2)=\sum_{k=1}^{N}\int_{h_{(k-1)}}^{h_{(k)}}\rho_{(k)}(1,n^2)dn \qquad (A.3)$$

denote mass terms.

The *rigidity coefficients* have the form

$$a_{11}=\oint K_{11}ds,\quad a_{12}(z)=\oint\left[x(z)K_{11}+K_{14}\frac{dy}{ds}\right]ds,$$

$$a_{13}(z)=\oint\left[y(z)K_{11}-K_{14}\frac{dx}{ds}\right]ds$$

$$a_{14}(z)=\oint K_{12}\frac{dx}{ds}ds,\quad a_{15}(z)=\oint K_{12}\frac{dy}{ds}ds,$$

$$a_{16}(z)=-\oint\left[K_{11}F_\omega(s,z)+K_{14}a(s,z)\right]ds$$

$$a_{17}(z)=\oint K_{13}(z)ds$$

$$a_{22}(z)=\oint\left[K_{11}x^2(z)+2x(z)K_{14}\frac{dy}{ds}+K_{44}\frac{dy}{ds}\frac{dy}{ds}\right]ds$$

$$a_{23}(z)=\oint\left[K_{11}x(z)y(z)-x(z)K_{14}\frac{dx}{ds}+y(z)K_{14}\frac{dy}{ds}-K_{44}\frac{dx}{ds}\frac{dy}{ds}\right]ds$$

$$a_{24}(z)=\oint\left(x(z)K_{12}\frac{dx}{ds}+K_{24}\frac{dx}{ds}\frac{dy}{ds}\right)ds$$

$$a_{25}(z)=\int\left(x(z)K_{12}\frac{dy}{ds}+K_{24}\frac{dy}{ds}\frac{dy}{ds}\right)ds$$

$$a_{26}(z)=-\oint\left[x(z)K_{11}F_\omega(s,z)+x(z)K_{14}a(s,z)+F_\omega(s,z)K_{14}\frac{dy}{ds}+K_{44}a(s,z)\frac{dy}{ds}\right]ds$$

$$a_{27}(z)=\oint\left[x(z)K_{13}(z)+K_{43}(z)\frac{dy}{ds}\right]ds$$

$$a_{33}(z)=\oint\left[K_{11}y^2(z)-2y(z)K_{14}\frac{dx}{ds}+K_{44}\frac{dx}{ds}\frac{dx}{ds}\right]ds$$

$$a_{34}(z)=\oint\left[y(z)K_{12}\frac{dx}{ds}-K_{24}\frac{dx}{ds}\frac{dx}{ds}\right]ds$$

$$a_{35}(z)=\oint\left[y(z)K_{12}\frac{dy}{ds}-K_{24}\frac{dx}{ds}\frac{dy}{ds}\right]ds \qquad (A.4)$$

$$a_{36}(z)=-\oint\left[y(z)K_{11}F_\omega+yK_{14}a(s,z)-F_\omega(s,z)K_{14}\frac{dx}{ds}-K_{44}a(s,z)\frac{dx}{ds}\right]ds$$

$$a_{37}(z)=\oint\left[y(z)K_{13}(z)-K_{43}(z)\frac{dx}{ds}\right]ds$$

$$a_{44}(z)=\oint\left[K_{22}\frac{dx}{ds}\frac{dx}{ds}+A_{44}\frac{dy}{ds}\frac{dy}{ds}\right]ds$$

$$a_{45}(z)=\oint\left[K_{22}\frac{dx}{ds}\frac{dy}{ds}-A_{44}\frac{dx}{ds}\frac{dy}{ds}\right]ds$$

$$a_{46}(z)=-\oint 5\left[F_\omega(s,z)K_{21}\frac{dx}{ds}+K_{24}a(s,z)\frac{dx}{ds}\right]ds$$

$$a_{47}(z)=\oint\left[K_{23}(z)\frac{dx}{ds}\right]ds$$

$$a_{55}(z)=\oint\left[K_{22}\frac{dy}{ds}\frac{dy}{ds}+A_{44}\frac{dx}{ds}\frac{dx}{ds}\right]ds$$

$$a_{56}(z)=-\oint\left[F_\omega(s,z)K_{21}\frac{dy}{ds}+K_{24}a(s,z)\frac{dy}{ds}\right]ds$$

$$a_{57}(z)=\oint\left[K_{23}(z)\frac{dy}{ds}\right]ds$$

$$a_{66}(z)=\oint\left[K_{11}F_\omega^2(s,z)+2K_{14}F_\omega(s,z)a(s,z)+K_{44}a^2(s,z)\right]ds$$

$$a_{67}(z)=-\oint\left[K_{13}(z)F_\omega(s,z)+K_{43}(z)a(s,z)\right]ds$$

$$a_{77}(z)=2\oint 2\left[\frac{A_c(z)}{\beta(z)}K_{23}(z)\right]ds$$

and note that the rigidity coefficients are symmetric, $a_{ij}=a_{ji}(i,j=1,2,\ldots 7)$.

Finally, the inertia coefficients are given by

$$[b_1,\ b_4(z),\ b_5(z),\ b_{10}(z)]=\oint m_o\left[1,\ y^2(z),\ x^2(z),\ F_\omega^2(s,z)\right]ds$$

$$[b_{14}(z),\ b_{15}(z),\ b_{18}(z)]=\oint m_2\left[\left(\frac{dx}{ds}\right)^2,\ \left(\frac{dy}{ds}\right)^2,a^2(s,z)\right]ds \qquad (A.5)$$

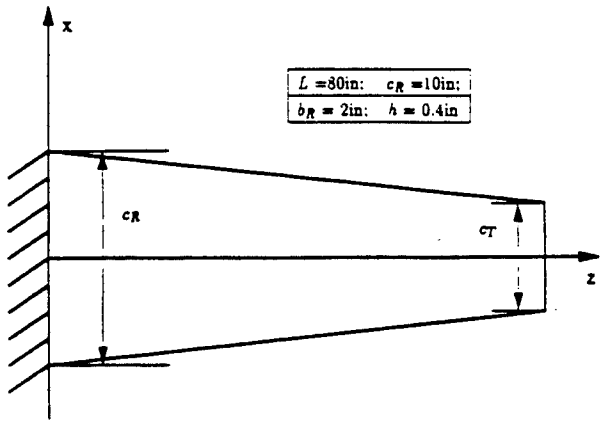

Fig. 1a Top view of the tapered wing

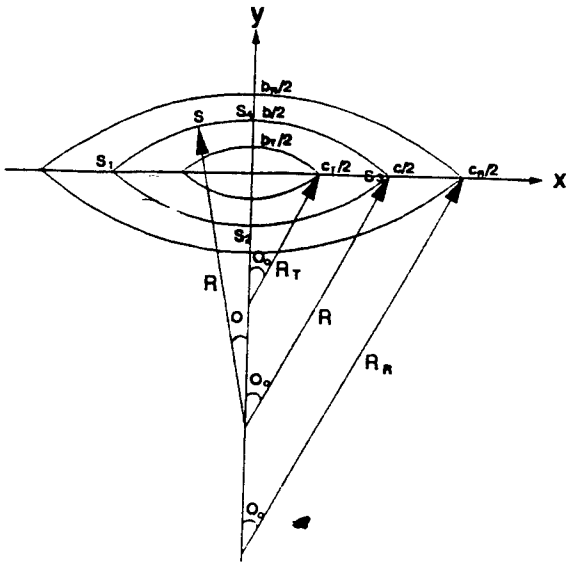

Fig. 1b Cross section of the tapered wing

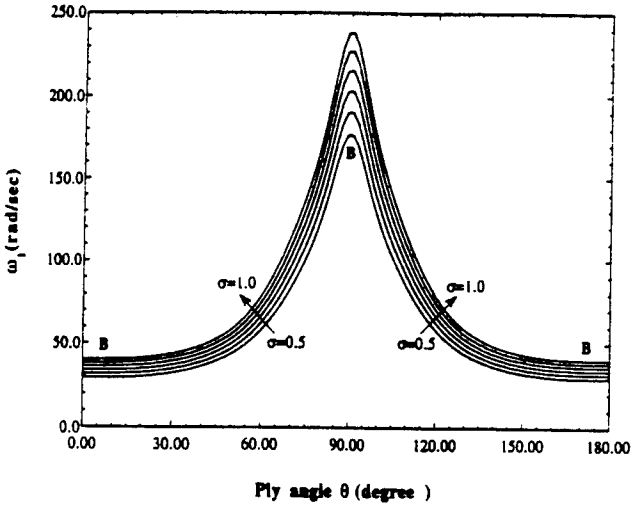

Fig. 2 The first eigenfrequency for various values of taper ratio

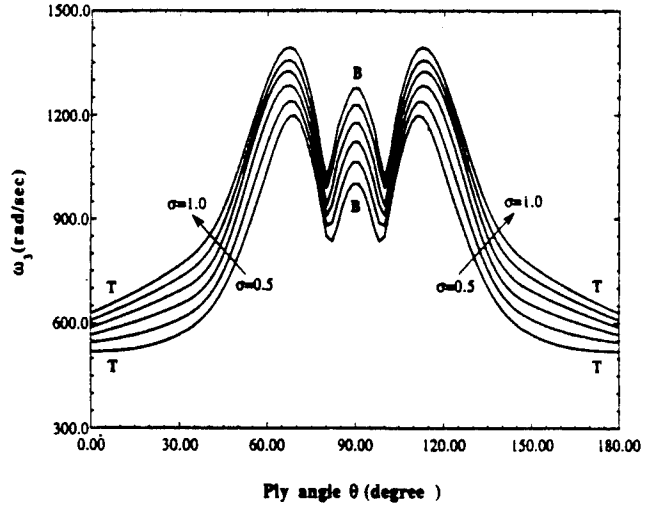

Fig. 3 The second eigenfrequency for various values of taper ratio

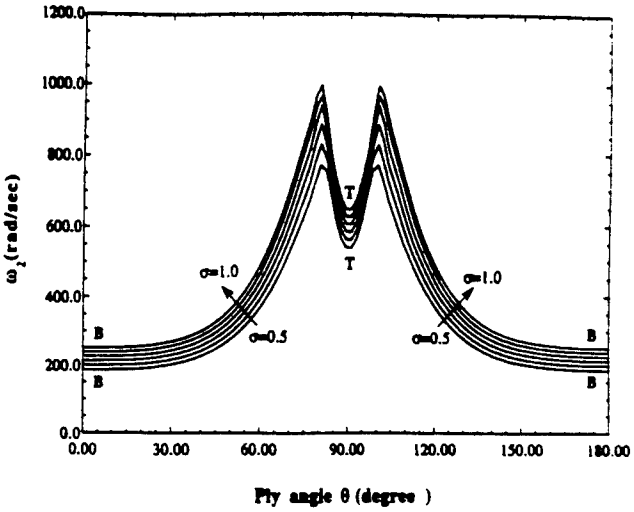

Fig. 4 The third eigenfrequency for various values of taper ratio

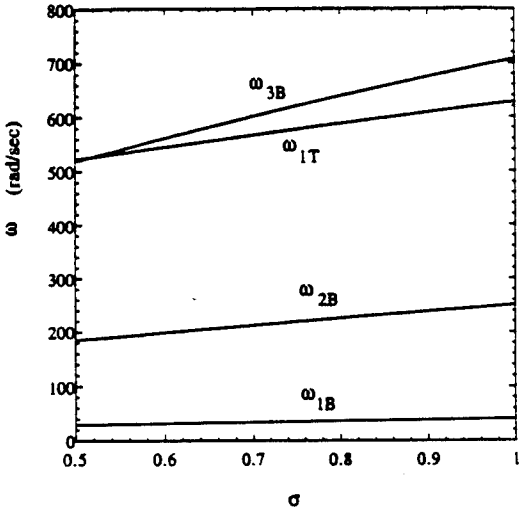

Fig. 5 The first four eigenfrequencies versus the taper ratio for $\theta = 0°$

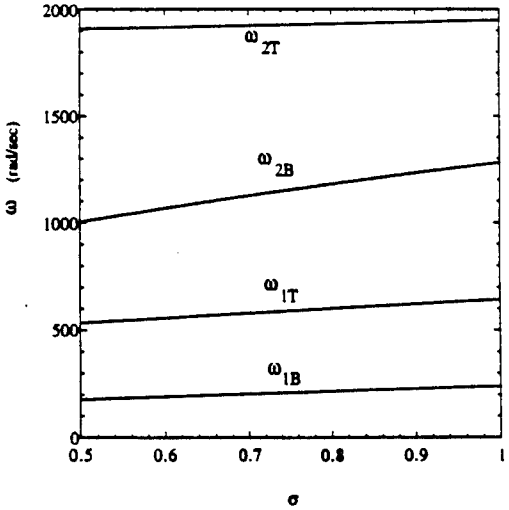

Fig. 6 The first four eigenfrequencies versus the taper ratio for $\theta = 90°$

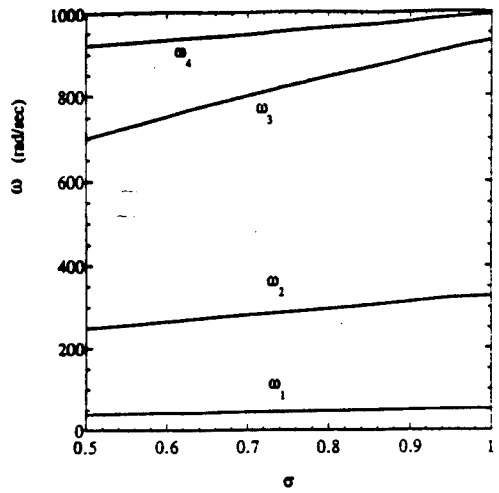

Fig. 7 The first four coupled eigenfrequencies versus the taper ratio for $\theta = 45°$

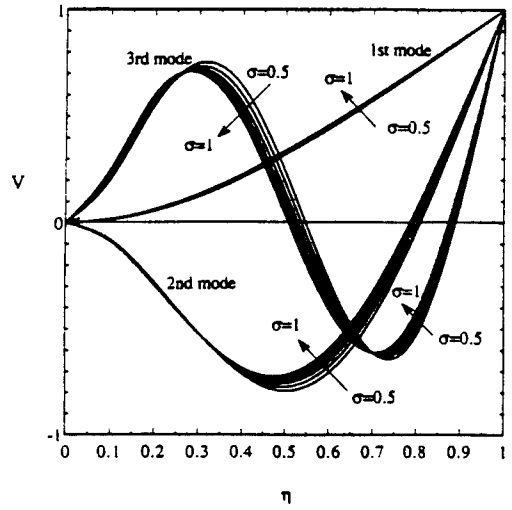

Fig. 8 The three lowest modes for $\theta = 45°$ and for various values of the taper ratio

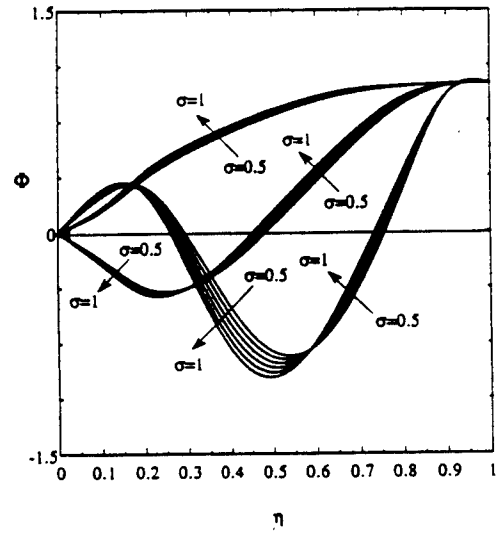

Fig. 9 The three lowest modes for $\theta = 45°$ and for various values of the taper ratio

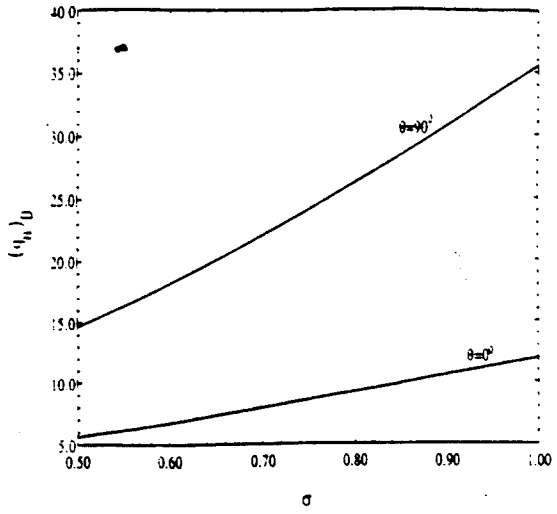

Fig. 10 The divergence speed versus the taper ratio of a swept-back wing ($\Lambda = 5°$) for $\theta = 0°$ and 90°

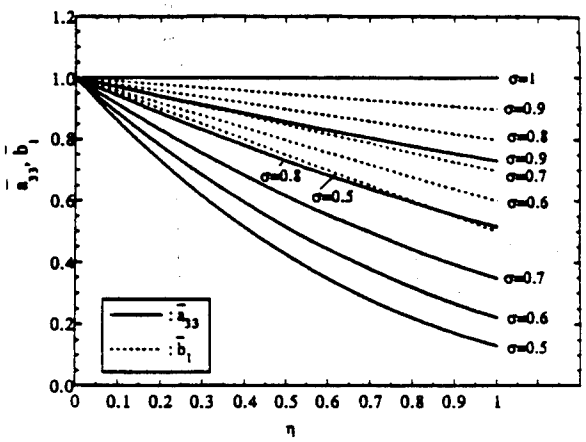

Fig. 11 The normalized bending stiffness and mass per unit span for $\theta = 0°$ or 90° and for various values of the taper ratio

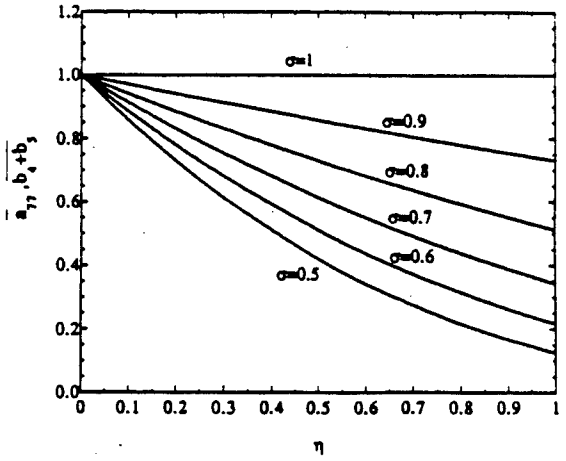

Fig. 12 The normalized torsional stiffness a_{77} and of the polar mass per unit span for $\theta = 0°$ or 90° and for various values of the taper ratio